THERMALLY CROSSLINKED POLYIMIDE HOLLOW FIBER MEMBRANES FOR NATURAL GAS PURIFICATION

A Dissertation
Presented to
The Academic Faculty

By

Chien-Chiang Chen

In Partial Fulfillment
Of the Requirements for the Degree
Doctor of Philosophy in the
School of Chemical & Biomolecular Engineering

Georgia Institute of Technology

December 2011

THERMALLY CROSSLINKED POLYIMIDE HOLLOW FIBER MEMBRANES FOR NATURAL GAS PURIFICATION

Approved by:

Dr. William Koros, Advisor
School of Chemical & Biomolecular Engineering
Georgia Institute of Technology

Dr. Dennis Hess
School of Chemical & Biomolecular Engineering
Georgia Institute of Technology

Dr. Tom Fuller
School of Chemical & Biomolecular Engineering
Georgia Institute of Technology

Dr. Stephen Miller
Chevron Fellow
Chevron Energy Technology Company

Dr. Anselm Griffin
School of Materials Science & Engineering
Georgia Institute of Technology

Date Approved: September 27, 2011

ACKNOWLEDGEMENTS

I would like to express my most earnest gratitude to my advisor Dr. Bill Koros for his unwavering support and guidance over the past several years. I consider myself particularly fortunate to have him as my mentor as he has been instrumental in my development, both on a professional and personal level. His enthusiasm, strong work ethic and relentless dedication will continue to be a great source of inspiration for me. I would also like to thank my committee members, Dr. Tom Fuller, Dr. Dennis Hess, Dr. Anselm Griffin, and Dr. Stephen Miller for their time and valuable insights. The funding support from Chevron is also greatly appreciated.

The whole of the Koros group has been a pleasure to work with. All members deserve thanks, but special credit goes to Dr. Wulin Qiu, Dr. Dhaval Bhandari, Dr. Naoki Bessho, Dr. Junqiang Liu, Dr. Mita Das, Dr. Ryan Adams, Dr. Jason Ward, Dr. JR Johnson and Dr. Oguz Karvan for their help and support. I would also like to thank Liren Xu for the numerous discussions, both technical and non-technical.

I must thank to my family for their unconditional support from thousand miles away. The friends I've made in Atlanta have helped me stay motivated throughout my PhD study. Thanks go out especially to Tsun-Yen Wu, Yungwen Lee, Yun Lee, and Yu-Ting Hsueh for enjoying my sense of humor and making Friday night fun.

None of this would have been possible without endless patience, encouragement, and understanding of my wife, Szu-Yu. She always willingly came to school with me on weekend and stayed awake with me whenever I have a deadline approaching. I cannot imagine my life without her, nor can I thank her enough.

TABLE OF CONTENT

LIST OF TABLES

LIST OF FIGURES

SUMMARY

World natural gas production is over 100 trillion scf/yr and is expected to grow as much as 50% by 2035. Carbon dioxide removal from natural gas is currently one of the largest industrial membrane gas separation applications. High energy efficiency, low capital, operating and maintenance costs make membranes an attractive approach for acid gas removal. Moreover, the compact and robust natures of hollow fiber membrane modules are desirable for offshore and remote applications. However, the use of polymeric membranes is limited by swelling-induced performance losses in aggressive feeds with high CO_2 content and heavy hydrocarbons.

The overarching goal of this research was to develop robust asymmetric hollow fiber membranes for CO_2 removal from aggressive natural gas feed streams and to understand their properties. Asymmetric hollow fiber membranes with defect-free selective skin layers on an optimized porous support substructure were successfully spun and subsequently stabilized by covalent crosslinking within the economical membrane formation process. Thermal treatment conditions, which promote sufficient crosslinking without introducing defects or undesired substructure resistance, were identified. It was found that crosslinking improves membrane efficiency and plasticization resistance as well as mechanical strength of fibers. The capability to maintain attractive separation performance under realistic operating conditions and durability against deleterious impurities suggests that the crosslinked fibers have great potential for use in diverse aggressive applications, even beyond the CO_2/CH_4 example explored in this work.

CHAPTER 1

INTRODUCTION

1.1 Membrane technology

Separation processes can represent 40-70% of both capital and operating costs in industry, and account for roughly half of all process energy used in the enormous chemicals and petroleum-refining industries [1]. More efficient separation technologies are essential for long-term sustainability of the industries by improving energy efficiency, reducing waste and CO_2 emissions. Membrane-based separations offer attractive alternatives to inefficient traditional thermally-driven processes. In seawater desalination, membranes are over 10 times more efficient than thermal options and have already become mainstream in this large-scale application [2]. In gas separations, membrane-based gas separation comprises a market of $150 million/year in 2000, and is expected to see continued growth of 7-8% annually to a market of $760 million/year by 2020 [3]. The major industrial applications of polymeric membranes include air separation, hydrogen separation, and natural gas treatment [3, 4]. However, large and growing opportunities for gas separations using membranes exist in refinery/petrochemical and natural gas industries [3], where the aggressive gas streams can significantly diminish membrane performance and lifetime; therefore more robust membranes are needed to enable their broad use in these applications of vast untapped potential for membranes. A percentage breakdown of the total membrane market by major separation categories in 2000 and predicted in 2020 is given in Figure 1.1.

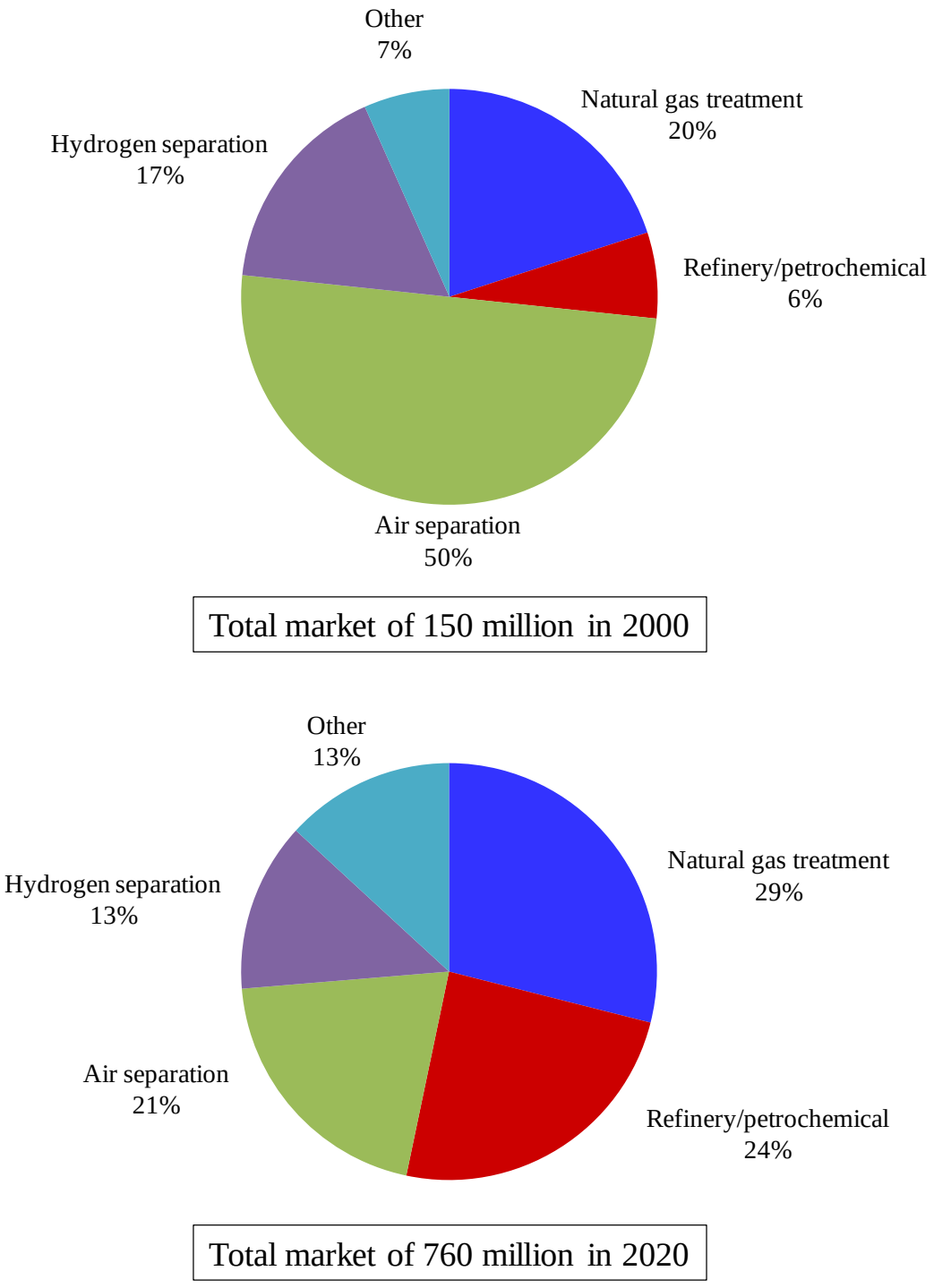

Figure 1.1: Percentage breakdown of membrane market in 2000 (a total of 150 million) and predicted in 2020 (a total of 760 million) [3].

Figure 1.2 summarizes the four essential elements that have enabled advancement of the membrane technology from the laboratory into commercial reality [2]. Research works in this field focus mostly on development of advanced materials. Creation of advanced materials is crucial, but is only the first key element needed. It is critical to integrate the four key elements in order to introduce a new type of membrane process or a new generation of an existing membrane process [2]. To meet these key requirements, most industrial gas separation membranes are formed into hollow fiber configuration. Hollow fiber modules offer much higher surface area per unit volume over other membrane configurations as shown in Figure 1.3. Such high efficiency modules, together with ability to form ultrathin selective layers in the fiber format via morphology control, provide the required high productivity per unit volume to maintain compact system size allows for large scale applications [2, 4]. In hollow fiber systems, shell side feeds are typically favorable for high pressure applications such as natural gas separations studied in this work. Fibers are much stronger under compression than expansion (the fiber collapse pressure is typically 2-4 times higher than the burst pressure) [4, 5], so the high wellhead pressures can be unitized to maximize productivity. Moreover, if individual fibers fail in shell side feed mode, they simply collapse and no longer contribute to the total membrane area; however, if bore side fed fibers fail, they serves as bypasses to contaminate the permeate with feed, thus destroying selectivity [4, 5].

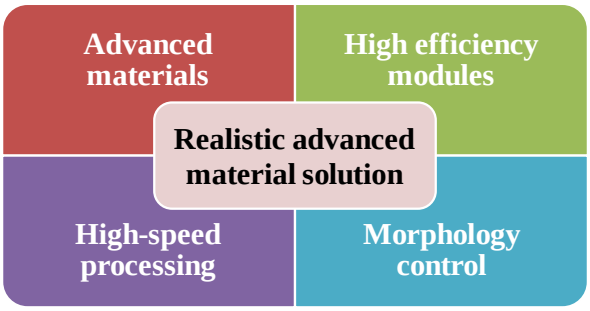

Figure 1.2: Enabling elements responsible for membrane technology advancement. Adapted from [2].

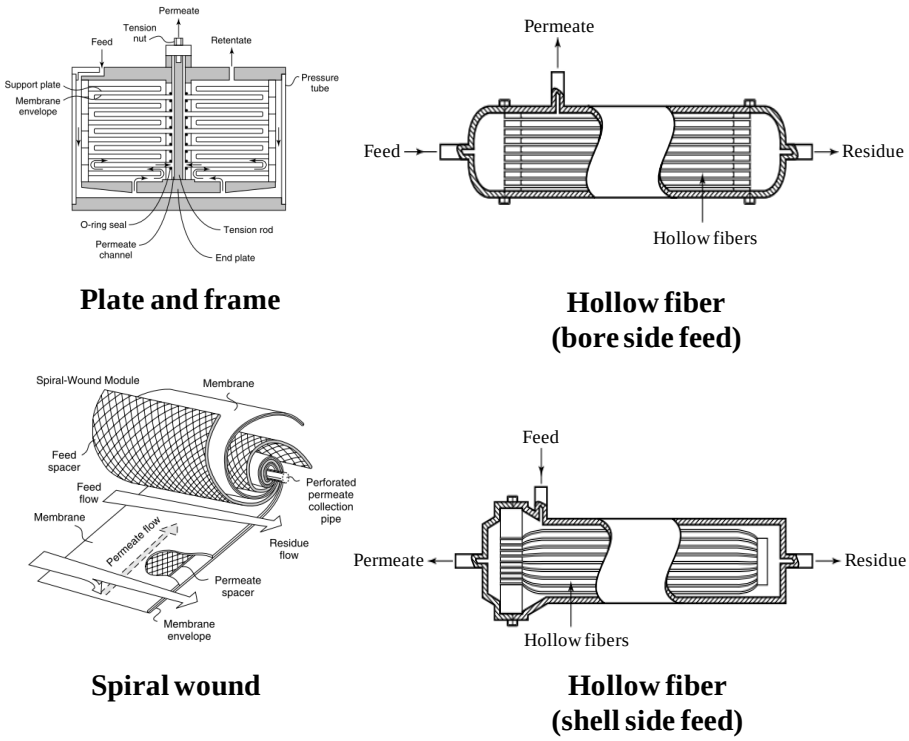

Figure 1.3: Schematics of major types of modules used for gas separation applications and comparison of surface area to volume ratios of various configurations [4, 6].

1.2 Natural gas processing

Oil, natural gas and coal are by far the most important energy source, accounting for more than 80% of the energy consumption in U.S. Of these three fossil fuels, natural gas has the smallest CO_2 footprint, and natural gas is an abundant U.S. resource. About 90% of natural gas consumption in U.S. is met by domestic production [7], thereby providing a secure, reliable and relatively environmentally friendly energy resource. Moreover, unlike declining proved reserves of crude oil shown in Figure 1.4, proved reserves of natural gas increased in the past twenty years thanks to advances in exploration and production technology. U.S. Energy Information Administration estimated that proved reserves accounts for less than 15% of the total recoverable natural gas resources in U.S. [8] and world natural gas production is expected to grow as much as 50% by 2035 [9].

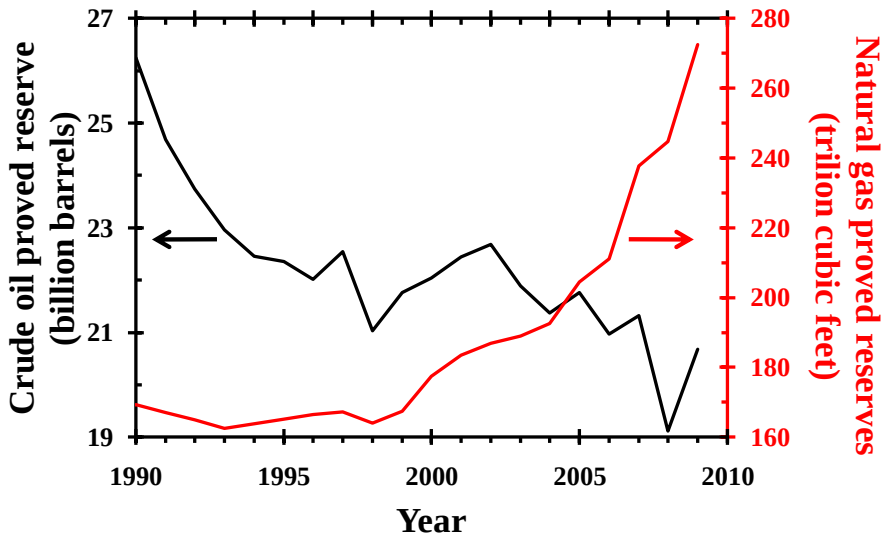

Figure 1.4: Proved reserves of crude oil [10] and natural gas [11] in U.S.

Raw natural gas varies substantially in composition from source to source. Natural gas contains mostly CH_4, but also contains various amount of impurities such as CO_2, N_2, H_2S, H_2O, and various hydrocarbons. All natural gas requires some processing to meet pipeline specifications as shown in Table 1.1. Carbon dioxide, as the most abundant contaminant in many wells, can exceed 50% in some natural gas feeds. In enhanced coal bed methane recovery and enhanced oil recovery applications, CO_2 content can be as much as 80-90% [12, 13]. Amine and physical absorption processes are widely used technologies for CO_2 removal, but the capital and operating costs surge with increasing CO_2 concentration and feed pressure. Membranes, on the other hand, are more efficient in high CO_2 partial pressure feeds due to the higher driving force for CO_2 permeation. High energy efficiency, low capital, operating and maintenance costs make membranes an attractive approach for acid gas removal. Moreover, the compact and robust natures of hollow fiber membrane modules are desirable for offshore and remote applications. Polymeric membranes are currently the most attractive option because of their cost and processability advantages over zeolite or ceramic membranes. However, the use of polymeric membranes is limited by swelling-induced performance losses in aggressive feeds with high CO_2 content and heavy hydrocarbons.

The overarching goal of this research is to develop robust asymmetric hollow fiber membranes for CO_2 removal from natural gas. Membranes that exhibit plasticization resistance against CO_2 have been shown to also have plasticization resistance to other contaminants such as aromatics [14-16]. Plasticization-resistant polyimide membranes may allow these polyimides to maintain attractive separation performance not only in natural gas but also in refinery and petrochemical industries,

such as olefin/paraffin [17] and aromatic/aliphatic separation [18]. While these applications are not pursed here, they would be interesting for study in other projects.

Table 1.1: U.S. natural gas pipeline specifications [19].

Component	Pipeline specification
CO_2	< 2%
H_2O	< 120 ppm
H_2S	< 4 ppm
C_{3+} content	950-1050 Btu/scf; Dew point < -20 ℃
Total Inerts (N_2, He, etc.)	< 4%

1.3 Research objectives

This research considers high pressure CO_2/CH_4 separation using thermally crosslinkable hollow fiber membranes. The earlier report of dense film properties of the same materials showed that the crosslinked films have excellent plasticization resistance against CO_2 [20, 21]. Given the promising results from dense films, this research addresses the challenges of transitioning this new crosslinking approach from dense films to industrially relevant asymmetric hollow fiber membranes. The primary objectives of this dissertation are as follows:

1. **Develop crosslinkable defect-free asymmetric hollow fiber membranes from a novel polyimide, 6FDA-DAM:DABA (3:2).**

The first challenge of this research is to produce crosslinkable defect-free asymmetric hollow fiber membranes from a novel polymer. Since the fibers will be crosslinked at high temperature (higher than 300 ℃), strategy to maintain skin integrity and substructure porosity are crucial to the later crosslinking step which could accentuate any incipient defect and introduce undesirable substructure resistance. The details of developing asymmetric hollow fibers with defect-free selective skin layers on an optimized porous support substructure are described. Fiber structure and transport properties were investigated.

2. **Investigate the effect of thermal treatment on degree of crosslinking, fiber morphology, and separation performance.**

The thermally crosslinkable fiber membranes developed in Objective 1 were crosslinked at various conditions and characterized. The effects of various thermal treatment conditions on crosslinking, fiber morphology, transport properties as well as plasticization resistance were investigated. In Objective 1 and 2, practical issues of fiber fabrication are considered. Detailed characterization and analysis were performed to guide and explain the process discussed, but the feasibility and practicality of implementation remain the focus of this work.

3. **Demonstrate the efficacy of thermally crosslinked hollow fiber membranes under aggressive feed streams and realistic operating conditions.**

Membrane suitability for practical applications is determined by long-term stability of permeance and selectivity under aggressive operating conditions (mixed gas,

high pressure and presence of contaminants). The effects of feed pressure, CO_2 concentration, operating temperature, permeate pressure and presence of contaminants were investigated to identify the application window of the crosslinked hollow fiber membranes for natural gas purification. The effects of physical aging and CO_2 conditioning on separation performance were also investigated.

1.4 Dissertation organization

This dissertation is organized in the following manners. Chapter 2 provides an overview of essential background material relevant to the research presented in this work. Chapter 3 describes the materials, experimental procedures and equipment used throughout this research. Chapter 4 identifies the experimental conditions for creating a defect-free asymmetric hollow fiber membrane from the thermally crosslinkable polymer. Chapter 5 discusses the effects of crosslinking conditions and the crosslinked fiber membrane performance under practical operating conditions. Effects of physical aging and CO_2 conditioning are also detailed. Chapter 6 contains the analysis of crosslinked fiber membrane performance in the presence of various model contaminants, including toluene, heptane and ethylene glycol. The stability against water-saturated acid gas is also presented. Chapter 7 summarizes the findings of this work and includes recommendations for future work to further advance the project.

1.5 References

1. A. Legault, *Mainstreaming efficient industrial separation systems*. OPEN Energy Technology Bulletin, 2008(55).

2. W.J. Koros, *Evolving beyond the thermal age of separation processes: membranes can lead the way.* AIChE Journal, 2004. **50**(10): p. 2326-2334.

3. R.W. Baker, *Future directions of membrane gas separation technology.* Industrial & Engineering Chemistry Research, 2002. **41**(6): p. 1393-1411.

4. W.J. Koros and G.K. Fleming, *Membrane-based gas separation.* Journal of Membrane Science, 1993. **83**(1): p. 1-80.

5. R.W. Baker, *Membrane separation systems: recent developments and future directions.* Elsevier Science: 1991.

6. R.W. Baker, *Membrane technology and applications.* Second ed.; Wiley: 2004.

7. *Annual Energy Outlook 2011 (AEO 2011). Report Number: DOE/EIA-0383ER(2011).* Energy Information Administration.

8. *Assumptions to the Annual Energy Outlook 2009, 2010, 2011*. Energy Information Administration.

9. *International Energy Outlook 2010. Report Number: DOE/EIA-0484(2010).* Energy Information Administration.

10. *U.S. crude oil proved reserves.* Energy Information Administration. http://www.eia.gov/dnav/pet/PET_CRD_PRES_DCU_NUS_A.htm. (accessed 08/2011).

11. *U.S. natural gas reserves summary*. Energy Information Administration. http://www.eia.gov/dnav/ng/ng_enr_sum_dcu_NUS_a.htm. (accessed 08/2011).

12. A. Tabe-Mohammadi, *A review of the applications of membrane separation technology in natural gas treatment.* Separation Science and Technology, 1999. **34**(10): p. 2095-2111.

13. A.K. Datta and P.K. Sen, *Optimization of membrane unit for removing carbon dioxide from natural gas.* Journal of Membrane Science, 2006. **283**(1-2): p. 291-300.

14. C. Staudt-Bickel, *Cross-linked copolyimide membranes for the separation of gaseous and liquid mixtures.* Soft Materials, 2003. **1**(3): p. 277-293.

15. I.C. Omole, D.A. Bhandari, S.J. Miller, and W.J. Koros, *Toluene impurity effects on CO_2 separation using a hollow fiber membrane for natural gas.* Journal of Membrane Science, 2011. **369**(1-2): p. 490-498.

16. J.K. Ward and W.J. Koros, *Crosslinkable mixed matrix membranes with surface modified molecular sieves for natural gas purification: II. Performance characterization under contaminated feed conditions.* Journal of Membrane Science, 2011. **377**(1-2): p. 82-88.

17. M. Das and W.J. Koros, *Performance of 6FDA-6FpDA polyimide for propylene/propane separations.* Journal of Membrane Science, 2010. **365**(1-2): p. 399-408.

18. N. Schmeling, R. Konietzny, D. Sieffert, P. Rolling, and C. Staudt, *Functionalized copolyimide membranes for the separation of gaseous and liquid mixtures.* Beilstein Journal of Organic Chemistry, 2010. **6**: p. 789-800.

19. R.W. Baker and K. Lokhandwala, *Natural gas processing with membranes: An overview.* Industrial & Engineering Chemistry Research, 2008. **47**(7): p. 2109-2121.

20. A.M. Kratochvil and W.J. Koros, *Decarboxylation-induced cross-linking of a polyimide for enhanced CO_2 plasticization resistance.* Macromolecules, 2008. **41**(21): p. 7920-7927.

21. W.L. Qiu, C.C. Chen, L. Xu, L. Cui, D.R. Paul, and W.J. Koros, *Sub-T_g cross-linking of a polyimide membrane for enhanced CO_2 plasticization resistance for natural gas separation.* Macromolecules, 2011. **44**(15): p. 6046-6056.

CHAPTER 2

BACKGROUND AND THEORY

2.1 Overview

This chapter provides essential background materials relevant to this research. The first section describes gas transport in polymeric membranes. The second section gives a review of non-ideal transport phenomena in polymeric membrane, and specifically focuses on plasticization and stabilization strategy. In the last part, the formation process and challenges in making successful asymmetric hollow fiber membranes are discussed.

2.2 Membrane transport theory

2.2.1 Permeation

Gas transport in nonporous polymeric membranes is commonly described by the sorption-diffusion theory [1]. Gas molecules sorb into the high pressure (upstream) side of the membrane, then diffuses through the membrane, and finally desorbs from the low pressure (downstream) side. Figure 2.1 shows a schematic of gas permeation through a polymeric membrane.

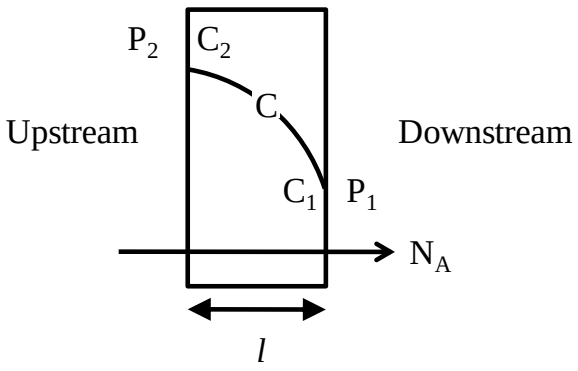

Figure 2.1: Schematic of gas permeation though a nonporous polymeric membrane.

Permeability and selectivity are the two key intrinsic properties commonly used to evaluate the membrane performance. Permeability is a measure of membrane productivity and is defined as the steady state gas flux (N_A) thorough the membrane normalized by partial pressure difference (Δp_A) across the membrane and the thickness (l) of the membrane:

$$P_A = \frac{N_A \cdot l}{\Delta p_A} \tag{2.1}$$

Penetrant transport through the membrane is driven by differences in chemical potential of penetrant across the membrane [2]. Therefore, in the case of non-ideal gases (such as CO_2/CH_4 mixed gas at high pressure commonly used in this study), the partial pressure difference (Δp_A) appearing in Equation 2.1 is replaced by the fugacity difference (Δf_A):

$$P_A = \frac{N_A \cdot l}{\Delta f_A} \tag{2.2}$$

The most common unit for permeability is “Barrer”, where

$$1\,Barrer = 1\times 10^{-10}\,\frac{cm^3(STP)\cdot cm}{cm^2\cdot s\cdot cmHg} \tag{2.3}$$

In the case of asymmetric membranes, where the thickness of the selective layer is not well defined, the membrane productivity is characterized by permeance, which is the fugacity driving force normalized flux:

$$\left(\frac{P}{l}\right)_A = \frac{N_A}{\Delta f_A} \tag{2.4}$$

Permeance is typically expressed in “Gas Permeation Unit” (GPU), which is defined as

$$1\,GPU = 1\times 10^{-6}\,\frac{cm^3(STP)}{cm^2\cdot s\cdot cmHg} \tag{2.5}$$

Membrane efficiency is evaluated by selectivity, which is defined as the ratio of the gas permeabilities or permeances:

$$\alpha_{A/B} = \frac{P_A}{P_B} = \frac{(P/l)_A}{(P/l)_B} \tag{2.6}$$

2.2.2 Sorption and diffusion in glassy polymers

Sorption in glassy polymers is commonly described by the dual mode model, which accounts for two separate environments for sorption. In this model, penetrant molecules can sorb into the densely packed region of the polymer (dissolved mode) and the non-equilibrium free volume microvoids in the polymer matrix (hole-filling or Langmuir mode) [2]. The dual mode sorption capacity is the sum of these two

contributions:

$$C = C_D + C_H \tag{2.7}$$

where C is the total concentration of penetrant in the polymer, C_D is the penetrant concentration in the dissolved mode, and C_H is the penetrant concentration in the Langmuir mode. C_D is described by a Henry's law relation and C_H is expressed in a Langmuir relation. The dual mode model can be written as

$$C = k_D p + \frac{C_H' bp}{1 + bp} \tag{2.8}$$

where k_D is the Henry's law constant, C_H' is the Langmuir capacity constant, b is the Langmuir affinity constant, and p is the penetrant pressure, or more accurately, fugacity.

Penetrant molecules diffuse through a dense non-porous polymeric membrane via random jumps through thermally activated penetrant-scale transient gaps in the polymer matrix [1]. The schematic of this diffusion process is illustrated in Figure 2.2.

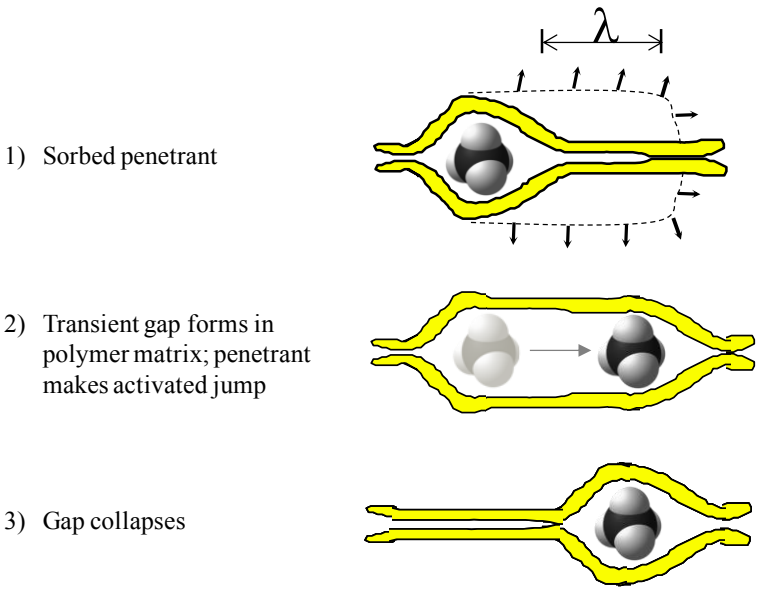

Figure 2.2: Schematics of diffusion through a polymer via transient gap formation, where λ is the average length of random diffusion jump.

The diffusivity of the penetrant in a given polymer is determined by the kinetic diameter of the penetrant molecules. Smaller molecules tend to have higher diffusivity. On the other hand, the solubility of the gas penetrant is strongly influenced by the condensability of the penetrant and the chemical affinity between polymer and penetrant. The critical temperature of a gas penetrant is a good indicator of condensability. Gases with higher critical temperature tend to be more condensable and hence more soluble in polymers. Kinetic diameters and critical temperatures for the gases used in this work are compared in Table 2.1. In the case of CO_2 removal from CH_4 using glassy polymers, CO_2 is the fast gas because of its higher condensability and smaller kinetic diameter compared to the slow gas CH_4. Therefore, the CO_2/CH_4 pair is considered a favorable separation using glassy polymer materials.

Table 2.1: Kinetic diameters and critical temperatures for gases used in this work [3].

	He	O_2	N_2	CO_2	CH_4
Kinetic diameter (Å)	2.6	3.46	3.64	3.3	3.8
Critical temperature (K)	5.2	154.4	126.1	304.2	190.7

2.2.3 Temperature dependence

Within a temperature range that does not span significant thermal transitions of the polymer, the temperature dependence of diffusion coefficient (*D*) and sorption coefficient (*S*) can be described by an Arrhenius expression and a van't Hoff expression,

respectively [4]:

$$D = D_0 \exp\left[\frac{-E_d}{RT}\right] \tag{2.9}$$

$$S = S_0 \exp\left[\frac{-\Delta H_s}{RT}\right] \tag{2.10}$$

where D_0 and S_0 are pre-exponential factors, E_d is the apparent activation energy for diffusion jump, ΔH_s is the apparent heat of sorption, R is the universal gas constant and T is the temperature in Kelvin. Since the permeability can be expressed as a product of the diffusion coefficient and the sorption coefficient, the temperature dependence of permeability (P) can be described by an apparent Arrhenius expression [4]:

$$P = D_0 S_0 \exp\left[\frac{-(E_d + \Delta H_s)}{RT}\right] \tag{2.11}$$

$$P = P_0 \exp\left[\frac{-E_p}{RT}\right] \tag{2.12}$$

where the pre-exponential factor, P_0, and the apparent activation energy for permeation, E_p, can be defined as

$$P_0 = D_0 S_0 \tag{2.13}$$

$$E_P = E_d + \Delta H_s \tag{2.14}$$

Diffusion coefficients typically increase with increasing temperature (E_D is positive) while sorption coefficients usually decrease with increasing temperature (ΔH_s is negative). In glassy polymers, the diffusion coefficient is generally a stronger function of temperature than the solubility coefficient (i.e. $E_D > |\Delta H_s|$), and thus permeability usually increases with increasing temperature [2].

2.3 Non-ideal transport phenomena in polymeric membrane

2.3.1 Plasticization

Plasticization occurs when a strongly sorbing penetrant reaches a concentration such that it swells and dilates the polymer matrix, increasing the mobility of polymer chain segments, thereby increasing the diffusion coefficients of all penetrants in the membrane. The phenomenon on the macro scale reflects a softening and a depression of the glass transition temperature of the material, while on the chain segmental scale it reflects an increase in mobility and permeability but a reduction in selectivity [5]. Plasticization behavior of membranes is commonly characterized by a permeation isotherm (permeability or permeance versus pressure plot) [6-10]. An upswing in permeability is a typical indication of swelling and plasticization. The plasticization pressure is usually defined as the pressure at which the permeability starts to increase with increasing pressure [5, 10]. Gases with high critical temperature, such as CO_2 and aromatics commonly present in raw natural gas, are known to strongly interact with glassy polymers. Therefore, plasticization is especially problematic in natural gas purification. The effects of CO_2 plasticization in CO_2/CH_4 separation is qualitatively depicted in Figure 2.3. As CO_2 partial pressure increases, the onset of plasticization occurs, which results in upswings in both CO_2 and CH_4 permeabilities. Since the slow gas CH_4 is more affected than the fast gas CO_2, plasticization results in a loss of selectivity. Moreover, the selectivity of plasticized membranes tends to decline over time [11, 12], i.e., plasticized membranes are inherently unstable.

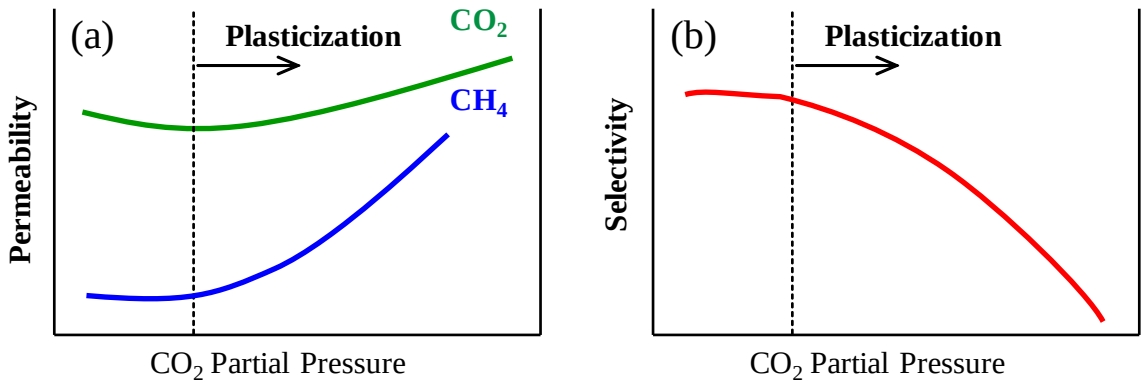

Figure 2.3: Schematics of (a) permeability increase and (b) selectivity decrease observed due to membrane plasticization.

Testing membranes with mixed gas feeds at relevant high pressure is important when penetrants (such as CO_2) can act as plasticizers. Unfortunately, most CO_2/CH_4 selectivities reported in the literature are obtained from pure gas permeation ("ideal" selectivity), or mixed gas permeation conducted at low feed pressure (less than 200 psia). Cellulose acetate membranes were the first commercial membrane system to separate CO_2 from natural gas and are still widely used. The effect of plasticization on cellulose acetate membranes and the importance of mixed gas testing are shown in Figure 2.4 [13, 14]. Pure gas selectivity is the ratio of pure gas permeabilities. The pure gas CO_2/CH_4 selectivity increases sharply as the pressure increases, because pure CO_2 permeability increases with increasing pressure (due to plasticization) while pure CH_4 permeability is relatively constant. The membrane separation performance is quite different when the membranes are tested with CO_2/CH_4 mixed gas. The mixed gas CO_2/CH_4 selectivity decreases as the pressure increases, because sorbed CO_2 plasticizes the membrane and thus causes the membrane to lose its size and shape discriminating ability. The pure gas CO_2/CH_4 selectivity can be vastly overestimated due to plasticization.

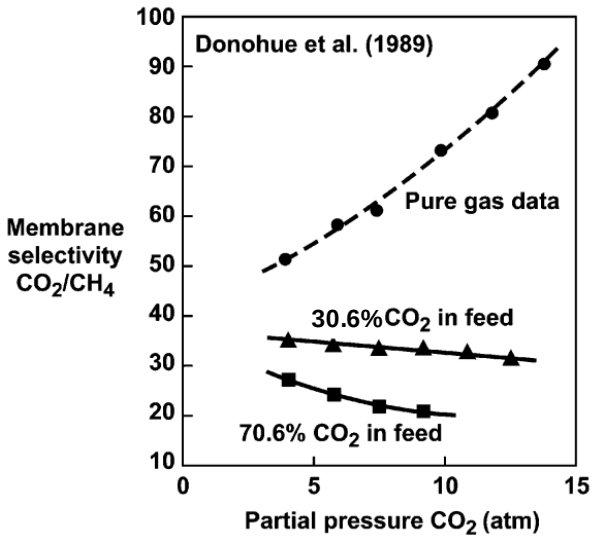

Figure 2.4: Graph showing the difference between pure gas and mixed gas selectivities of cellulose acetate films [13, 14].

Most plasticization studies are carried out using thick dense films (typically ~50 µm). On the other hand, most commercial gas separation membranes have an asymmetric morphology that contains a thin selective layer (typically less than 1 µm). Thin films have been shown to have different and more severe plasticization behaviors as compared to thick dense films of the same materials [9, 15, 16]. In thin films, plasticization usually occurs immediately without the initial drop in the permeability versus pressure plot, especially for the very thin polymer layers such as those found in asymmetric hollow fibers [17-20]. Figure 2.5 compares the CO_2 permeation isotherm of Matrimid® dense film and asymmetric hollow fiber. Plasticization occurs at lower CO_2 pressure in an asymmetric hollow fiber form and shows more pronounced effect than in a dense film form [8, 21]. Since plasticization effects are exaggerated in thin membrane structures, the suppression of plasticization is essential to membrane viability for practical applications.

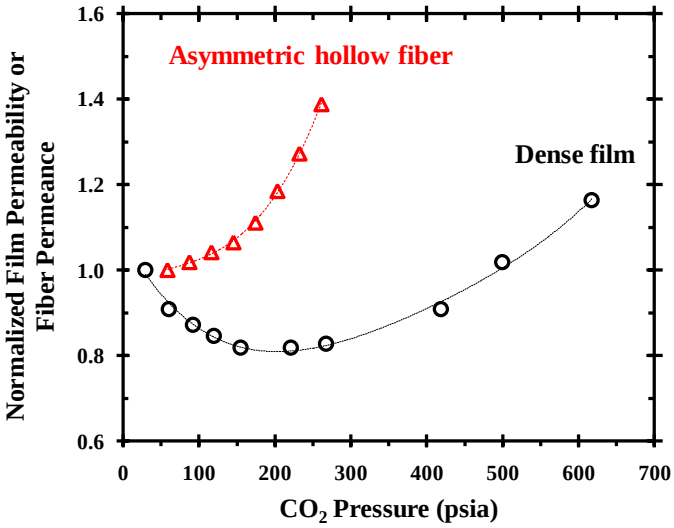

Figure 2.5: Comparison of plasticization effect on Matrimid® dense film [8] and asymmetric hollow fiber [21].

Several approaches such as thermal treatment [8, 22, 23], polymer blending [24, 25], semi-interpenetrating polymer networks [26] and crosslinking [17-19, 27-32] have been applied to suppress plasticization. Covalent crosslinking using a class of crosslinkable polyimides has been demonstrated to be effective for stabilizing the membranes against CO_2 plasticization [27-30]. The diol crosslinking agents used in these works formed ester linkages through a carboxylic acid pendant group, thus preserving polymer network and increasing plasticization resistance. The diol crosslinking approach has been successfully extended to industrial relevant asymmetric hollow fibers [18, 20]. Despite the attractive properties of the ester crosslinked membranes, these ester crosslinks can potentially be hydrolyzed in aggressive acid gas conditions present in high CO_2 feed streams, which would reverse the effects of crosslinking and greatly reduce the membrane performance. Recently, decarboxylation-induced thermal cross-linking was

discovered using the same carboxylic acid containing polyimide [33]. This new crosslinking mechanism occurs through the decarboxylation of the carboxylic acid pendant group at high temperatures, which creates free radical sites capable of crosslinking at proposed sites along the polymer backbone [33]. The structure of the crosslinkable polyimide used in this work and the crosslinking mechanism [33, 34] are shown in Figure 2.6. The 6FDA moiety and DAM moiety provide high permeability due to their bulky groups which inhibit chain packaging. The DABA moiety provides a carboxylic acid pendant group as a crosslinking site. Dense film study using the same thermally crosslinkable polyimide have shown that the crosslinked films exhibit excellent plasticization resistance [34]. This research focuses on extending the dense film success to a realistic asymmetric hollow fiber membrane and evaluating its separation performance under aggressive conditions for natural gas purification.

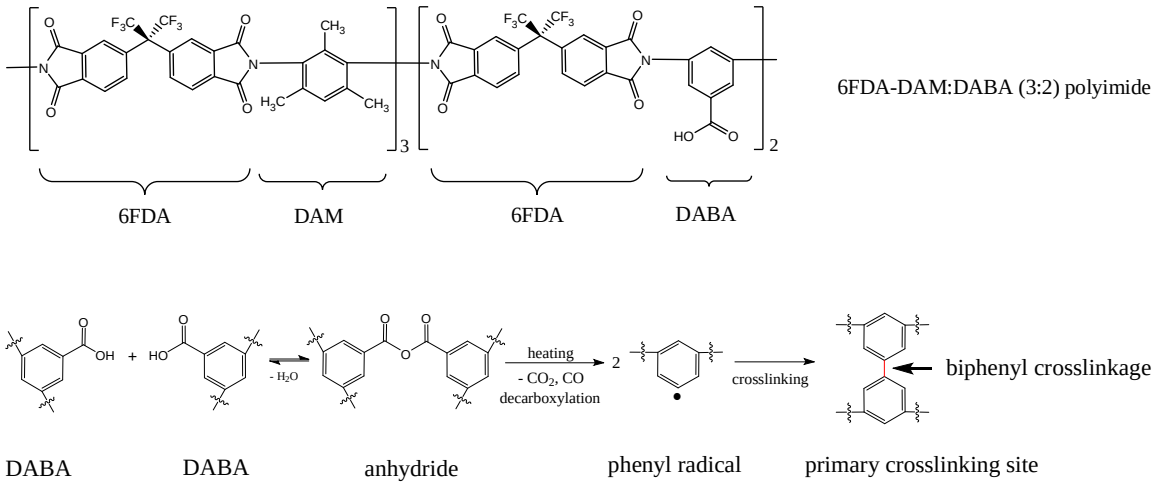

Figure 2.6: Chemical structure of 6FDA-DAM:DABA (3:2) and crosslinking mechanism of decarboxylation, radical induced crosslinking (DRIC) [33, 34]. Crosslinking bond is noted with an arrow.

2.3.2 Antiplasticization

Some low molecular weight penetrants, when incorporated into a polymer matrix at low percentages, appear to retard the segmental motion of the polymer chain, thereby decreasing the permeabilities of all penetrants. Evidence of this phenomenon includes increases in modulus and strength with losses in elongation at break and impact resistance [35, 36], which are the opposite to the effects of plasticization; therefore, this phenomenon is referred as antiplasticization and the penetrants are called antiplasticizers. The effects of antiplasticization on transport properties of polymeric membrane have been studied using a variety of polymers and antiplasticizers [35-44]. Antiplasticization leads to reduced permeabilities with complex effects on selectivities [35]. In some cases, increasing antiplasticizer concentration beyond certain level can result in increased permeabilities as antiplasticization was replaced by a plasticization response [44, 45].

2.3.3 Physical aging

Glassy polymers are not in a state of equilibrium and Figure 2.7 illustrates the non-equilibrium nature of glassy polymers in terms of a specific volume versus temperature relationship [2, 46]. Above the glass transition temperature (T_g), the polymer exists in an equilibrium state; however, as the polymer is cooled from a rubbery state, and passes through glass transition, long-range polymer chain movements become drastically hindered and form segmental microvoids. These microvoids—known as "excess free volume" or "unrelaxed volume" —are temporarily trapped in the polymer matrix. Below the glass transition temperature, the polymer densifies over extended time scales and approaches equilibrium packing by diffusing the excess free volume from the matrix.

This process is known as physical aging and can result in significant time-dependent membrane transport properties [12, 46-52]. During the aging process, permeabilities decrease and selectivities increase as the polymer matrix densifies.

The state of a glassy polymer and its corresponding aging behavior depend not only on the immediate environment but also on its previous history (such as process conditions, thermal history, exposure to sorbing species, etc.) [53]. Moreover, due to its partially diffusion-like mechanism, physical aging accelerates with increasing temperature and decreasing membrane thickness. Thin films have been shown to age much faster than thick films of the same materials [51, 52]. Since commercial applications usually utilize asymmetric membranes with thin selective layers, physical aging is an important topic of study.

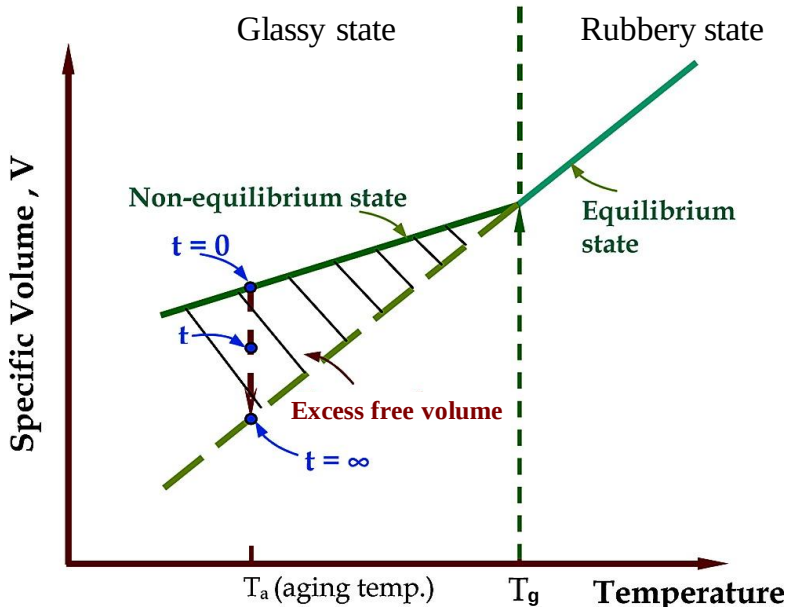

Figure 2.7: Schematic illustration of the volume relaxation (or physical aging) process of a glassy polymer. Adapted from Ref [46].

2.3.4 Conditioning

Conditioning is defined to be the hysteretic change in physical properties of glassy polymers following the initial exposure to high activities of a penetrant [16, 54-58]. Specifically, when the concentration of a strongly sorbing penetrant in the polymer reaches the point of physical swelling, the polymer chain configuration is altered to accommodate the sorbed penetrant. Once the penetrant is removed, the polymer may not immediately return to its original state and it is left in a swollen state with increased free volume. A membrane is considered to be "conditioned" and the extra free volume generated during conditioning causes an increase in sorption capacity and hysteresis in sorption and permeation analyses [55-58].

2.4 Asymmetric hollow fiber membranes

2.4.1 Formation of asymmetric hollow fiber membranes

In this research, asymmetric hollow fiber membranes were formed via a dry-jet/wet-quench spinning process illustrated in Figure 2.8 along with the key spinning variables in Table 2.2. Polymer solution (dope) and bore fluid were coextruded through a spinneret into the air gap ("dry-jet") and then into an aqueous quench bath ("wet-quench") where polymer solution solidifies due to a phase separation prior to being collected on a take-up drum. The qualitative dope composition trajectories during the skin layer and the substructure formation are shown in Figure 2.9. The dope composition should be in the one phase region and close to the binodal line to facilitate rapid phase separation in the quench bath. When the dope is extruded through the air gap, evaporation of the volatile solvent and non-solvent causes the composition of the outermost region to

approach the vitrified region. This composition pathway is believed to aid in skin formation [59-62]. When the fiber reaches the quench bath, water (non-solvent) diffuses into the nascent fiber and brings the composition of the underlying substrate into the two phase region where the dope phase separates and forms a porous substructure without causing vitrified skin layer defects. The bore of the hollow fiber is created by extruding a bore fluid along with the dope. The bore fluid is a neutral fluid which takes up space and prevents the nascent fiber from collapsing during spinning. In this way, dry-jet/wet-quench spinning results in the desirable asymmetric morphology, a dense selective skin layer with a porous substructure underneath.

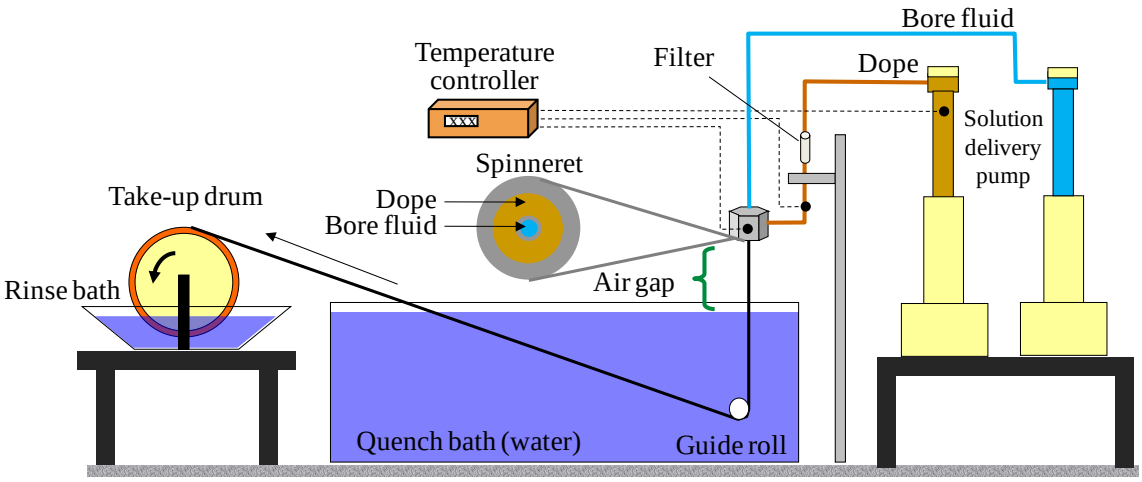

Figure 2.8: Dry-jet/wet-quench spinning process for producing asymmetric hollow fiber membranes.

Table 2.2: Key variables in dry-jet/wet-quench spinning process.

Dope composition	Air gap height	Spinneret temperature
Take-up rate	Quench bath temperature	Dope flow rate
Bore fluid composition	Quench bath composition	Humidity

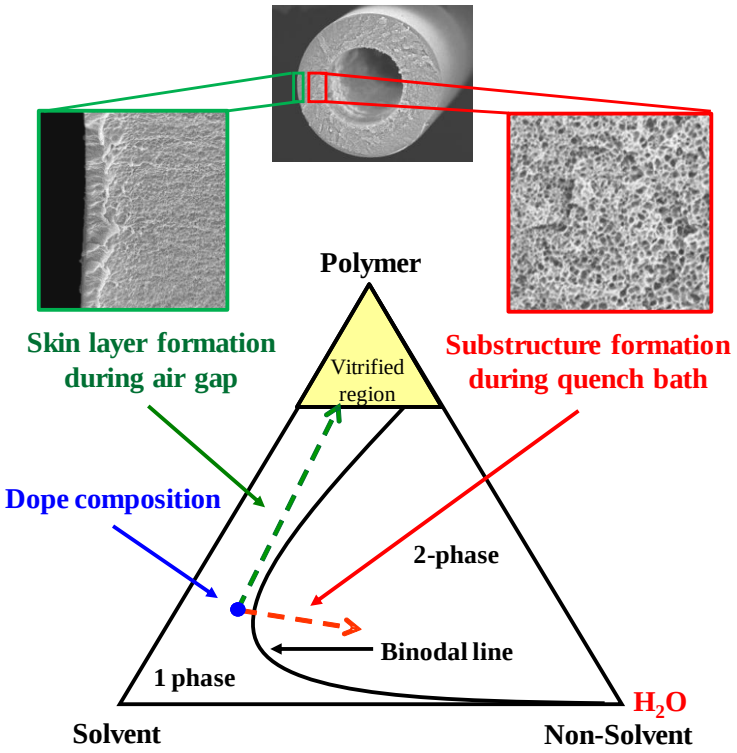

Figure 2.9: Ternary diagram showing the asymmetric membrane formation process.

2.4.2 Essential properties for aggressive applications

2.4.2.1 Skin integrity

Due to the complexity of membrane formation in spinning and the ultra-thin nature of a selective skin, most commercial membranes rely on post-treatment process to "caulk" defects and thus improve membrane selectivity. Even though post-treated membranes exhibit attractive selectivities and are efficient for some nonaggressive applications (such as air separation), defect-free membranes offer advantages in stability under aggressive feeds. Defect-free fiber membranes have better contaminant resistance as compared to defective fiber membranes made from similar materials [63]. Moreover,

the selectivity enhancement from post-treatment vanished with time when held at high pressure feed (20/80 CO_2/CH_4 mixture at 1000 psia) or exposed to toluene-contaminated feeds [20, 61]. Therefore, a *defect-free integral skin layer* is essential to robust performance of asymmetric hollow fiber membranes for aggressive applications.

2.4.2.2 Substructure porosity

The ideal substructure should have highly porous and interconnected pore structures that can support large pressure drops without imposing additional resistance to gas transport. If the substructure resistance (non-selective) cannot be neglected as compared to the skin layer resistance, it can reduce both permeance and selectivity due to the larger reduction in the fast gas permeance [64, 65]. The reduced selectivity due to substructure resistance has been observed in essentially defect-free asymmetric membranes [66-68]. Moreover, the effects of substructure resistance become much more pronounced for ultrathin asymmetric membranes made from advanced polymers which have high permeabilities and selectivities [65]. Simultaneous formation of defect-free thin skin layer and highly permeable substructure from these advanced polymers is challenging but must be achieved for practical applications.

2.4.2.3 Macroscopic properties

As mentioned earlier, hollow fiber modules provide very high volumetric productivity due to the ability to pack a huge membrane area into a single module. Smaller diameter fibers are favored since they allow more membrane area per module as shown in Table 2.3. Moreover, smaller diameter fibers can also withstand higher pressures. In practical gas separation applications, a general optimal fiber dimension is

~200 µm in outside diameter and ~100 µm in inside diameter [69]. Several non-ideal macroscopic morphologies can jeopardize the mechanical strength of the fiber and must be minimized for high pressure applications. Some examples include non-concentric bores, irregular bores, oval fibers and presence of macrovoids [69]. Examples of these undesirable macroscopic morphologies are shown in Figure 2.10. If the mechanical integrity is insufficient, macroscopic fiber failure can occur at high pressure as shown in Figure 2.11. In this research, fibers with the ability to withstand external feed pressure of at least 1000 psia are considered to have sufficient mechanical strength for high pressure CO_2/CH_4 separations.

Table 2.3: Effect of fiber outside diameter on membrane area in a module of 20 cm in diameter and 1 m long. 25% of the module volume is filled with fibers [70].

Fiber diameter (µm)	100	250	500
Number of fibers/module (thousands)	1000	250	40
Membrane area (m^2)	315	155	65
Membrane area to module volume ratio (m^2/m^3)	10000	5000	2000

(a) non-concentric bore

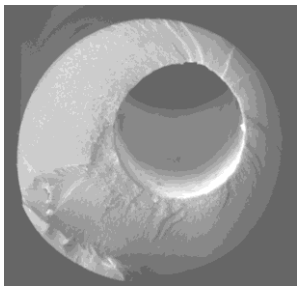

(b) irregular bore

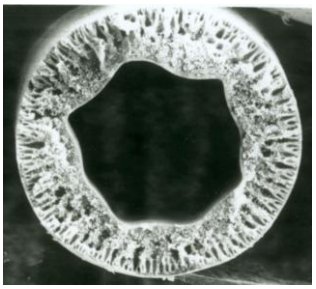

(c) oval

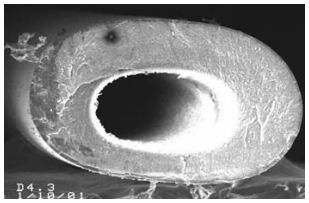

(d) macrovoids

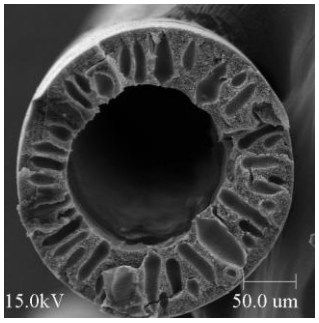

Figure 2.10: SEM images of fibers with undesirable macroscopic morphologies. (a) fiber with an non-concentric bore, (b) fiber with an irregular bore [71], (c) oval fiber [62], and (d) fiber with macrovoids [72].

(a) Fiber collapse

(b) Fiber burst

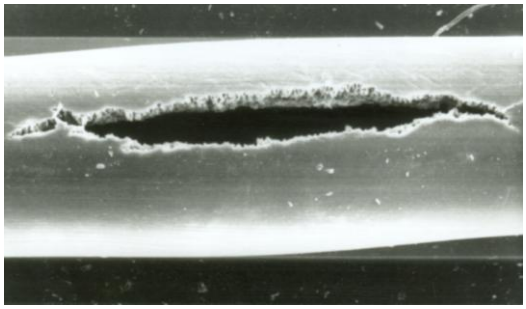

Figure 2.11: SEM images showing the fiber collapse due to (a) an external feed pressure difference of 500 psia, and (b) an internal feed pressure difference of 550 psia [71].

2.4.2.4 Additional challenges faced in asymmetric hollow fibers

As reviewed in section 2.3.1, many efforts have been devoted to stabilize membrane against membrane plasticization. Despite improved plasticization resistance, most works were conducted on thick dense films and has not yet been successfully extended to industrially relevant asymmetric hollow fibers. The delicate morphology of hollow fibers poses new challenges in these stabilization approaches faced in dense films. For instance, the aggressive conditions need to promote crosslinking can cause undesirable substructure resistance [19, 67] and destruction of skin layer integrity [62, 73]. These negative impacts on fiber morphology as well as separation performance must be minimized while still promoting sufficient crosslinking to stabilize membrane against plasticization.

In addition to key requirements of performance and durability, the membranes must be economically feasible for large scale production. The thermally crosslinkable polyimide used in this work can be spun into defect-free asymmetric hollow fibers at a commercial production rate (50 m/min) and subsequently stabilized by covalent crosslinking via thermal treatment. This post-spinning, solid-state thermal crosslinking is especially attractive for scale-up, because it allows the process to be easily integrated into current commercial membrane formation process, where crosslinking can take place during the drying step as shown Figure 2.12 [74].

.

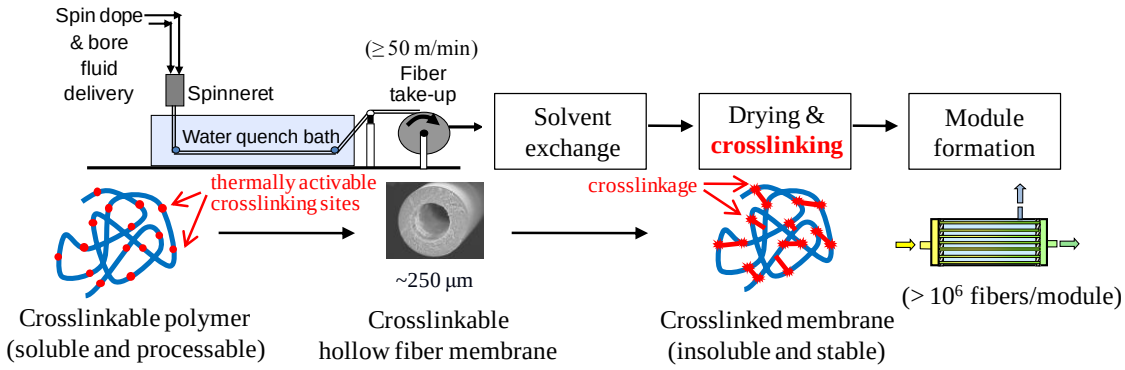

Figure 2.12: Schematic showing crosslinkable polymer can be fitted into current industrial process for manufacturing asymmetric hollow fiber membranes. Adapted from Ref. [74].

2.5 References

1. W.J. Koros and G.K. Fleming, *Membrane-based gas separation.* Journal of Membrane Science, 1993. **83**(1): p. 1-80.

2. K. Ghosal and B.D. Freeman, *Gas separation using polymer membranes: an overview.* Polymers for Advanced Technologies, 1994. **5**(11): p. 673-697.

3. S. Matteucci, Y. Yampolskii, B.D. Freeman, and I. Pinnau, *Transport of gases and vapors in glassy and rubbery polymers*, in *materials science of membranes for gas and vapor separation.* 2006, John Wiley & Sons, Ltd. p. 1-47.

4. L.M. Costello and W.J. Koros, *Effect of structure on the temperature dependence of gas transport and sorption in a series of polycarbonates.* Journal of Polymer Science Part B-Polymer Physics, 1994. **32**(4): p. 701-713.

5. A.F. Ismail and W. Lorna, *Penetrant-induced plasticization phenomenon in glassy polymers for gas separation membrane.* Separation and Purification Technology, 2002. **27**(3): p. 173-194.

6. E.S. Sanders, S.M. Jordan, and R. Subramanian, *Penetrant-plasticized permeation in polymethylmethacrylate.* Journal of Membrane Science, 1992. **74**(1-2): p. 29-36.

7. E.S. Sanders, *Penetrant-induced plasticization and gas permeation in glassy-polymers.* Journal of Membrane Science, 1988. **37**(1): p. 63-80.

8. A. Bos, I.G.M. Punt, M. Wessling, and H. Strathmann, *Plasticization-resistant glassy polyimide membranes for CO_2/CH_4 separations.* Separation and Purification Technology, 1998. **14**(1-3): p. 27-39.

9. C.A. Scholes, G.Q. Chen, G.W. Stevens, and S.E. Kentish, *Plasticization of ultra-thin polysulfone membranes by carbon dioxide.* Journal of Membrane Science, 2010. **346**(1): p. 208-214.

10. A. Bos, I.G.M. Punt, M. Wessling, and H. Strathmann, *CO_2-induced plasticization phenomena in glassy polymers.* Journal of Membrane Science, 1999. **155**(1): p. 67-78.

11. J.D. Wind, D.R. Paul, and W.J. Koros, *Natural gas permeation in polyimide membranes.* Journal of Membrane Science, 2004. **228**(2): p. 227-236.

12. J.H. Kim, W.J. Koros, and D.R. Paul, *Effects of CO_2 exposure and physical aging on the gas permeability of thin 6FDA-based polyimide membranes - Part 1. Without crosslinking.* Journal of Membrane Science, 2006. **282**(1-2): p. 21-31.

13. R.W. Baker and K. Lokhandwala, *Natural gas processing with membranes: An*

overview. Industrial & Engineering Chemistry Research, 2008. **47**(7): p. 2109-2121.

14. M.D. Donohue, B.S. Minhas, and S.Y. Lee, *Permeation behavior of carbon dioxide-methane mixtures in cellulose acetate membranes.* Journal of Membrane Science, 1989. **42**(3): p. 197-214.

15. M. Wessling, M.L. Lopez, and H. Strathmann, *Accelerated plasticization of thin-film composite membranes used in gas separation.* Separation and Purification Technology, 2001. **24**(1-2): p. 223-233.

16. N.R. Horn and D.R. Paul, *Carbon dioxide plasticization and conditioning effects in thick vs. thin glassy polymer films.* Polymer, 2011. **52**(7): p. 1619-1627.

17. Y. Liu, T.S. Chung, R. Wang, D.F. Li, and M.L. Chng, *Chemical cross-linking modification of polyimide/poly(ether sulfone) dual-layer hollow-fiber membranes for gas separation.* Industrial & Engineering Chemistry Research, 2003. **42**(6): p. 1190-1195.

18. I.C. Omole, S.J. Miller, and W.J. Koros, *Increased molecular weight of a cross-linkable polyimide for spinning plasticization resistant hollow fiber membranes.* Macromolecules, 2008. **41**(17): p. 6367-6375.

19. J.H. Ren, R. Wang, T.S. Chung, D.F. Li, and Y. Liu, *The effects of chemical modifications on morphology and performance of 6FDA-ODA/NDA hollow fiber membranes for CO2/CH4 separation.* Journal of Membrane Science, 2003. **222**(1-2): p. 133-147.

20. D.W. Wallace, J. Williams, C. Staudt-Bickel, and W.J. Koros, *Characterization of crosslinked hollow fiber membranes.* Polymer, 2006. **47**(4): p. 1207-1216.

21. G.C. Kapantaidakis, G.H. Koops, M. Wessling, S.P. Kaldis, and G.P. Sakellaropoulos, *CO_2 plasticization of polyethersulfone/polyimide gas-separation membranes.* AIChE Journal, 2003. **49**(7): p. 1702-1711.

22. X. Duthie, S. Kentish, S.J. Pas, A.J. Hill, C. Powell, K. Nagai, G. Stevens, and G. Qiao, *Thermal treatment of dense polyimide membranes.* Journal of Polymer Science Part B-Polymer Physics, 2008. **46**(18): p. 1879-1890.

23. A.F. Ismail and N. Yaacob, *Performance of treated and untreated asymmetric polysulfone hollow fiber membrane in series and cascade module configurations for CO_2/CH_4 gas separation system.* Journal of Membrane Science, 2006. **275**(1-2): p. 151-165.

24. A. Bos, I. Punt, H. Strathmann, and M. Wessling, *Suppression of gas separation membrane plasticization by homogeneous polymer blending.* AIChE Journal,

2001. **47**(5): p. 1088-1093.

25. X.J. Duthie, S.E. Kentish, C.E. Powell, G.G. Qiao, K. Nagai, and G.W. Stevens, *Plasticization suppression in grafted polyimide−epoxy network membranes.* Industrial & Engineering Chemistry Research, 2007. **46**(24): p. 8183-8192.

26. A. Bos, I.G.M. Punt, M. Wessling, and H. Strathmann, *Suppression of CO_2-plasticization by semiinterpenetrating polymer network formation.* Journal of Polymer Science Part B-Polymer Physics, 1998. **36**(9): p. 1547-1556.

27. A.M.W. Hillock and W.J. Koros, *Cross-linkable polyimide membrane for natural gas purification and carbon dioxide plasticization reduction.* Macromolecules, 2007. **40**(3): p. 583-587.

28. J.D. Wind, C. Staudt-Bickel, D.R. Paul, and W.J. Koros, *Solid-state covalent cross-linking of polyimide membranes for carbon dioxide plasticization reduction.* Macromolecules, 2003. **36**(6): p. 1882-1888.

29. C. Staudt-Bickel and W.J. Koros, *Improvement of CO_2/CH_4 separation characteristics of polyimides by chemical crosslinking.* Journal of Membrane Science, 1999. **155**(1): p. 145-154.

30. J.D. Wind, C. Staudt-Bickel, D.R. Paul, and W.J. Koros, *The effects of crosslinking chemistry on CO_2 plasticization of polyimide gas separation membranes.* Industrial & Engineering Chemistry Research, 2002. **41**(24): p. 6139-6148.

31. L. Hu, X. Xu, and M.R. Coleman, *Impact of H^+ ion beam irradiation on Matrimid® . II. Evolution in gas transport properties.* Journal of Applied Polymer Science, 2007. **103**(3): p. 1670-1680.

32. M.S. McCaig and D.R. Paul, *Effect of UV crosslinking and physical aging on the gas permeability of thin glassy polyarylate films.* Polymer, 1999. **40**(26): p. 7209-7225.

33. A.M. Kratochvil and W.J. Koros, *Decarboxylation-induced cross-linking of a polyimide for enhanced CO_2 plasticization resistance.* Macromolecules, 2008. **41**(21): p. 7920-7927.

34. W.L. Qiu, C.C. Chen, L. Xu, L. Cui, D.R. Paul, and W.J. Koros, *Sub-T_g cross-linking of a polyimide membrane for enhanced CO_2 plasticization resistance for natural gas separation.* Macromolecules, 2011. **44**(15): p. 6046-6056.

35. Y. Maeda and D.R. Paul, *Effect of antiplasticization on selectivity and productivity of gas separation membranes.* Journal of Membrane Science, 1987. **30**(1): p. 1-9.

36. N.M. Larocca and L.A. Pessan, *Effect of antiplasticisation on the volumetric, gas sorption and transport properties of polyetherimide.* Journal of Membrane Science, 2003. **218**(1-2): p. 69-92.

37. Y. Maeda and D.R. Paul, *Effect of antiplasticization on gas sorption and transport .1. Polysulfone.* Journal of Polymer Science Part B-Polymer Physics, 1987. **25**(5): p. 957-980.

38. Y. Maeda and D.R. Paul, *Effect of antiplasticization on gas sorption and transport. 2. Poly(phenylene oxide).* Journal of Polymer Science Part B-Polymer Physics, 1987. **25**(5): p. 981-1003.

39. Y. Maeda and D.R. Paul, *Effect of antiplasticization on gas sorption and transport. 3. Free-volume interpretation.* Journal of Polymer Science Part B-Polymer Physics, 1987. **25**(5): p. 1005-1016.

40. F.A. Ruiz-Trevino and D.R. Paul, *Gas permselectivity properties of high free volume polymers modified by a low molecular weight additive.* Journal of Applied Polymer Science, 1998. **68**(3): p. 403-415.

41. A. Garcia, M. Iriarte, C. Uriarte, and A. Etxeberria, *Study of the relationship between transport properties and free volume based in polyamide blends.* Journal of Membrane Science, 2006. **284**(1-2): p. 173-179.

42. S.E. Vidotti, A.C. Chinellato, G.H. Hu, and L.A. Pessan, *Effects of low molar mass additives on the molecular mobility and transport properties of polysulfone.* Journal of Applied Polymer Science, 2006. **101**(2): p. 825-832.

43. C. García, M. López-González, J. de Abajo, L. Garrido, and J. Guzmán, *Effects of tricresylphosphate on gas transport coefficients in Matrimid and 6FDA-TMPD polyimides.* Macromolecules, 2011. **44**(10): p. 3862-3873.

44. J.S. Lee, W. Madden, and W.J. Koros, *Antiplasticization and plasticization of Matrimid® asymmetric hollow fiber membranes-Part A. Experimental.* Journal of Membrane Science, 2010. **350**(1-2): p. 232-241.

45. J.S. Lee, W. Madden, and W.J. Koros, *Antiplasticization and plasticization of Matrimid® asymmetric hollow fiber membranes. Part B. Modeling.* Journal of Membrane Science, 2010. **350**(1-2): p. 242-251.

46. Y. Huang and D.R. Paul, *Effect of film thickness on the gas-permeation characteristics of glassy polymer membranes.* Industrial & Engineering Chemistry Research, 2007. **46**(8): p. 2342-2347.

47. L. Cui, W. Qiu, D.R. Paul, and W.J. Koros, *Physical aging of 6FDA-based*

polyimide membranes monitored by gas permeability. Polymer, 2011. **52**(15): p. 3374-3380.

48. J.H. Kim, W.J. Koros, and D.R. Paul, *Effects of CO_2 exposure and physical aging on the gas permeability of thin 6FDA-based polyimide membranes - Part 2. With crosslinking.* Journal of Membrane Science, 2006. **282**(1-2): p. 32-43.

49. D. Punsalan and W.J. Koros, *Thickness-dependent sorption and effects of physical aging in a polyimide sample.* Journal of Applied Polymer Science, 2005. **96**(4): p. 1115-1121.

50. Y. Huang and D.R. Paul, *Effect of temperature on physical aging of thin glassy polymer films.* Macromolecules, 2005. **38**(24): p. 10148-10154.

51. Y. Huang and D.R. Paul, *Physical aging of thin glassy polymer films monitored by gas permeability.* Polymer, 2004. **45**(25): p. 8377-8393.

52. P.H. Pfromm and W.J. Koros, *Accelerated physical aging of thin glassy polymer-films - evidence from gas-transport measurements.* Polymer, 1995. **36**(12): p. 2379-2387.

53. B.W. Rowe, B.D. Freeman, and D.R. Paul, *Influence of previous history on physical aging in thin glassy polymer films as gas separation membranes.* Polymer, 2010. **51**(16): p. 3784-3792.

54. M.R. Coleman and W.J. Koros, *Conditioning of fluorine containing polyimides. 1. Effect of exposure to high pressure carbon dioxide on permeability.* Macromolecules, 1997. **30**(22): p. 6899-6905.

55. G.K. Fleming and W.J. Koros, *Carbon dioxide conditioning effects on sorption and volume dilation behavior for bisphenol A-polycarbonate.* Macromolecules, 1990. **23**(5): p. 1353-1360.

56. S.M. Jordan, W.J. Koros, and G.K. Fleming, *The effects of CO_2 exposure on pure and mixed gas permeation behavior - comparison of glassy polycarbonate and silicone-rubber.* Journal of Membrane Science, 1987. **30**(2): p. 191-212.

57. A.M. Kratochvil and W.J. Koros, *Effects of supercritical CO_2 conditioning on cross-linked polyimide membranes.* Macromolecules, 2010. **43**(10): p. 4679-4687.

58. M.R. Coleman and W.J. Koros, *Conditioning of fluorine-containing polyimides. 2. Effect of conditioning protocol at 8% volume dilation on gas-transport properties.* Macromolecules, 1999. **32**(9): p. 3106-3113.

59. D.T. Clausi and W.J. Koros, *Formation of defect-free polyimide hollow fiber membranes for gas separations.* Journal of Membrane Science, 2000. **167**(1): p.

79-89.

60. S.B. Carruthers. *Integral-skin formation in hollow fiber membranes for gas separations* Ph.D. Dissertation, The University of Texas at Austin, Austin, TX, 2001.

61. I.C. Omole. *Crosslinked polyimide hollow fiber membranes for aggressive natural gas feed streams.* Ph.D. Dissertation, Georgia Institute of Technology, Atlanta, GA, 2008.

62. D.W. Wallace. *Crosslinked hollow fiber membranes for natural gas purification and their manufacture from novel polymers.* Ph.D. Dissertation, The University of Texas at Austin, Austin, TX, 2004.

63. M. Al-Juaied and W.J. Koros, *Performance of natural gas membranes in the presence of heavy hydrocarbons.* Journal of Membrane Science, 2006. **274**(1-2): p. 227-243.

64. D.T. Clausi, S.A. McKelvey, and W.J. Koros, *Characterization of substructure resistance in asymmetric gas separation membranes.* Journal of Membrane Science, 1999. **160**(1): p. 51-64.

65. I. Pinnau and W.J. Koros, *Relationship between substructure resistance and gas separation properties of defect-free integrally skinned asymmetric membranes.* Industrial & Engineering Chemistry Research, 1991. **30**(8): p. 1837-1840.

66. M.R. Kosuri and W.J. Koros, *Defect-free asymmetric hollow fiber membranes from Torlon®, a polyamide-imide polymer, for high-pressure CO_2 separations.* Journal of Membrane Science, 2008. **320**(1-2): p. 65-72.

67. Y. Li, C. Cao, T.S. Chung, and K.P. Pramoda, *Fabrication of dual-layer polyethersulfone (PES) hollow fiber membranes with an ultrathin dense-selective layer for gas separation.* Journal of Membrane Science, 2004. **245**(1-2): p. 53-60.

68. I. Pinnau and W.J. Koros, *Influence of quench medium on the structures and gas permeation properties of polysulfone membranes made by wet and dry wet phase inversion.* Journal of Membrane Science, 1992. **71**(1-2): p. 81-96.

69. S.A. McKelvey, D.T. Clausi, and W.J. Koros, *A guide to establishing hollow fiber macroscopic properties for membrane applications.* Journal of Membrane Science, 1997. **124**(2): p. 223-232.

70. R.W. Baker, *Membrane technology and applications.* Second ed.; Wiley: 2004.

71. S.A. McKelvey. *Formation and characterization of hollow fiber membranes for gas separation.* Ph.D. Dissertation, The University of Texas at Austin, Austin, TX,

1997.

72. S. Husain. *Formation of non-crosslinked asymmetric hollow fiber mixed matrix polymer/molecular sieve membranes.* Ph.D. Dissertation, Georgia Institute of Technology, Atlanta, GA, 2006.

73. C.C. Chen, S.J. Miller, and W.J. Koros, *Plasticization-resistant hollow fiber membranes for CO_2/CH_4 separation based on a thermally crosslinkable polyimide.* Journal of Membrane Science, 2011. **382(1-2):** p.212-221.

74. W.J. Koros and R. Mahajan, *Pushing the limits on possibilities for large scale gas separation: which strategies?* Journal of Membrane Science, 2000. **175**(2): p. 181-196.

CHAPTER 3

MATERIALS AND EXPERIMENTAL METHODS

3.1 Overview

This chapter contains a description of the materials and experimental methods. Section 3.2 describes the polymer synthesis procedure and gases used for membrane formation and characterization. Section 3.3 discusses the procedures for formation of asymmetric hollow fiber membranes and thermal crosslinking of membranes. Section 3.4 outlines characterization techniques and equipment.

3.2 Materials

3.2.1 Polymer synthesis

The polymer selected for this study is a thermally crosslinkable polyimide, 6FDA-DAM:DABA (3:2). The polymer was synthesized by a two-step polycondensation reaction. The first step produces a high molecular weight polyamic acid via the reaction of stoichiometric amounts of the dianhydride, 4,4'-(hexafluoroisopropylidene)diphthalic anhydride (6FDA), and diamines, 2,4,6-trimethyl-1,3-diaminobenzene (DAM) and 3,5-diaminobenzoic acid (DABA), in 1-methyl-2-pyrrolidinone (NMP) at low temperature (~5 ℃). The second step closes the imide ring via chemical imidization with beta-picolin and acetic anhydride. The reaction scheme is shown in Figure 3.1. The resulting polyimide was precipitated and washed with methanol, and then air-dried in the fume hood for 1~2 days before dried in the vacuum oven at 210 ℃ for 24 h. The detailed

synthesis procedure can be found in Appendix A.

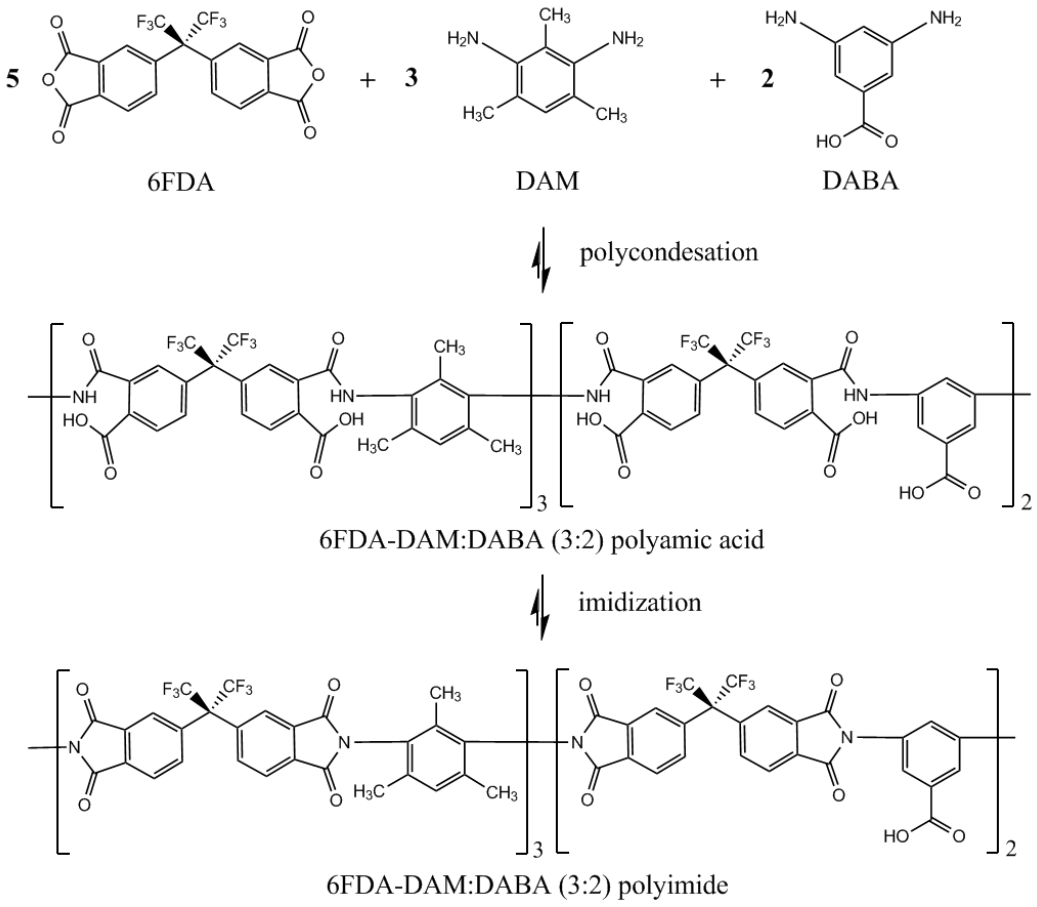

Figure 3.1: Reaction scheme for 6FDA-DAM:DABA (3:2) synthesis.

3.2.2 Gases

All pure gases (He, O_2, N_2, CH_4, CO_2, Ar) used were of purity greater than 99.999% and purchased from Airgas. Gas mixtures were provided by either Airgas or Praxair.

3.3 Membrane preparation

3.3.1 Dope formulation and cloud point experiment

The dope typically consists of the polymer, solvents, and non-solvents. NMP (N-methylpyrrolidone) was chosen as the non-volatile solvent because it is relatively environmentally benign. THF (tetrahydrofuran) is chosen as the volatile solvent to facilitate the skin formulation because of its high volatility [1, 2]. Ethanol (EtOH) was selected as the non-solvent, because it provides a greater compositional window for dope formulation than water, which has an excessive non-solvent power [2, 3]. Lithium nitrate ($LiNO_3$) was added to enhance phase separation [3].

Ternary phase diagram was constructed using the cloud point technique. A series of dope samples of fixed polymer content with increasing ethanol (non-solvent) content were made. The one-phase dopes are clear while the two-phase dopes are cloudy. The binodal point is the composition where phase separation occurs. By repeating this procedure for different polymer contents, the binodal line was determined.

3.3.2 Syringe tests

Syringe tests can be used as a screening tool to identify potential dope formulation and spinning conditions by simulating fiber spinning process [4]. Dopes were

loaded into disposable syringes, and heated up to "spinning temperature", and then were extruded through an air gap and into a water quench bath. After dehydration, the morphology of these solid fibers was carefully examined by scanning electron microscope (SEM).

3.3.3 Formation of asymmetric hollow fiber membranes

Asymmetric hollow fiber membranes were formed via a dry-jet/wet-quench spinning process [1, 5], which is described in section 2.4.1. The spin dopes were made in Qorpak® glass bottle sealed with Teflon® cap liners, and dissolved on a roller under a heat lamp (~50 ℃). Once the dope was homogenous, it was cooled down at room temperature before being transferred into a 500-mL Isco syringe pump and allowed to degas for ~24 hr at 50 ℃. A bore fluid mixture of 80/20 NMP/water was loaded into a 100-mL Isco syringe pump. The dope and bore fluid were filtered in-line between the Isco delivery pumps and the spinneret with 60 μm and 2 μm sintered metal filters, respectively. Two thermocouples were attached to the dope delivery pump and the spinneret, and one was immersed in the dope stream prior to the filter block. The spinning was carried out at 70 ℃ by heating the dope delivery pump, tubing, dope filter and spinneret using multiple heating tapes controlled by temperature controllers. The dope and bore fluid were co-extruded through an adjustable air gap into the water quench bath (height = 1 m) at ~50 ℃, passed over a Teflon guide in the quench bath and collected on a polyethylene rotating take-up drum (diameter = 0.32 m). The take-up drum was partially immersed in a separate water bath at room temperature. Once cut off from the take-up drum, the fibers were soaked sequentially in at least four separate water baths for 3~4 days to remove the last traces of solvent, and then solvent exchanged with

sequential 1 hr baths of ethanol and hexane. After air-drying in the fume hood for 1 hr, the fibers were dried in the vacuum oven at 75~85 ℃ for ~3 hr.

3.3.4 Thermal treatment

Thermal treatment was carried out with a controlled thermal treatment protocol under a continuous gas purge at 200 mL/min. A three-zone tube furnace ((Thermcraft, Inc., model XST-3-0-24-3C) was outfitted with a multi-channel PID temperature controller (Omega Engineering, Inc., model CN1507TC) to achieve uniform temperature profile inside the quartz tube (55 mm ID x 59 mm OD, National Scientific Company, GE Type 214 quartz tubing). The tube is sealed with a metal flange with two silicon O-rings (MTI Corporation, model EQ-FI-60) on the both ends. Fibers were placed on an aluminum sheet supported by a stainless steel perforated plate (as shown in Figure 3.2). The thermal treatment protocol (as shown in Figure 3.3) is: (1) heating at 10 ℃/min to temperature 50 ℃ below the final temperature, (2) heating to the final temperature at a rate of 1 ℃/min, (3) isothermal soaking at the final temperature for a given period of time. Thermal treated fibers were unloaded after the furnace was cooled down naturally to room temperature.

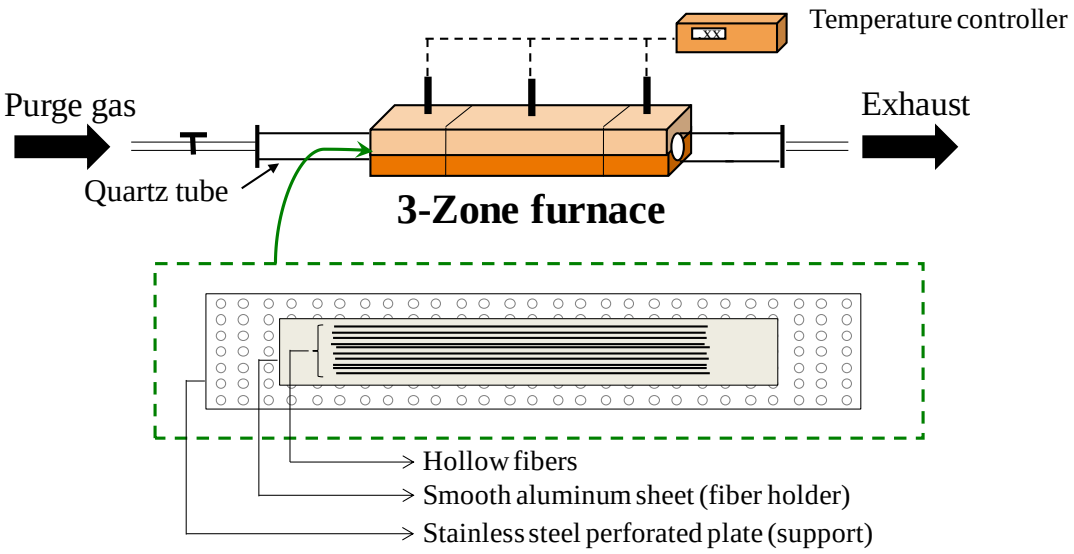

Figure 3.2: Schematic showing the experimental setup for fiber thermal treatment.

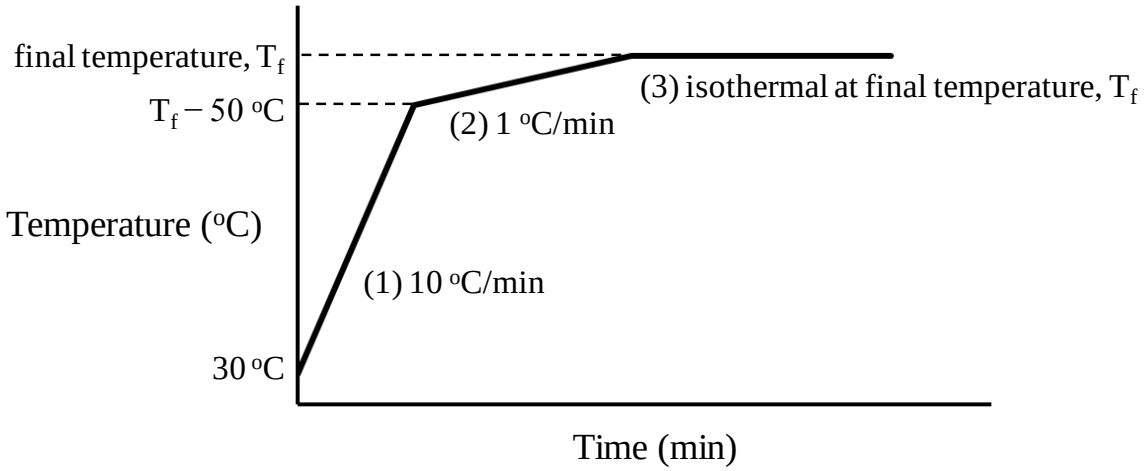

Figure 3.3: Thermal treatment protocol.

3.4 Characterization techniques

3.4.1 Pure gas permeation

Hollow fibers were potted into laboratory-scale modules as shown in Figure 3.4. The detailed module making procedure can be found elsewhere [6, 7]. For pure gas permeation experiment, a typical module contained 4~10 fibers with active membrane length of 18~20 cm. Pure gas permeation measurements were conducted in a temperature-controlled box using a bore side feed at 100 psig. The permeate flow rate was measured from the shell side with a bubble flowmeter at atmospheric pressure. The schematic of the set-up is shown in Figure 3.5. This configuration allows multiple fiber modules to be tested with a common feed at the same time by measuring the permeate flow rate of each module. The permeance can be calculated using the following equation

$$\frac{P_i}{l} = 10^{-6} \cdot \frac{Q_p \cdot 273.15}{A \cdot T \cdot \Delta p \cdot 5.17} \tag{3.1}$$

where Q_p is the permeate flow rate in mL/sec, A is the active membrane area in cm^2, T is the room temperature in Kelvin, Δp is the transmembrane pressure difference in psia. The calculated permeance is in "Gas Permeation Units" (GPU) defined as

$$1\,GPU = 1 \times 10^{-6} \frac{cm^3(STP)}{cm^2 \cdot s \cdot cmHg} \tag{3.2}$$

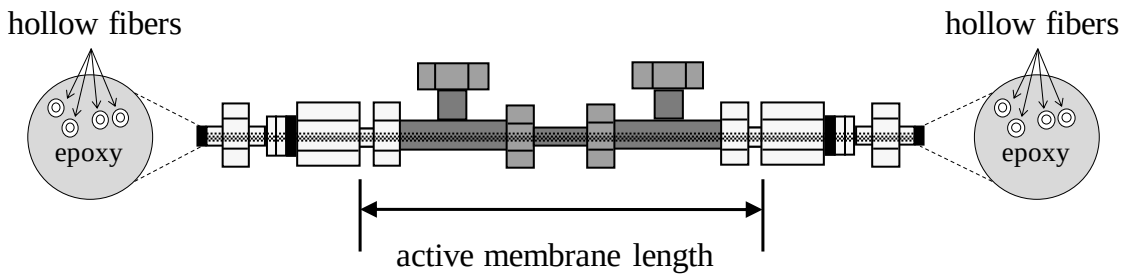

Figure 3.4: Schematic of laboratory-scale hollow fiber membrane module.

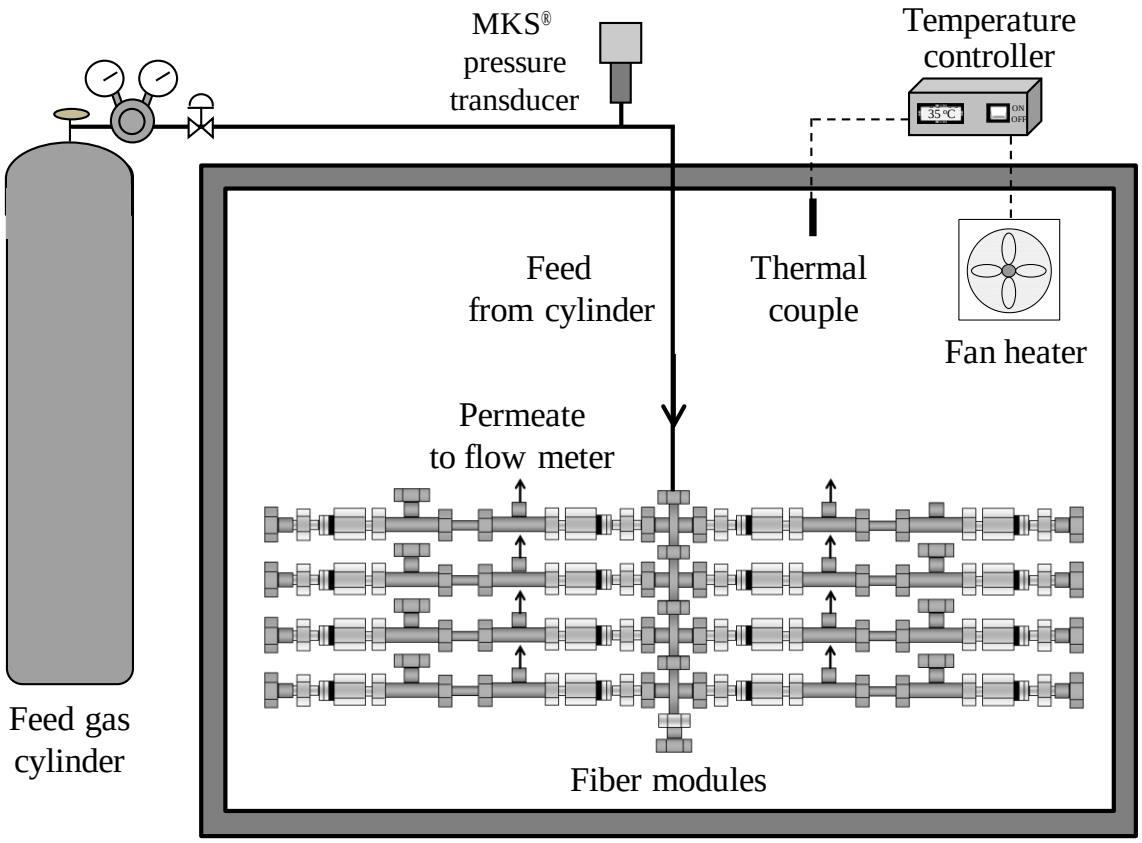

Figure 3.5: Schematic of a constant pressure testing system for pure gas permeation measurements. Permeate flow rate is measured from the shell side using a bubble flowmeter at atmospheric pressure.

3.4.2 Mixed gas permeation

Mixed gas permeation measurements were carried out using a shell side feed as shown in Figure 3.6. The permeate flow rate was measured from the bore side with a bubble flowmeter at atmospheric pressure (unless noted otherwise). The stage cut (permeate flow/feed flow) was maintained below 1% to minimize the feed composition variation as the membrane selectively permeates the gases along the module. The number (1~4) and active membrane length (12~18 cm) of fibers in a module depends on testing conditions (feed composition and pressure) and fiber properties. For instance, when testing highly permeable fiber with a high content of fast gas (such as 70/30 CO_2/CH_4 mixture) at high pressure (800-1000 psia), a single fiber module with active length of ~12 cm is used to reduce the membrane area and thus the flow rate of vented retentate stream needed to maintain low stage cuts. The compositions of feed, retentate, and permeate were analyzed 3~5 times by gas chromatography. The permeance in the unit of GPU can be calculated using the following equation

$$\frac{P_i}{l} = 10^{-6} \cdot \frac{Q_p \cdot y_i \cdot 273.15}{A \cdot T \cdot (p_x \cdot x_i \cdot \varphi_{x,i} - p_y \cdot y_i \cdot \varphi_{y,i}) \cdot 5.17} \qquad (3.3)$$

where Q_p is the permeate flow rate in mL/sec, A is the active membrane area in cm^2, T is the temperature in Kelvin, p_x and p_y are the feed and permeate pressures in psia respectively, x_i and y_i are the mole fraction of component i in the upstream and permeate respectively, $\varphi_{x,i}$ and $\varphi_{x,i}$ are fugacity coefficients of component i in the upstream and permeate respectively. The fugacity coefficients of CO_2 and CH_4 in the binary mixtures were estimated from the virial equation of state truncated after the second coefficient [8].

Upstream mole fraction (x_i) uses log-mean average of mole fractions of *i* in the feed and retentate, which are essentially the same at low stage cut.

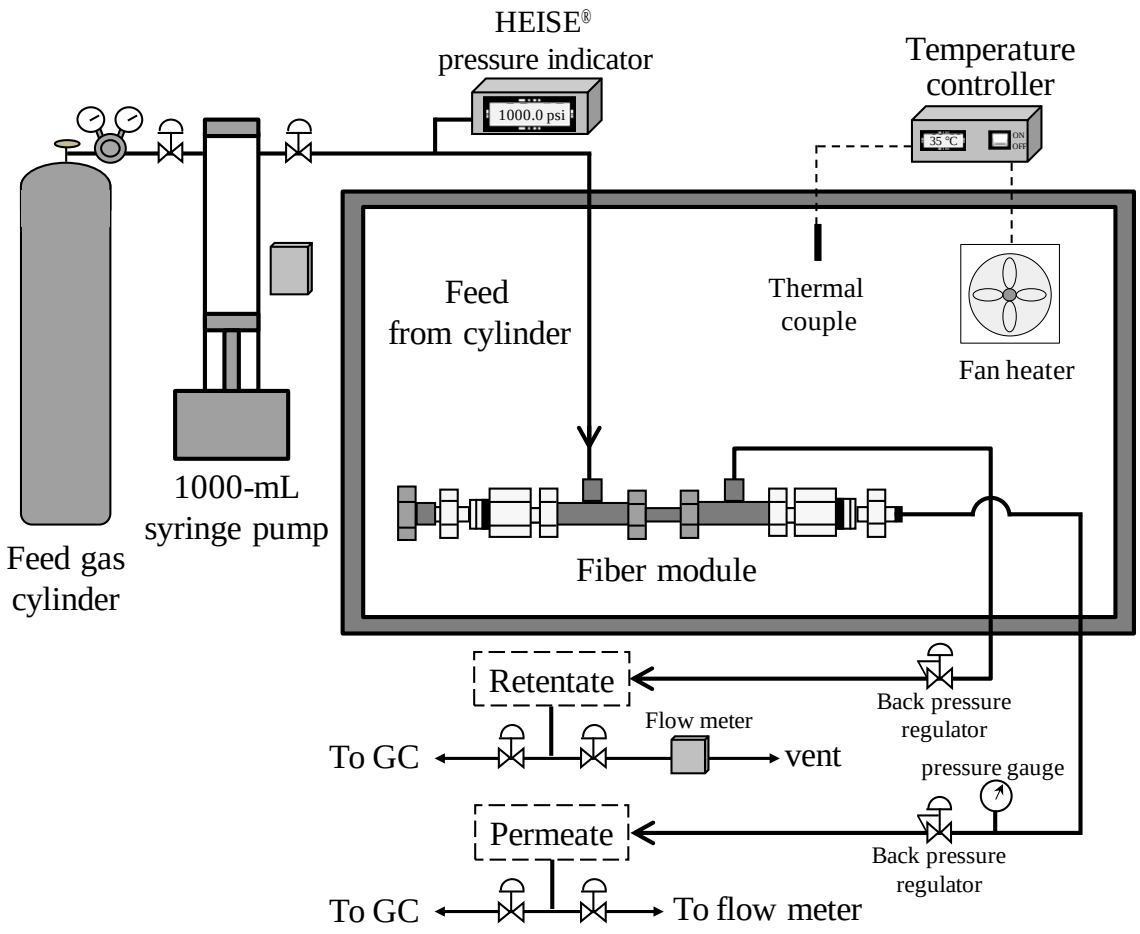

Figure 3.6: Schematic of a constant pressure testing system for mixed gas permeation measurements. Permeate flow rate is measured from the bore side using a bubble flowmeter at atmospheric pressure.

3.4.3 Dissolution tests

Dissolution tests serve as a quick method for determining the existence of crosslinking. NMP is a strong solvent for the uncrosslinked polymer and its high boiling point (204 ℃) allows dissolution tests at elevated temperature. The solubility was determined visually by soaking fibers in vials of NMP at a given temperature and time.

3.4.4 Scanning electron microscopy (SEM)

The geometry and morphology of pristine and thermally treated fiber membranes were examined using a high resolution scanning electron microscope (Leo 1530, Leo Electron Microscopy). The fibers were soaked in hexane and then shear fractured in liquid nitrogen to preserve fiber morphology. The fiber samples were mounted on a SEM mount and sputter-coated with gold before being examined.

3.4.5 Polymer characterization

3.4.5.1 Gel permeation chromatography (GPC)

Molecular weight (Mw) and polydispersity (PDI) of polymer samples from various batched were analyzed using gel permeation chromatography (GPC) by American Polymer Standards Corporation (Mentor, OH). The samples were dissolved in THF at 1 mg/mL concentration. Polystyrene standards are used to calibrate the GPC.

3.4.5.2 Differential scanning calorimetry (DSC)

Glass transition temperature of polymers was analyzed using a differential scanning calorimeter (Q200, TA Instruments). The measurement was carried out using a

standard heating-cooling-heating procedure at heating/cooling rates of 10 K/min in nitrogen atmosphere. The sample was heated beyond its expected glass transition temperature but below its decomposition temperature determined from TGA. The glass transition temperature was determined as the inflection point of the change in the heat flow during the second heating cycle.

3.4.5.3 Thermal gravimetric analysis (TGA)

Thermogravimetric analysis (TGA) was conducted on a thermogravimetric analyzer (Q5000, TA Instruments) at a heating rate of 10 K/min under nitrogen atmosphere.

3.4.5.4 Thermal gravimetric analysis-mass spectrometry (TGA-MS)

TGA-MS was performed in a thermogravimetric analyzer (Q500, TA Instruments) coupled to a mass spectrometer (ThermoStar, Pfeiffer Vacuum) at a heating rate of 10 K/min under nitrogen atmosphere.

3.5 References

1. S.B. Carruthers, G.L. Ramos, and W.J. Koros, *Morphology of integral-skin layers in hollow-fiber gas-separation membranes.* Journal of Applied Polymer Science, 2003. **90**(2): p. 399-411.

2. D.T. Clausi and W.J. Koros, *Formation of defect-free polyimide hollow fiber membranes for gas separations.* Journal of Membrane Science, 2000. **167**(1): p. 79-89.

3. D.W. Wallace, C. Staudt-Bickel, and W.J. Koros, *Efficient development of effective hollow fiber membranes for gas separations from novel polymers.* Journal of Membrane Science, 2006. **278**(1-2): p. 92-104.

4. S.B. Carruthers. *Integral-skin formation in hollow fiber membranes for gas separations* Ph.D. Dissertation, The University of Texas at Austin, Austin, TX, 2001.

5. S.C. Pesek and W.J. Koros, *Aqueous quenched asymmetric polysulfone hollow fibers prepared by dry wet phase-separation.* Journal of Membrane Science, 1994. **88**(1): p. 1-19.

6. D.Q. Vu, W.J. Koros, and S.J. Miller, *High pressure CO_2/CH_4 separation using carbon molecular sieve hollow fiber membranes.* Industrial & Engineering Chemistry Research, 2002. **41**(3): p. 367-380.

7. D.W. Wallace. *Crosslinked hollow fiber membranes for natural gas purification and their manufacture from novel polymers.* Ph.D. Dissertation, The University of Texas at Austin, Austin, TX, 2004.

8. D.Q. Vu. *Formation and characterization of asymmetric carbon molecular sieve and mixed matrix membranes for natural gas purification.* The University of Texas at Austin, Austin, TX, 2001.

CHAPTER 4

SPINNING DEFECT-FREE ASYMMETRIC HOLLOW FIBER MEMBRANES FROM A NOVEL CROSSLINKABLE POLYIMIDE

4.1 Overview

In Chapter 1, the case was made for the need of robust polymeric membranes—especially in industrially relevant asymmetric hollow fiber form—for natural gas purification. Chapter 2 and 3 follow up with essential background related to gas transport in polymeric membranes, the challenge and potential solution for aggressive stream applications, and the specifics of asymmetric hollow fiber formation and characterization. The first challenge of this research is to produce crosslinkable defect-free asymmetric hollow fiber membranes from a novel polymer. In this chapter, the details of developing such fiber membranes are described. The analyses of fiber structure and transport properties are discussed. The defect-free hollow fibers developed in this chapter will be used for subsequent thermal crosslinking study described in Chapter 5.

4.2 First attempt spinning

4.2.1 Polymer properties

Four separate batches of the crosslinkable polyimide, 6FDA-DAM:DABA (3:2), were used during the course of this research. It has been shown that high molecular weight polymer (yet still processable) is an essential property for fiber spinning using PDMC polyimide, which is esterified counterpart of 6FDA-DAM:DABA (3:2) [1, 2]. It

is believe that increasing polymer molecular weight can enhance spinnability [2] and the ability to form defect-free skin layers [3]. The molecular weights and polydispersity indices of polymer batches used for each spinning are given in Table 4.1. All polymer batches have a high molecular weight (> 100 kDa) and thus good spinnability, which allows spinning speeds greater than 50 m/min.

Table 4.1: Characteristics of polymers used for fiber spinning.

Batch #	Polymer name	Mw (kDa)	PDI (Mw/Mn)	Used for
1	6FDA-DAM:DABA (3:2)	105	4.3	1st spinning
2	6FDA-DAM:DABA (3:2)	102	4.0	2nd spinning
3	6FDA-DAM:DABA (3:2)	200	4.7	3rd spinning
4	6FDA-DAM:DABA (3:2)	229	4.2	4th spinning

4.2.2 Exploration of potential dope formulation and spinning conditions

In this research, 6FDA-DAM:DABA (3:2) will be crosslinked by thermal treatment (below T_g of the polymer, ~390 ℃) after essentially defect-free asymmetric hollow fiber membrane formation is achieved. Forming such fibers from the more hydrophilic carboxylic acid polymer to avoid defect development and substructure collapse during thermal treatment is important. Moreover, it is highly desirable to produce asymmetric hollow fibers with defect-free selective skin layers on an optimized

porous support substructure to provide a final robust defect-free crosslinked membrane. 6FDA-DAM:DABA is itself a challenge, since phase separation in the aqueous quench bath is suppressed due to carboxylic acid groups. Wallace [4] showed that the binodals of DABA containing polyimide are shifted toward non-solvent compared to Matrimid®, a commercial polyimide widely used for gas separations as shown in Figure 4.1. The less hydrophobic nature of the polymer increases phase separation time during spinning. Inadequate phase separation during spinning may lead to oval, crushed or even unspinnable fibers. Initial dope composition and spinning conditions are guided by the work of Wallace [4] and Omole [1] on esterified 6FDA-DAM:DABA (3:2) or PDMC which has similar chemical structure.

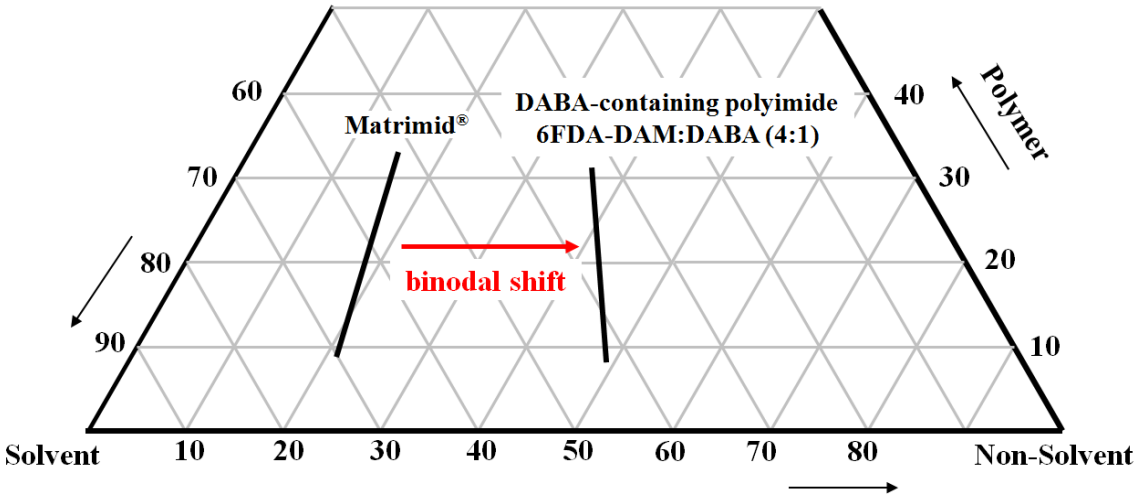

Figure 4.1: Binodals of 6FDA-DAM:DABA (4:1) and Matrimid® [4].

The first step in fiber spinning is dope formulation. The binodals were determined by presetting (1) volatile solvent THF at 15 wt% to aid skin formation during air gap and (2) lithium nitrate ($LiNO_3$) at 6.5 wt% to accelerate phase separation during quenching, and adjusting NMP and ethanol concentration. As expected, binodals of 6FDA-DAM:DABA (3:2) shift toward non-solvent compared to conventional polyimides used for hollow fiber gas separation membranes, i.e. 6FDA-DAM:DABA (3:2) is less hydrophobic than conventional polyimides. To the best of our knowledge, no defect-free hollow fibers have been spun previously from this polymer. In initial dope formulation, 30-35 wt% polymer was chosen since higher polymer concentration is preferable to promote skin formation. Syringes tests were conducted to simulate fiber spinning. The results showed: (1) dope made of 30 wt% polymer has acceptable viscosity while dope made of 35 wt% polymer is so viscous that it would be difficult to process during spinning; (2) warm quench bath (41 ℃) helps phase separation and thereby forms a more porous substructure as shown in Figure 4.2. Based on the above results, the initial dope formulation and water quench temperature was determined.

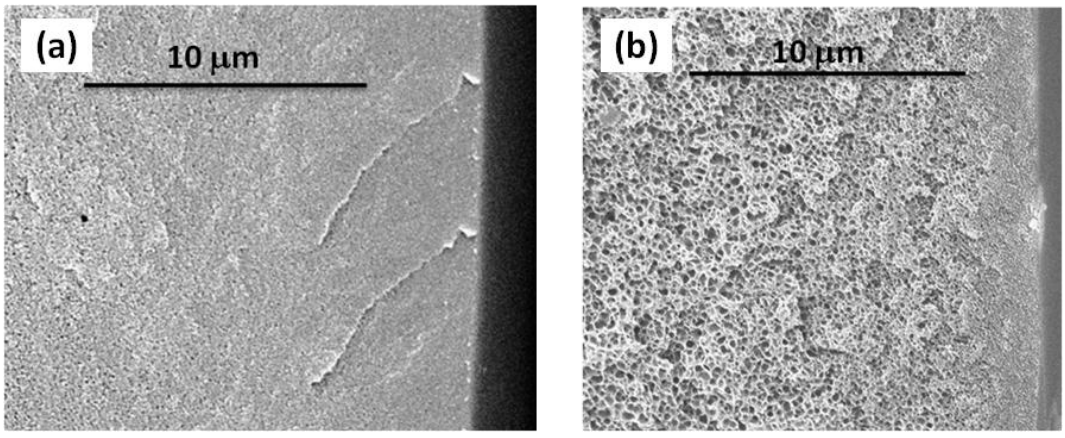

Figure 4.2: SEM images of syringed solid fibers quenched at different temperature (a) 23 ℃ (b) 41 ℃. The bars on the fibers serve as a visual aid.

4.2.3 Fiber spinning – 1st spinning

The initial spinning conditions were designed to (1) promote skin formation, evaporation of volatile dope components in the air gap was maximized by heating the spinneret to 70 ℃ and increasing the air gap to 20-30 cm; (2) accelerate phase separation during quenching, the quench bath was heated to ~50 ℃. The preferred hollow fiber formation conditions are summarized in Table 4.2. The fiber morphology was examined by SEM. Figure 4.3 (a) shows that the fiber is circular in cross-section and macrovoid-free, suggesting that adequate phase separation occurred during quenching. The non-concentric fibers were caused by the slightly misaligned spinneret, which was corrected in the 2nd spinning. Figure 4.3(c) shows that the fiber skin is quite thick, so further optimization must be done to reduce the skin thickness.

Table 4.2: Hollow fiber formation conditions in the 1st spinning (G-1).

G-1 Dope formulation		**Spinning conditions**	
Polymer	30 wt %	Dope extrusion rate	180 mL/h
NMP	21.5 wt %	Bore fluid	60 mL/h, 80/20 (NMP/water)
THF	15 wt %	Spinneret temperature	70 ℃
LiNO3	6.5 wt %	Air gap*	20-30 cm
Ethanol	27 wt %	Quench bath	Height = 1 m, tap water, ~50 ℃
		Take-up rate	35 – 50 m/min

*: Ambient temperature ~ 26 ℃, relative humidity ~ 46 %

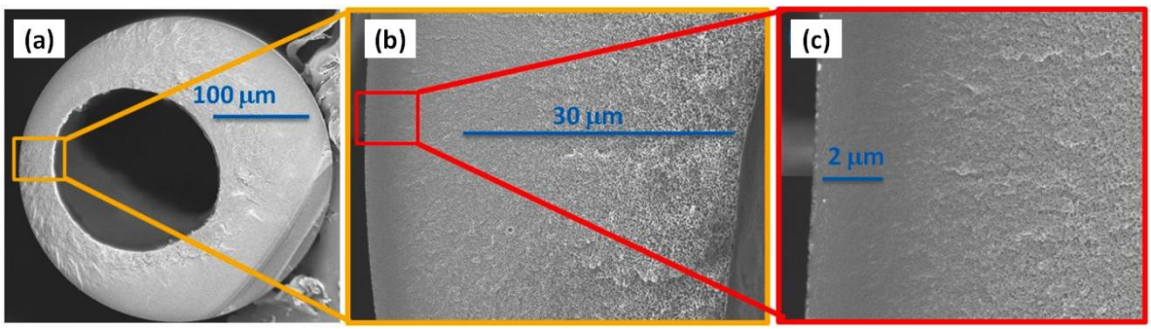

Figure 4.3: SEM images of (a) fiber cross-section, (b) fiber wall, and (c) outer skin region of the fiber from the 1st spinning. The bars on the fibers serve as a visual aid.

The transport properties of the fibers were characterized by pure gas permeation and the results are shown in Table 4.3. It should be noticed that since uncrosslinked fibers are prone to plasticization by CO_2 over time, "ideal" CO_2/CH_4 selectivity obtained from pure gas permeation may overestimate the performance. The "real" CO_2/CH_4 selectivity must be measured by mixed gas permeation, which is discussed in Chapter 5.

The fibers showed selectivities close to dense film values (O_2/N_2 selectivity of 4.5, CO_2/CH_4 selectivity of 34), indicating that no serious defects exist. As mentioned earlier, the skin integrity is believed to be crucial in this research, because any minor defects may deteriorate during subsequent thermal treatment. PDMS (silicon rubber) coating was conducted using a standard procedure [4] to examine the skin integrity of fibers. The "caulked" fibers showed higher selectivities (O_2/N_2 selectivity of 4.9, CO_2/CH_4 selectivity of 45), indicating that the initial fiber skin is slightly defective. High selectivities (greater than dense film values) may be attributed to shear induced molecular orientation on the skin layer [1, 5-8], but the surface orientation effect may decrease after thermal treatment or aging because of polymer chain relaxation.

Table 4.3: Pure gas permeation on hollow fibers from the 1st spinning (G-1). Test conditions: 35 ℃, 100 psig, bore side feed.

	Selectivity			Permeance (GPU)		
State #	O_2/N_2	He/N_2	CO_2/CH_4	O_2	He	CO_2
1-1	4.3	27	36	29	180	230
1-2	4.3	29	37	23	159	181

4.3 Defect-free fiber spinning

4.3.1 Identifying possible causes of skin defect

Based on the characteristics of fibers from the 1st spinning, the goals of the 2nd spinning are to obtain defect-free skin for better membrane efficiency and robustness, also the thinner skin for higher membrane productivity. First, the dope formulation was revisited to identify possible cause of defective skin. During the passage through air gap, the dope composition of the outer layer was changed due to THF evaporation, ethanol evaporation, and moisture absorptions as illustrated in Figure 4.4. Composition trajectories were estimated based on the assumption noted in the figure caption. The estimated composition trajectory, as noted in the figure caption, of the outer layer of the 1st dope (G-1) during passage through the air gap traverses the binodal line, suggesting interfacial phase separation in the air gap, which may be detrimental to skin formation [3]. Thus, the minor defects were likely caused by early phase separation of the nascent skin during passage through the air gap.

4.3.2 Fiber spinning – 2nd spinning

The dope formulation was modified to reduce skin thickness by lowering polymer concentration from 30 wt% to 25 wt% and lowering THF concentration from 15 wt% to 10 wt%. The lower polymer concentration also promotes a more porous substructure. In order to prevent early phase separation of the nascent skin, the dope (G-2) was formulated to be slightly away from the binodal as shown in Figure 4.4. The air gap was lowered to reduce skin thickness. The preferred hollow fiber formation conditions are summarized in Table 4.4.

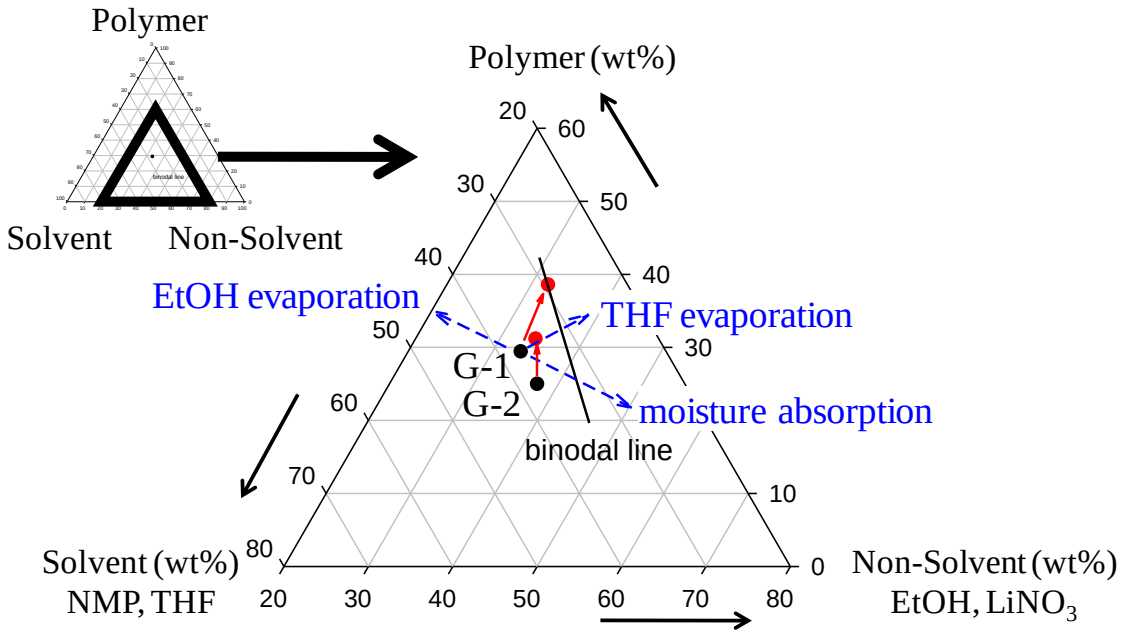

Figure 4.4: Ternary phase diagram illustrating dope composition trajectories. Blue arrows represent trajectories caused by THF evaporation, ethanol evaporation, and moisture absorptions, respectively. G-1 and G-2 are dopes for the 1st and the 2nd spinning, respectively. Red arrows represent estimated composition trajectories of outer layer of dopes during air gap. This trajectory was estimated by assuming complete evaporation of THF (P_{sat} = 142 torr at 20 ℃) and one-third evaporation of ethanol (P_{sat} = 44 torr at 20 ℃) at 70 ℃ (spinning temperature) during 30 cm air gap.

Table 4.4: Hollow fiber formation conditions in the 2nd spinning (G-2).

G-2 Dope formulation		**Spinning conditions**	
Polymer	25 wt %	Dope extrusion rate	180-240 mL/h
NMP	27.5 wt %	Bore fluid	60-80 mL/h, 80/20 (NMP/water)
THF	10 wt %	Spinneret temperature	70 ℃
LiNO3	6.5 wt %	Air gap*	5-20 cm
Ethanol	31 wt %	Quench bath	Height = 1 m, tap water, ~50 ℃
		Take-up rate	25 – 50 m/min

*: Ambient temperature ~ 26 ℃, relative humidity ~ 50 %

The fiber showed acceptable macroscopic morphology (circular and concentric in cross-section, no macrovoids) and the fiber skin is thinner compared to fibers from the 1st spinning as shown in Figure 4.5.

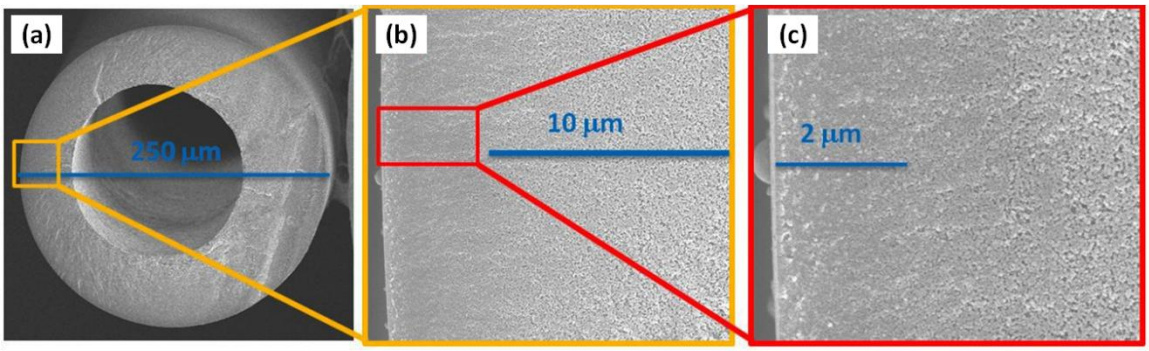

Figure 4.5: SEM images of (a) fiber cross-section, (b) fiber wall, and (c) outer skin region of the fiber from the 2nd spinning. The bars on the fibers serve as a visual aid.

Pure gas permeation was carried out and the results are shown in Table 4.5. Fibers from the 2nd spinning showed higher permeances than fibers from the 1st spinning. This indicates that modified dope formulation and lowered air gap reduced the skin layer thickness as expected. Fibers from the 2nd spinning also showed higher selectivities. The skin integrity of as-spun fibers was confirmed by PDMS coating and the caulked fibers showed similar selectivities.

Table 4.5: Pure gas permeation on hollow fibers from the 2nd spinning (G-2). Test conditions: 35 ℃, 100 psig, bore side feed.

	Selectivity			Permeance (GPU)		
State #	O_2/N_2	He/N_2	CO_2/CH_4	O_2	He	CO_2
2-3	4.5	29	43	36	229	288
2-4	4.8	32	43	54	366	426
2-5	4.5	31	44	47	322	395
2-6	4.3	28	42	57	380	502
2-7	4.9	35	51	62	450	552

4.3.3 Analysis of subtle differences in fiber structure

In order to investigate the differences in fiber structure, three analyses were performed on the permeation results. (1) *Skin thickness*: Apparent skin thickness can be estimated by dividing the dense film permeability by the fiber permeance. Nitrogen permeation results were used to calculate the skin thickness. (2) *Skin perfection*: The extent of raised selectivities after caulking is associated with skin perfection. The higher selectivity by caulking, the more defective the skin. (3) *Substructure resistance*: The fast gas permeance is reduced more by substructure resistance than the slow gas, and therefore substructure resistance can be examined by comparing the selectivity of a high permeability/low permeability gas pair such as He/N_2 to the selectivity of a low permeability gas pair such as O_2/N_2. Thus, a depression of the ratio of He/N_2 selectivity to O_2/N_2 selectivity is an indication of substructure resistance [9, 10]. The results of analyses are summarized in Table 4.6. The fibers from the 2nd spinning have thinner skin layer, more perfect skin, and less substructure resistance as compared to the fibers from the 1st spinning.

Table 4.6: Analyses for skin thickness, skin perfection, and substructure resistance.

	1st spinning	2nd spinning*
Apparent skin thickness (μm)	1.1	0.7
% change of α CO_2/CH_4 after caulking	26%	1%
(α He/N_2)/(α O_2/N_2) before caulking	6.3	6.8

*: Average from 5 sets of fibers spun with various air gap length and take-up rate

4.4 Thermal treatment and crosslinking

The effects of thermal treatment on slightly defective fibers (from the 1st spinning) were investigated. Different thermal treatments reduced the fiber selectivities to different degrees as shown in Figure 4.6. The decrease in selectivity may be attributed to defect development and/or substructure collapse. Thermal treatments can be categorized in two groups: (1) thermal treatment below 220 ℃ (in the green box), which is unlikely to collapse substructure, but may aggravate defective skin and thus decrease CO_2/CH_4 selectivities to ~20 and O_2/N_2 selectivities to ~3.5; and (2) thermal treatment above 300 ℃ (in the blue box), which is likely to collapse substructure and aggravate defective skin and thus decrease CO_2/CH_4 selectivities to lower than 10 and O_2/N_2 selectivities to lower than 2.

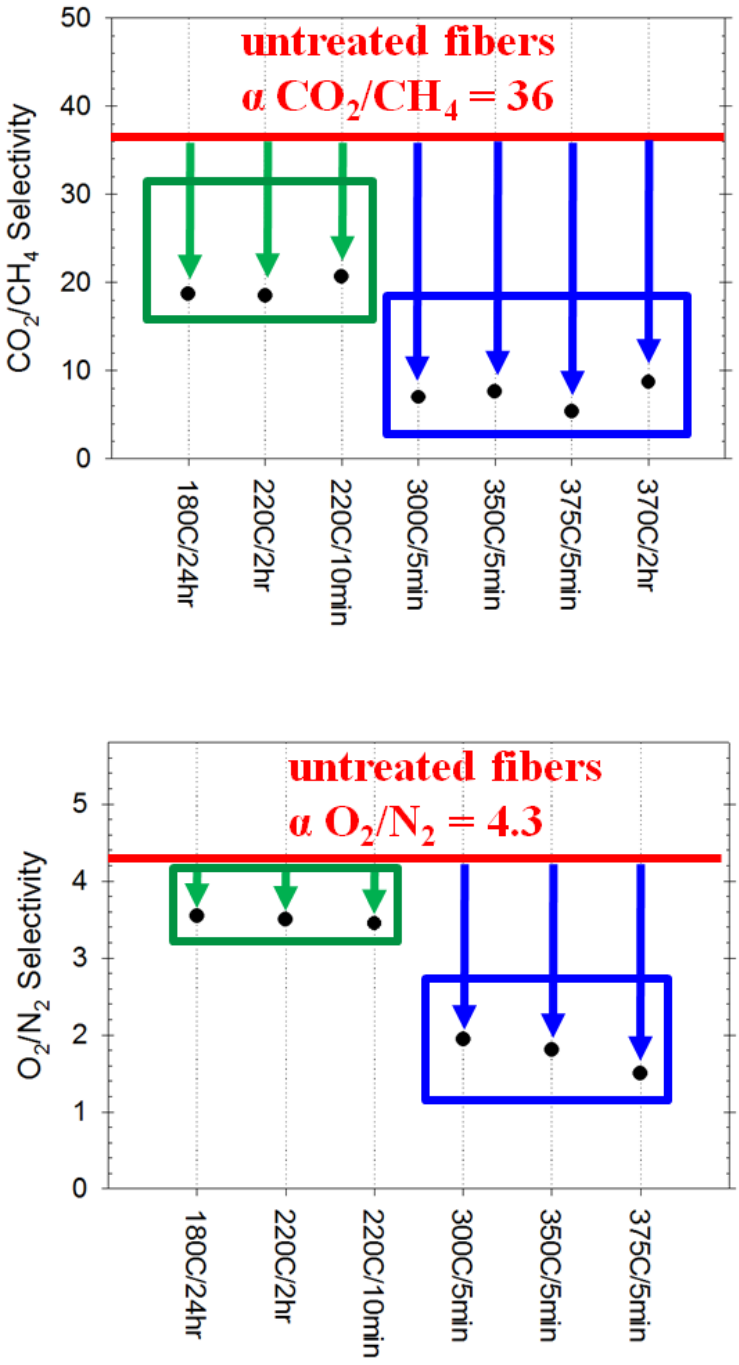

Figure 4.6: Effect of thermal treatment on slightly defective fibers (from the 1st spinning). Red lines represent the selectivities of untreated fibers. Black dots represent the selectivities of treated fibers, and green or blue arrows indicate the changes of selectivities compared to untreated fibers.

To decouple the effects of defect development and substructure collapse, thermally treated fibers were coated with PDMS. If selectivities recover after coating, it indicates thermal treatment aggravates defective skin. Caulking raised the selectivities of all fibers, but to different degrees as shown in Figure 4.7. Accelerated physical aging during thermal treatment tends to decrease permeance but increase selectivity [11], while substructure collapse tends to decrease both permeance and selectivity [9]. Therefore, selectivity is used to distinguish these two effects. After caulking, 180 ℃ and 220 ℃ treated fibers showed higher selectivities, which may be caused by accelerated aging process (indicated by green arrow); while 370 ℃ treated fibers showed much lower selectivities with little improvement upon caulking, which may be caused by substructure collapse (indicated by blue arrow). The reduction in selectivity after 180 ℃ and 220 ℃ treatment (without caulking) may be due to defect development at elevated temperature (indicated by brown arrow). While caulking can raise the selectivities of defective fibers, the benefit diminishes as the feed conditions become more aggressive [4] or feed contains toluene [1]. The negative impact of thermal treatment on slightly defective fibers emphasizes the importance of producing defect-free hollow fibers without substrate resistance for subsequent thermal treatment in this study.

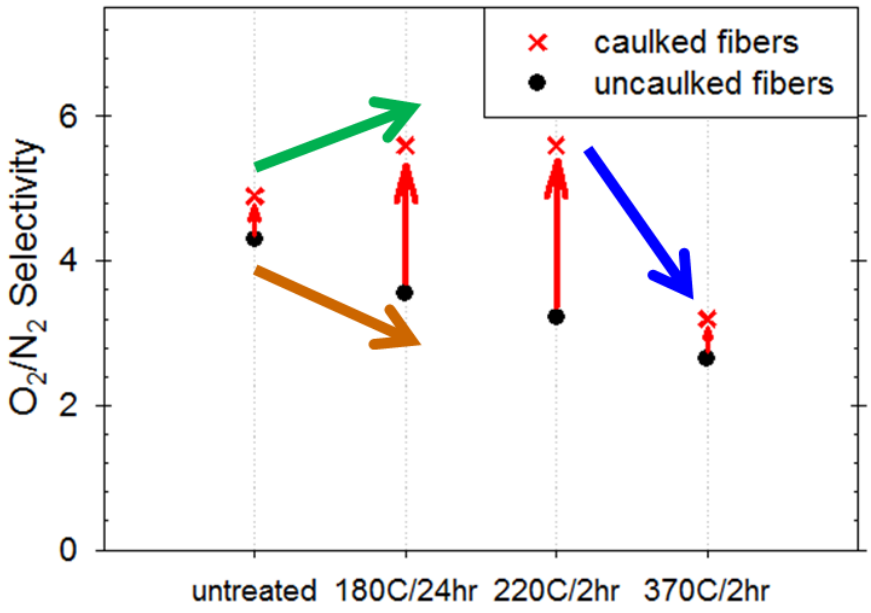

Figure 4.7: Selectivities of caulked thermally treated fibers from 1st spinning.

Thermal treatment of defect-free fibers from the 2nd spinning was conducted. Unlike previous slightly defective fibers, defect-free fibers maintained high selectivities (O_2/N_2 selectivity of ~5, CO_2/CH_4 selectivity of ~40) after 220 ℃ and 350 ℃ treatment, suggesting that thermal treatment neither damaged the skin nor caused serious substructure collapse of these defect-free fibers. This is also supported by SEM images as shown in Figure 4.8. Dissolution tests were conducted to determine the existence and stability of crosslinking. Untreated fibers are soluble in NMP at room temperature while 350 ℃ treated fibers are not dissolved in hot NMP at 110 ℃ for more than 3 days, indicating that stable crosslinking occurred.

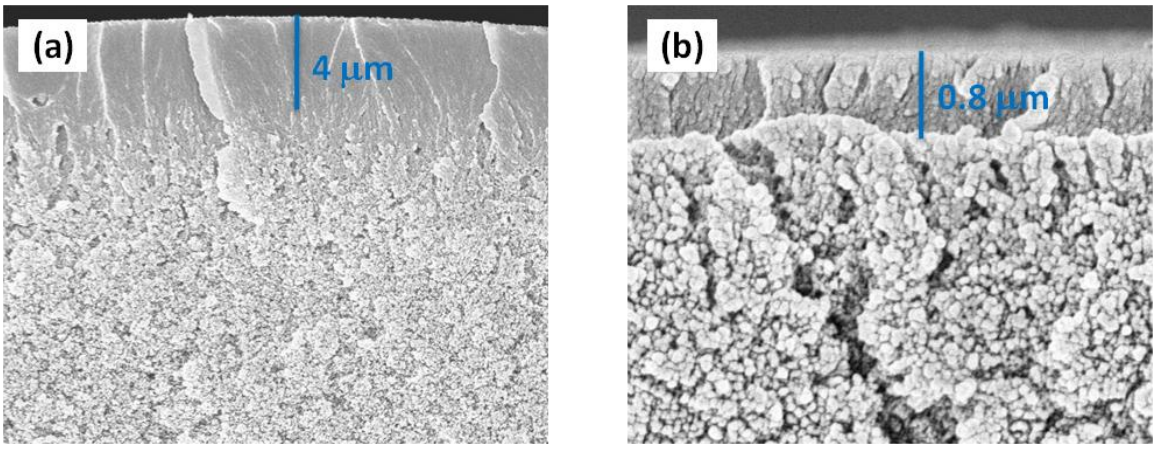

Figure 4.8: SEM images of outer skin region of 350C-1hr treated (a) slightly defective fiber and (b) defect-free fiber.

4.5 Effect of spinning conditions on uncrosslinked and crosslinked fiber

In the 2nd spinning, 5 sets of fibers (spun with air gap distance of 5-20 cm and take-up rate of 25-50 m/min) showed defect-free selectivities, the skin thickness is well correlated with air gap residence time as shown in Figure 4.9. The shorter the residence time in the air gap, the thinner the skin. Fiber diameter is decreased with an increase in the take-up rate as shown in Figure 4.10. Take-up rate of 50 m/min is comparable to commercial production rates and the outside diameters of spun fibers are within the desired limit of 300 μm [12, 13]. These sets of fibers were crosslinked at 350 ℃ for 1 hr, and tested by mixed gas permeation. All crosslinked fibers showed similar selectivities (as shown in Figure 4.11) while fibers spun with shorter air gap residence time showed higher CO_2 permeances after crosslinking (as shown in Figure 4.12). These results suggest that spinning conditions may be further optimized to improve fiber productivity by further reducing the skin thickness, which is discussed in the next section.

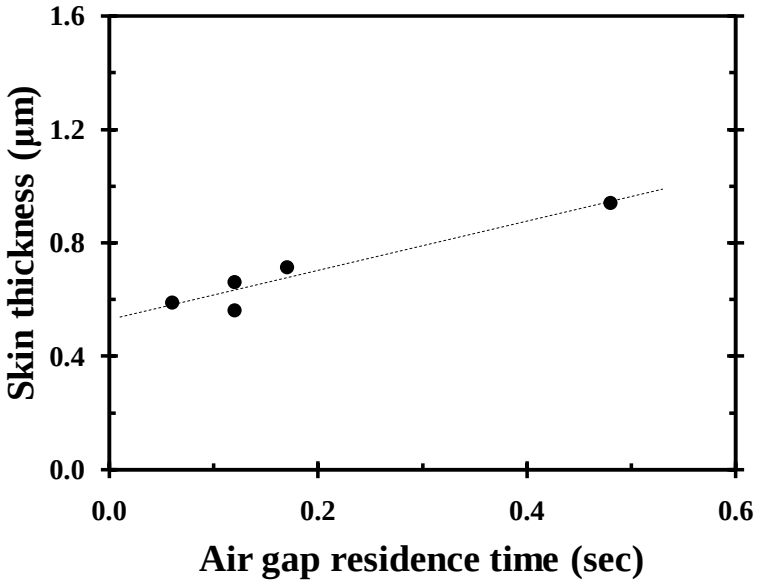

Figure 4.9: Effect of air gap residence time on fiber skin thickness. Air gap residence time is estimated by dividing air gap length by take-up rate. Skin thickness is estimated by dividing the dense film N_2 permeability by the fiber N_2 permeance.

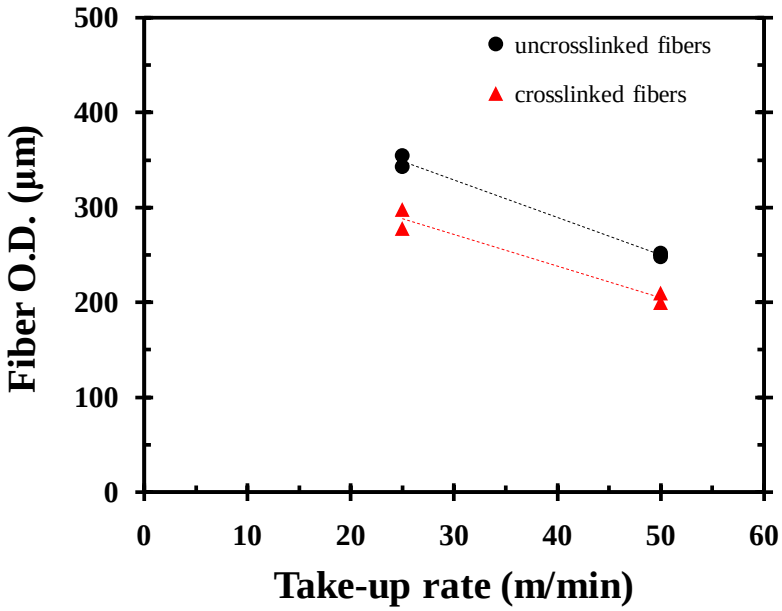

Figure 4.10: Effect of take-up rate on outside diameter (O.D.) of uncrosslinked and crosslinked fibers.

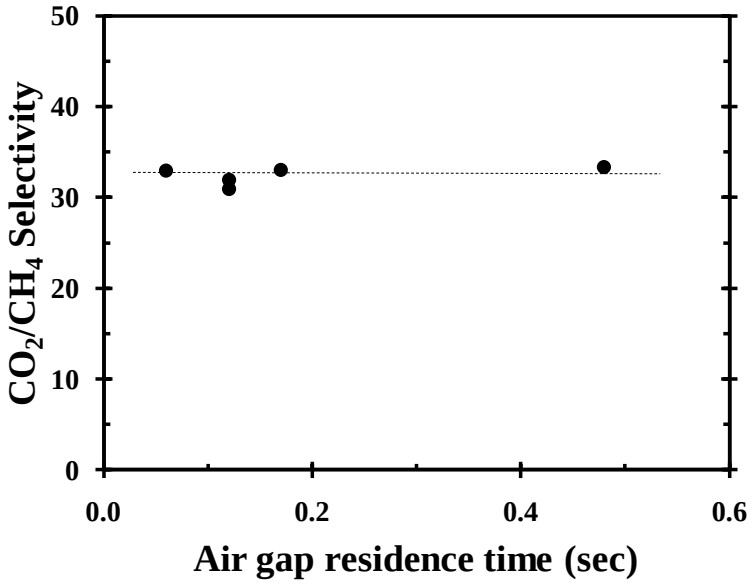

Figure 4.11: Effect of air gap residence time on CO_2/CH_4 mixed gas selectivity of fibers crosslinked at 350 ℃ for 1 hr. Test conditions: 35 ℃, 50/50 CO_2/CH_4 shell side feed at 200 psia. Permeances were calculated using fugacity.

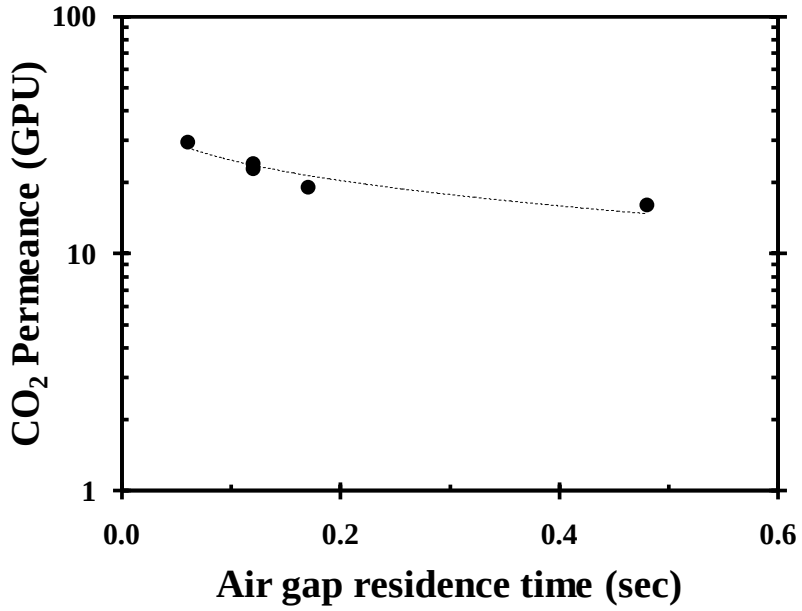

Figure 4.12: Effect of air gap residence time on CO_2 permeance of fibers crosslinked at 350 ℃ for 1 hr. Test conditions: 35 ℃, 50/50 CO_2/CH_4 shell side feed at 200 psia. Permeances were calculated using fugacity.

4.6 Further attempt to reduce skin thickness – 3rd and 4th spinning

The 3rd spinning was conducted with lower air gap (2.5 cm) or faster take-up rate (75 m/min) which were designed to further shorten the air gap residence time and thus reduce the skin thickness. The hollow fiber formation conditions in the 3rd spinning are summarized in Table 4.7. The fiber showed decent macroscopic morphology (circular and concentric in cross-section, no macrovoids) as shown in Figure 4.13. Pure gas permeation was carried out and the results are shown in Table 4.8. Although the fibers have defect-free or nearly defect-free skin (as suggested by their good selectivities), the fibers must retain skin integrity during thermal crosslinking. Unlike the good reproducibility of crosslinked 2nd spinning fibers, selectivities of crosslinked 3rd spinning fibers varied and were lower than crosslinked 2nd spinning fibers. The lowered selectivities suggest that the skin of 3rd spinning fibers were damaged during thermal crosslinking.

Table 4.7: Hollow fiber formation conditions in the 3rd spinning (G-3).

G-3 Dope formulation		**Spinning conditions**	
Polymer	25 wt %	Dope extrusion rate	180 mL/h
NMP	27.5 wt %	Bore fluid	60 mL/h, 80/20 (NMP/water)
THF	10 wt %	Spinneret temperature	70 ℃
LiNO3	6.5 wt %	Air gap*	2.5-5 cm
Ethanol	31 wt %	Quench bath	Height = 1 m, tap water, ~50 ℃
		Take-up rate	50 – 75 m/min

*: Ambient temperature ~ 23 ℃, relative humidity ~ 27 %

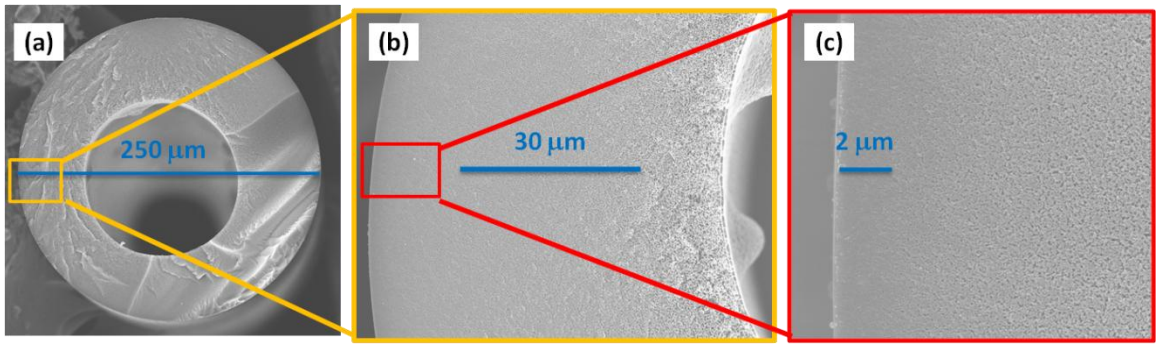

Figure 4.13: SEM images of (a) fiber cross-section, (b) fiber wall, and (c) outer skin region of the fiber from the 3rd spinning. The bars on the fibers serve as a visual aid.

Table 4.8: Pure gas permeation on hollow fibers from the 3rd spinning (G-3). Test conditions: 35 ℃, 100 psig, bore side feed.

	Selectivity			Permeance (GPU)		
State #	O_2/N_2	He/N_2	CO_2/CH_4	O_2	He	CO_2
3-2	4.3	36	40	59	494	510
3-3	4.5	39	40	56	497	465

From the characteristics of uncrosslinked and crosslinked fibers, dope composition and spinning conditions for producing fibers, which can be thermally crosslinked without sacrificing selectivities, were identified. Large quantity of defect-free fibers was spun with optimized conditions (as summarized in Table 4.9) for the subsequent thermal treatment/crosslinking study, which will be discussed in Chapter 5. As expected, the fiber showed desirable morphology (a thin skin layer with a porous substructure underneath) and maintained high selectivities after thermal crosslinking.

Table 4.9: Hollow fiber formation conditions in the 4th spinning (G-4). Note that ethanol content was slightly reduced according to minor shift of binodals.

G-4 Dope formulation		**Spinning conditions**	
Polymer	25 wt %	Dope extrusion rate	180 mL/h
NMP	31.5 wt %	Bore fluid	60 mL/h, 80/20 (NMP/water)
THF	10 wt %	Spinneret temperature	70 ℃
LiNO3	6.5 wt %	Air gap*	5 cm
Ethanol	27 wt %	Quench bath	Height = 1 m, tap water, ~50 ℃
		Take-up rate	50 m/min

*: Ambient temperature ~ 26 ℃, relative humidity ~ 43 %

4.7 Summary and conclusions

Defect-free asymmetric hollow fiber membranes were successfully spun from a novel crosslinkable polyimide, 6FDA-DAM:DABA (3:2). The fibers were spun at take-up rate of 50 m/min, which is comparable to commercial production rates. Post-spin thermal crosslinking was implemented to these defect-free fibers without damaging the delicate skin and porous substructure, thus preserving high selectivities. In a comparison study on *slightly defective fibers*, thermal treatment caused a severe and irreparable loss in selectivity, indicating that defect-free property is critical to these crosslinkable fibers. The effects of various crosslinking conditions on fiber morphology and transport properties as well as CO_2 plasticization resistance will be described in Chapter 5.

4.8 References

1. I.C. Omole. *Crosslinked polyimide hollow fiber membranes for aggressive natural gas feed streams.* Ph.D. Dissertation, Georgia Institute of Technology, Atlanta, GA, 2008.

2. I.C. Omole, S.J. Miller, and W.J. Koros, *Increased molecular weight of a cross-linkable polyimide for spinning plasticization resistant hollow fiber membranes.* Macromolecules, 2008. **41**(17): p. 6367-6375.

3. S.B. Carruthers. *Integral-skin formation in hollow fiber membranes for gas separations* Ph.D. Dissertation, The University of Texas at Austin, Austin, TX, 2001.

4. D.W. Wallace. *Crosslinked hollow fiber membranes for natural gas purification and their manufacture from novel polymers.* Ph.D. Dissertation, The University of Texas at Austin, Austin, TX, 2004.

5. S.A. Gordeyev and S.J. Shilton, *Forced convection spinning of gas separation hollow fibre membranes: some underlying factors, mechanisms and effects.* Journal of Membrane Science, 2004. **229**(1-2): p. 225-233.

6. A.F. Ismail, I.R. Dunkin, S.L. Gallivan, and S.J. Shilton, *Production of super selective polysulfone hollow fiber membranes for gas separation.* Polymer, 1999. **40**(23): p. 6499-6506.

7. A.F. Ismail, S.J. Shilton, I.R. Dunkin, and S.L. Gallivan, *Direct measurement of rheologically induced molecular orientation in gas separation hollow fibre membranes and effects on selectivity.* Journal of Membrane Science, 1997. **126**(1): p. 133-137.

8. A. Niwa, H. Kawakami, T. Kanamori, T. Shinbo, A. Kaito, and S. Nagaoka, *Surface orientation effect of asymmetric polyimide hollow fibers on their gas transport properties.* Journal of Membrane Science, 2004. **230**(1-2): p. 141-148.

9. D.T. Clausi and W.J. Koros, *Formation of defect-free polyimide hollow fiber membranes for gas separations.* Journal of Membrane Science, 2000. **167**(1): p. 79-89.

10. I. Pinnau and W.J. Koros, *Relationship between substructure resistance and gas separation properties of defect-free integrally skinned asymmetric membranes.* Industrial & Engineering Chemistry Research, 1991. **30**(8): p. 1837-1840.

11. Y. Huang and D.R. Paul, *Effect of temperature on physical aging of thin glassy polymer films.* Macromolecules, 2005. **38**(24): p. 10148-10154.

12. O.M. Ekiner, Vassilatos, G.J., *Polymeric membranes.* U.S. Patent 5,085,774, 1992.

13. S.B. Carruthers, G.L. Ramos, and W.J. Koros, *Morphology of integral-skin layers in hollow-fiber gas-separation membranes.* Journal of Applied Polymer Science, 2003. **90**(2): p. 399-411.

CHAPTER 5

THERMALLY CROSSLINKABLE HOLLOW FIBER MEMBRANES FOR NATURAL GAS PURIFICATION

5.1 Overview

In Chapter 4, crosslinkable asymmetric hollow fiber membranes were spun from a carboxylic acid containing polyimide, 6FDA-DAM:DABA. Dope and spinning conditions were optimized to obtain fibers with a defect-free selective skin layer, which is found to be an essential property for high performance of the resulting crosslinked hollow fiber membranes. In this chapter, detailed characterization of crosslinked hollow fiber membranes is discussed. The first part of this chapter discusses the effects of various thermal treatments on crosslinking, fiber morphology, transport properties as well as plasticization resistance. The second part discusses membrane performance under aggressive operating conditions. The crosslinked fibers were tested using high CO_2 content feeds at a variety of feed pressures, temperatures, and permeate pressures. The last part of this chapter discusses the effects of physical aging and CO_2 conditioning on separation performance.

5.2 Thermal analysis: DSC and TGA-MS

6FDA-DAM:DABA (2:1) dense films have been decarboxylated crosslinked at 389 ℃ (15 ℃ above T_g) [1]. Sub-T_g annealing is preferable for asymmetric hollow fibers, since it reduces the negative impact on fiber skin and porous substructure. Differential

scanning calorimetry (DSC) shows that the T_g of 6FDA-DAM:DABA (3:2) polymer powders and hollow fibers were similar (~390 ℃). The decarboxylation temperature (accompanied by CO_2 evolution) was measured by thermogravimetric analysis–mass spectrometry (TG-MS) as shown in Figure 5.1. Significant amounts of CO_2 were evolved from 6FDA-DAM:DABA (3:2) between ~350 ℃ and the polymer degradation temperature, while no noticeable amounts of CO_2 were evolved in 6FDA-DAM (without DABA group) before polymer degradation. The results indicate that DABA moieties are responsible for the evolved CO_2 prior to polymer degradation.

As mentioned in section 2.4.2, the delicate morphology of hollow fibers poses additional challenges to most approaches to improving plasticization resistance. Moreover, the asymmetric morphology with a thin selective layer also adds complexity to various characterization techniques, such as FT-IR and X-ray diffraction. Therefore, in this work, crosslinking effects on fibers were characterized using dissolution test for existence and stability of crosslinking, SEM for fiber morphology, and most importantly, mixed gas permeation for transport properties as well as plasticization resistance. To get more fundamental understanding of crosslinking effects on chemical structure and polymer microstructure, study of dense films is preferable due to their relative simplicity. The parallel work on dense films of the same material was done by Dr. Wulin Qiu in Koros research group. The study revealed the insight of crosslinking effects on the material properties. For instance: (1) the crosslinking mechanism was further characterized by FT-IR; (2) The average interchain spacing was determined by wide angle X-ray diffraction and was found to increase as a result of decarboxylation-induced crosslinking. More characterization on dense films can be found in reference [2].

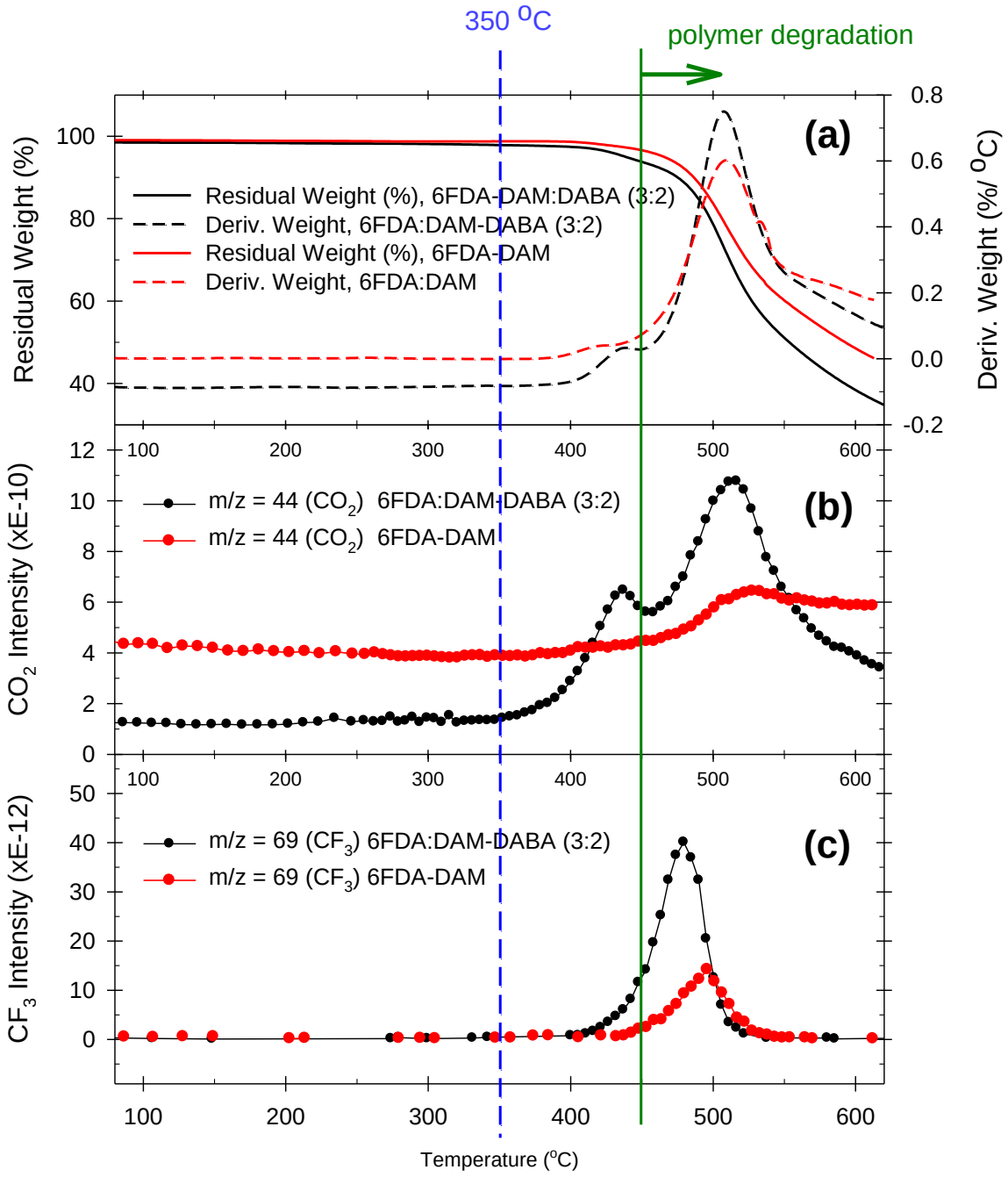

Figure 5.1: TG–MS spectra of 6FDA-DAM:DABA (3:2) and 6FDA-DAM. (a) TGA trace, (b) evolved CO_2 and (c) evolved CF_3.

5.3 Effects of crosslinking conditions

5.3.1 Effects of thermal treatment protocol and atmosphere

Dense film study using the same thermally crosslinkable polyimide has shown that crosslinking initiates at about 300 ℃, and the dense film can be highly crosslinked at 350 or 370 ℃ for 1 hr [2]. Chapter 4 shows that the defect-free fibers can be crosslinked without damaging the delicate skin and porous substructure by thermally treated at 350 ℃ for 1 hr under argon purge, herein, referred as the baseline conditions. A detailed comparison of fibers crosslinked at different temperature (300 ℃ and 350 ℃) and soak time (1 hr and 10 hr) under various atmospheres (argon, argon with trace O_2 or N_2O, CO_2, N_2, and air) were investigated. Dissolution tests serve as a quick method for determining the existence and stability of crosslinking. Untreated fiber easily dissolved in NMP at room temperature. Fibers thermally treated at 300 ℃ for 10 hr swelled in NMP at room temperature and nearly dissolved in hot NMP at 110 ℃, suggesting that little crosslinking occurred. Fibers thermally treated at 350 ℃ for 1 hr were insoluble in hot NMP at 110 ℃ for more than 3 days, indicating that stable crosslinking occurred. Note that hot water-containing NMP used here could hydrolyze some types of crosslinkage (such as ester linkages [3] or amide linkages) or may even lead to polymer backbone scission, and thus dissolve the ester bond or amide bond crosslinked membranes.

Transport properties of untreated and thermally treated fibers were tested with a 50% CO_2/50% CH_4 mixed gas feed at 200 psia. As shown in Figure 5.2, temperature has a significant effect while shorter soak time (350 ℃ for 1 hr or 10 min) has a negligible effect. In comparison with 350 ℃ treated fibers, 300 ℃ treated fibers show higher permeances and lower selectivities close to untreated fibers, suggesting a very low degree

of crosslinking. This is also supported by dissolution in hot NMP, in agreement with the dense film study [2]. Argon with trace strong oxidizer (500 ppm O_2 or N_2O) was employed as an attempt to facilitate crosslinking at lower temperature (300 ℃). Neither oxidizer shows noticeable effect at 350 ℃ or promotes crosslinking at 300 ℃, again supported by dissolution in hot NMP. These results suggest that temperature is the controlling factor. Under the investigated gas atmospheres, crosslinking should be carried out at 350 ℃ since it provides sufficient polymer chain mobility to bring reactive sites together as well as sufficient energy to overcome the activation energy barrier for crosslinking.

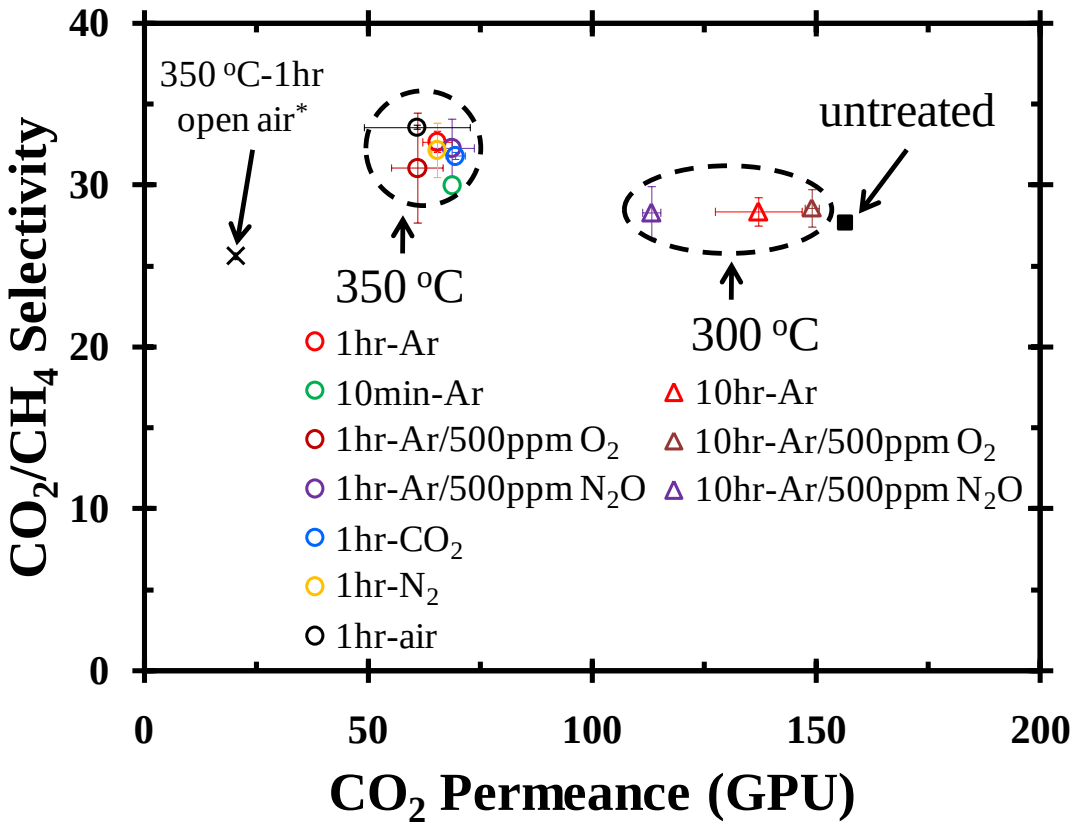

Figure 5.2: Effects of crosslinking conditions on CO_2 permeance and CO_2/CH_4 selectivity. *open air: atmosphere (static). Purge gas at 200 mL/min. Test conditions: 50% CO_2/50% CH_4 mixed gas feed, 200 psia, 35 ℃. Permeances were calculated using fugacity.

Dense film analogs showed that crosslinking caused an increase in permeabilities while a different trend is observed with asymmetric hollow fibers studied here. The higher selectivity observed in the crosslinked fibers suggests that the decrease in permeance can be attributed to skin layer densification during 350 ℃ thermal treatment. The reduction in permeance (2.4 times) after crosslinking (Figure 5.2, from 156 to 65 GPU) is roughly equal to the increase (2.5 times) in observed skin layer thickness after crosslinking (Figure 5.3, from ~0.4 μm to ~1 μm).

To alleviate skin densification, i.e. maximize permeance retention, during thermal treatment, crosslinking was carried out under CO_2 purge. Because of its high solubility in polymer, it was suggested that sorbed CO_2 may "puff up" the polymer matrix and thus mitigate skin densification during thermal treatment. However, as shown in Figure 5.2, CO_2 purge shows little effect on crosslinked fiber performance. Crosslinking was also carried out under N_2 purge, and the crosslinked fibers showed similar performance as well. Nitrogen is preferable to argon, since N_2 is the most economical inert gas alternative. To explore more economic crosslinking conditions, crosslinking was conducted under open-air atmosphere without inert gas purge. In comparison with purge gas conditions, crosslinking under open-air conditions resulted in an about 20% decrease in selectivity and a more than 50% decrease in permeance. As shown Figure 5.3 (c), the reduction in both permeance and selectivity can be attributed to skin and transition layer densification; the latter can cause undesirable substructure resistance (less selective) and thus reduce selectivity. To identify the possible cause of the intensive densification, crosslinking was carried out with dry air purge. Crosslinking under dry air purge resulted in similar morphology and transport properties with crosslinking under inert gas purge, suggesting that the adverse effect may be caused by trace humidity. Clearly, crosslinking should be conducted in a controlled environment to avoid undesired transition layer densification.

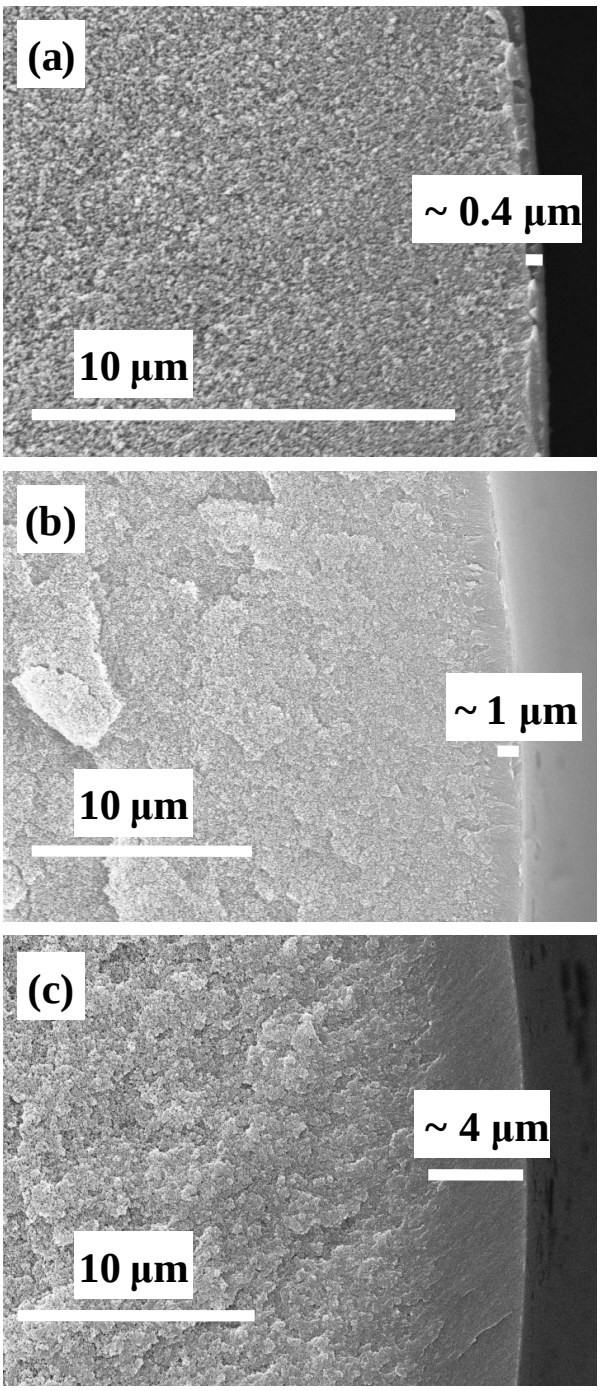

Figure 5.3: SEM images of outer skin region of fiber thermally treated at various conditions. (a) 300 ℃ for 10 hr under inert gas purge (argon or N_2 at 200 mL/min); (b) 350 ℃ for 1 hr under inert gas purge (argon or N_2 at 200 mL/min); (c) 350 ℃ for 1 hr under open air atmosphere (static).

5.3.2 Effects of thermal treatment conditions on plasticization resistance

To evaluate the membrane performance under aggressive feeds, the fibers were tested using a 50% CO_2/50% CH_4 mixed gas feed at high pressures up to 800 psia. As shown in Figure 5.4 (a), the crosslinked fibers showed higher selectivity, indicating that crosslinking improve the membrane efficiency. The reduction in selectivity with increasing pressure observed for crosslinked fibers can be explained by dual mode sorption theory. In the absence of plasticization, the sorption coefficient decreases with increasing pressure as Langmuir sorption sites are filled. Since CO_2 is more condensable, it has a competitive advantage over CH_4 in sorption. The sorption advantage of CO_2 is reduced with increasing pressure and thus resulting in a decrease in CO_2/CH_4 selectivity. The retained selectivities from 200 to 800 psia for the 350 ℃ treated fibers and the 300 ℃ treated fibers are 85% and 68%, respectively, indicating that crosslinking helps eliminate 17% of the selectivity loss associated with plasticization. More pronounced indication of plasticization effects and the benefit of crosslinking can be observed in CH_4 permeance as a function of feed pressure shown in Figure 5.4 (b). For untreated fibers, CH_4 permeance increased rapidly with increasing feed pressure, indicating that increased CO_2 partial pressure swelled the membrane and caused a loss of CH_4 at high pressures. Moreover, untreated fibers became defective during exposure to 600-800 psia feed, which may be because of the softening of polymer due to plasticization [4]. On the contrary, the 350 ℃ treated fibers showed typical dual mode behavior, decreasing CH_4 permeance with increasing feed pressure, indicating that the crosslinked fibers have excellent plasticization resistance against CO_2. The 300 ℃ treated fibers showed improved plasticization resistance due to limited crosslinking. However, despite being

masked by downward trend with pressure caused by the saturation of Langmuir sorption sites, the CH_4 permeance slightly increased with increasing feed pressure, suggesting that some swelling still occurred. It should be noted that plasticized membranes are inherently unstable, i.e., the selectivity have a tendency to decline over time [5, 6]. The time stability test (discussed later) demonstrated that the crosslinked fibers do not show such instability. In summary, crosslinking improves membrane efficiency and stability, and eliminates swelling-induced hydrocarbon loss at high pressures.

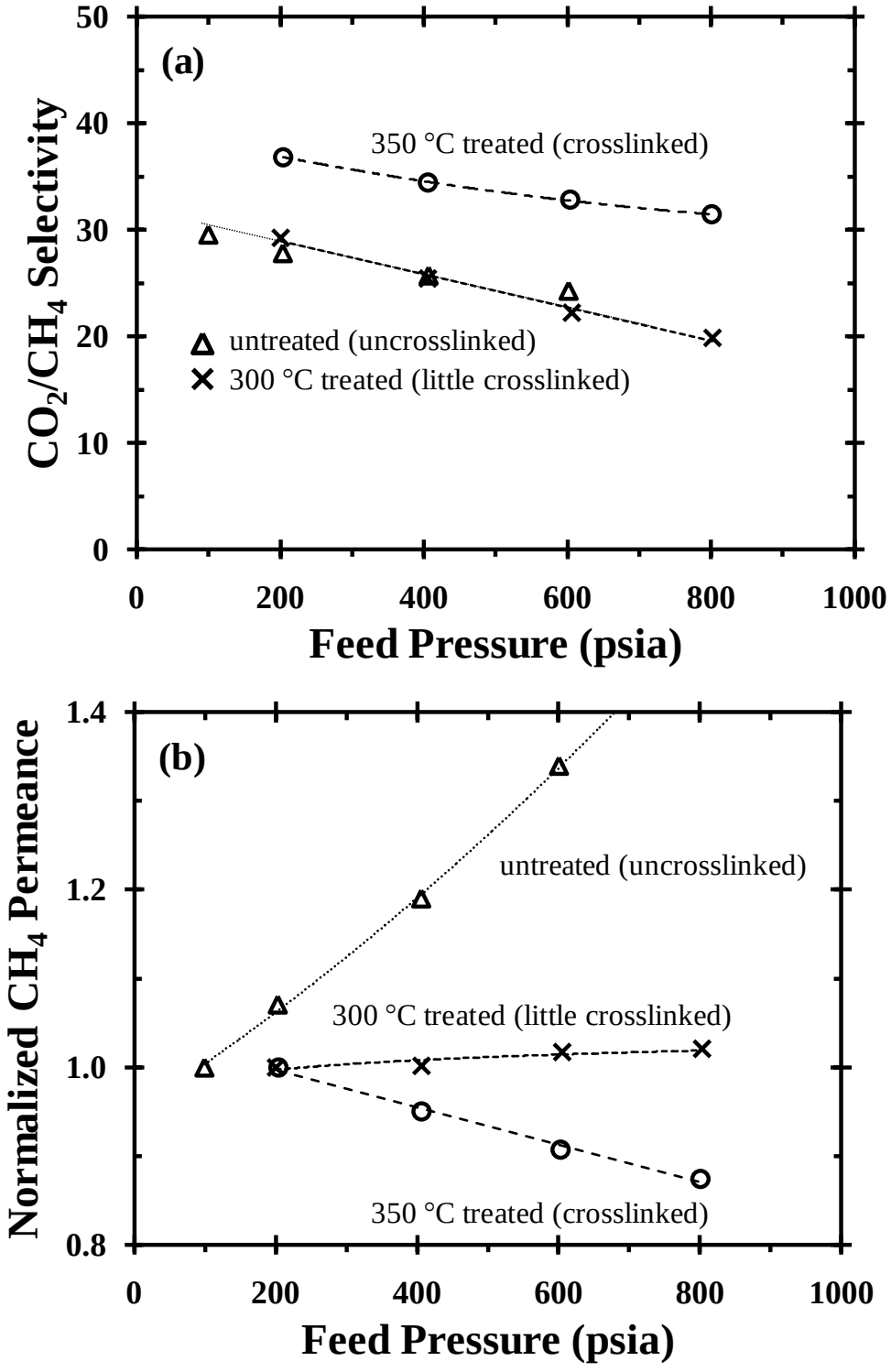

Figure 5.4: Effects of thermal treatment on (a) CO_2/CH_4 selectivity and (b) CH_4 permeance of untreated and thermally treated fibers. Test conditions: 50% CO_2/50% CH_4 mixed gas feed, 35 ℃. Permeances were calculated using fugacity at corresponding feed pressures and normalized by the permeance at the lowest pressure. The lines are used to guide the eye.

5.4 Membrane performance under aggressive operating conditions

5.4.1 Pressure effects and plasticization resistance for 70% CO_2 feeds

Plasticization resistance of the crosslinked fibers were tested further with even higher CO_2 content feed, 70% CO_2/30% CH_4, to explore the possibility of use in more aggressive applications. Figure 5.5 shows the effects of feed pressure on (a) CO_2 and CH_4 permeance and (b) CO_2/CH_4 selectivity. There is no increase in CO_2 and CH_4 permeance, i.e. no indication of plasticization up to a total feed pressure of 1000 psia. Again, the reduction in permeances and selectivity with increasing pressure can be attributed to dual mode sorption effects. These results indicate that the crosslinked fibers have excellent plasticization resistance against CO_2 (at least CO_2 partial pressure of 700 psia).

5.4.2 Time stability under high CO_2 content feeds

The performance stability over time under high pressures was tested using 50% CO_2/50% CH_4 and 70% CO_2/30% CH_4 feed at 1000 psia to simulate long-term exposure to aggressive natural gas feed streams with high CO_2 partial pressures. The results of the time stability test are shown in Figure 5.6 and Figure 5.7. These results indicate that the crosslinked fibers maintained good permeance and selectivity over 95 hr testing with 50% CO_2/50% CH_4 feed and 45 hr testing with 70% CO_2/30% CH_4 feed. The good performance stability and the absence of plasticization under these conditions suggest that crosslinked fibers are promising for industrial applications.

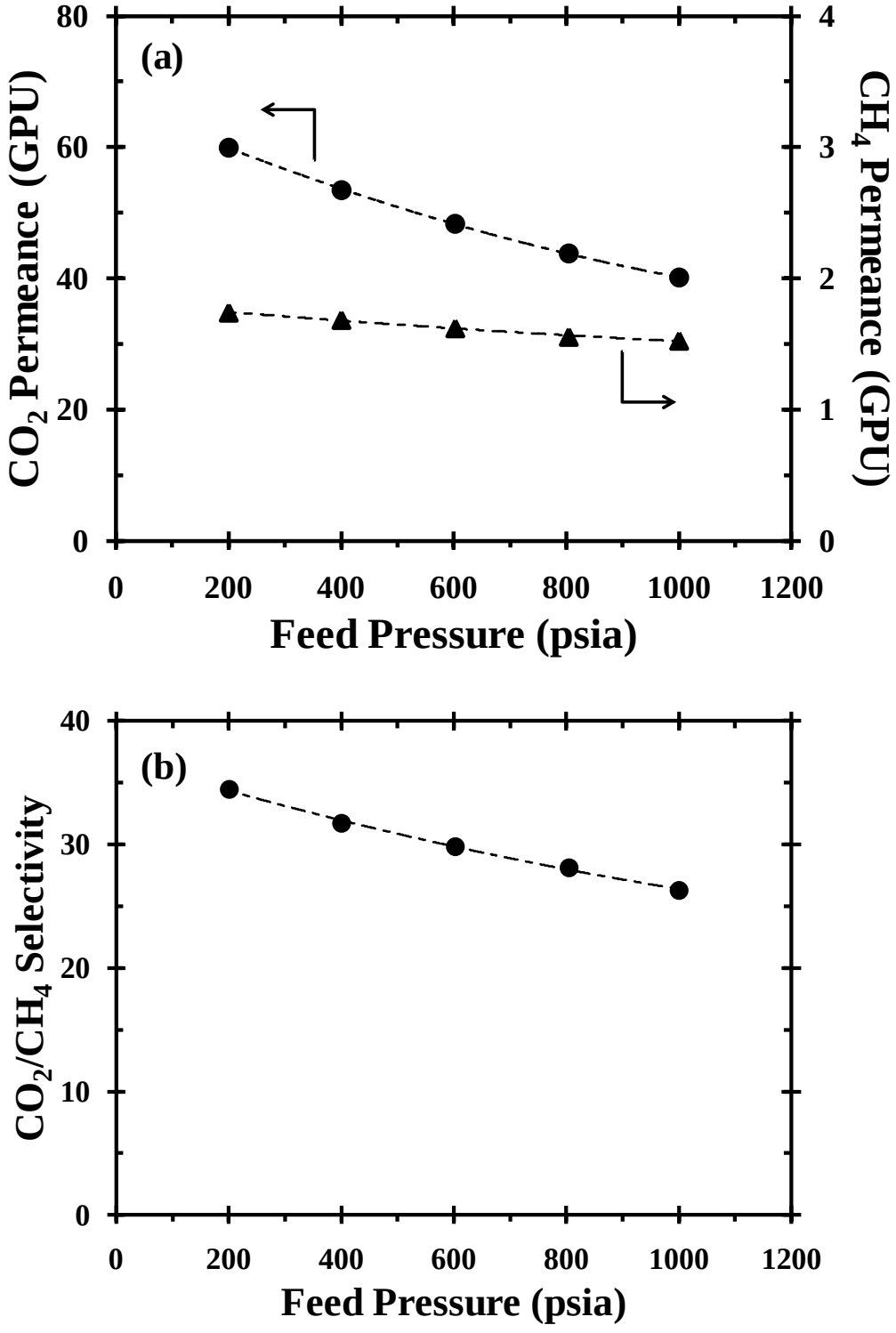

Figure 5.5: Effects of feed pressure on (a) CO_2 and CH_4 permeance (b) CO_2/CH_4 selectivity of 350 ℃ crosslinked fibers. Test conditions: 70% CO_2/30% CH_4 mixed gas feed, 35 ℃. Permeances were calculated using fugacity at corresponding feed pressures.

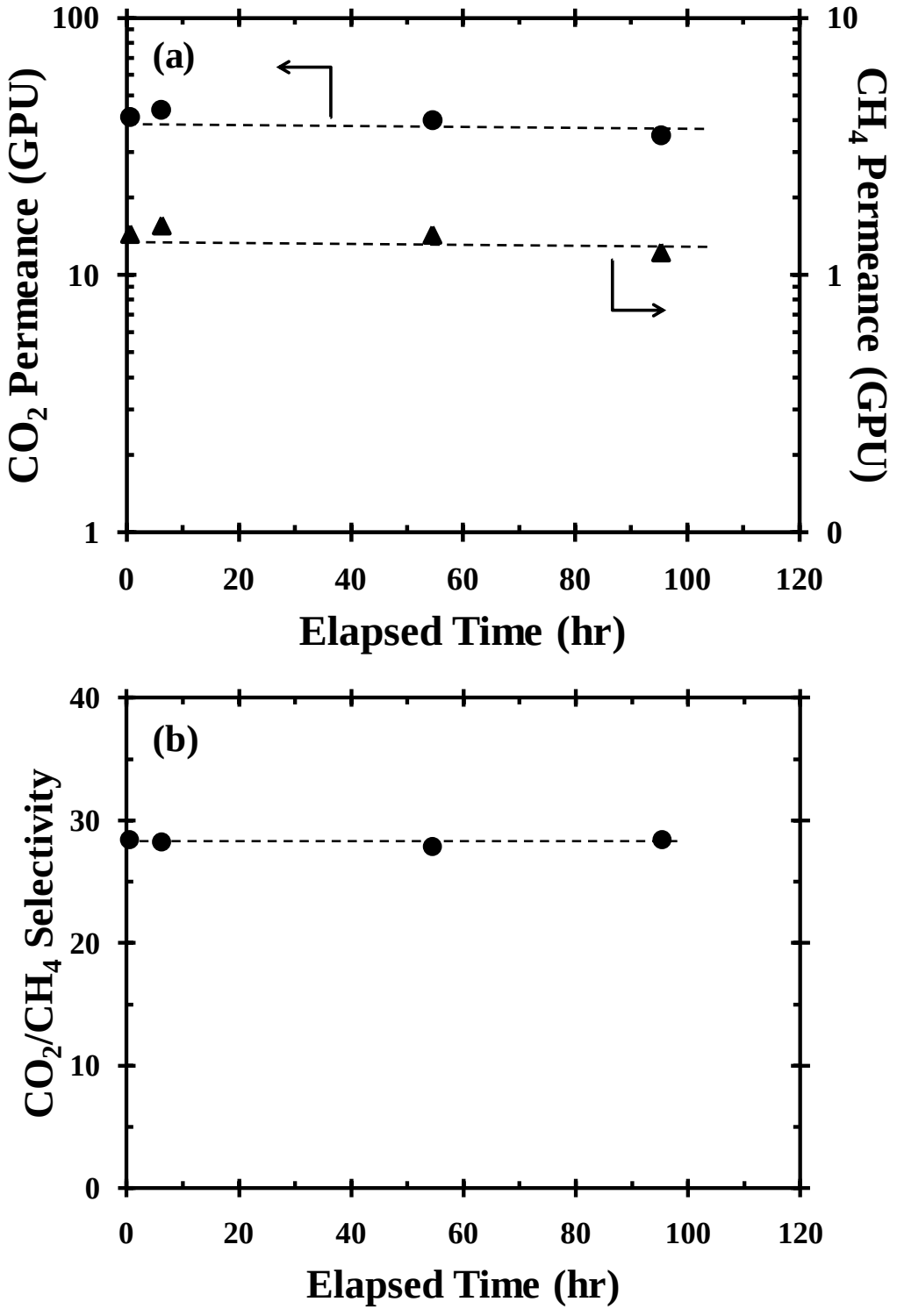

Figure 5.6: Stability over time of (a) CO_2 and CH_4 permeance (b) CO_2/CH_4 selectivity of 350 ℃ crosslinked fibers under 50% CO_2/50% CH_4 mixed gas feed at 1000 psia, 35 ℃. Permeances were calculated using fugacity.

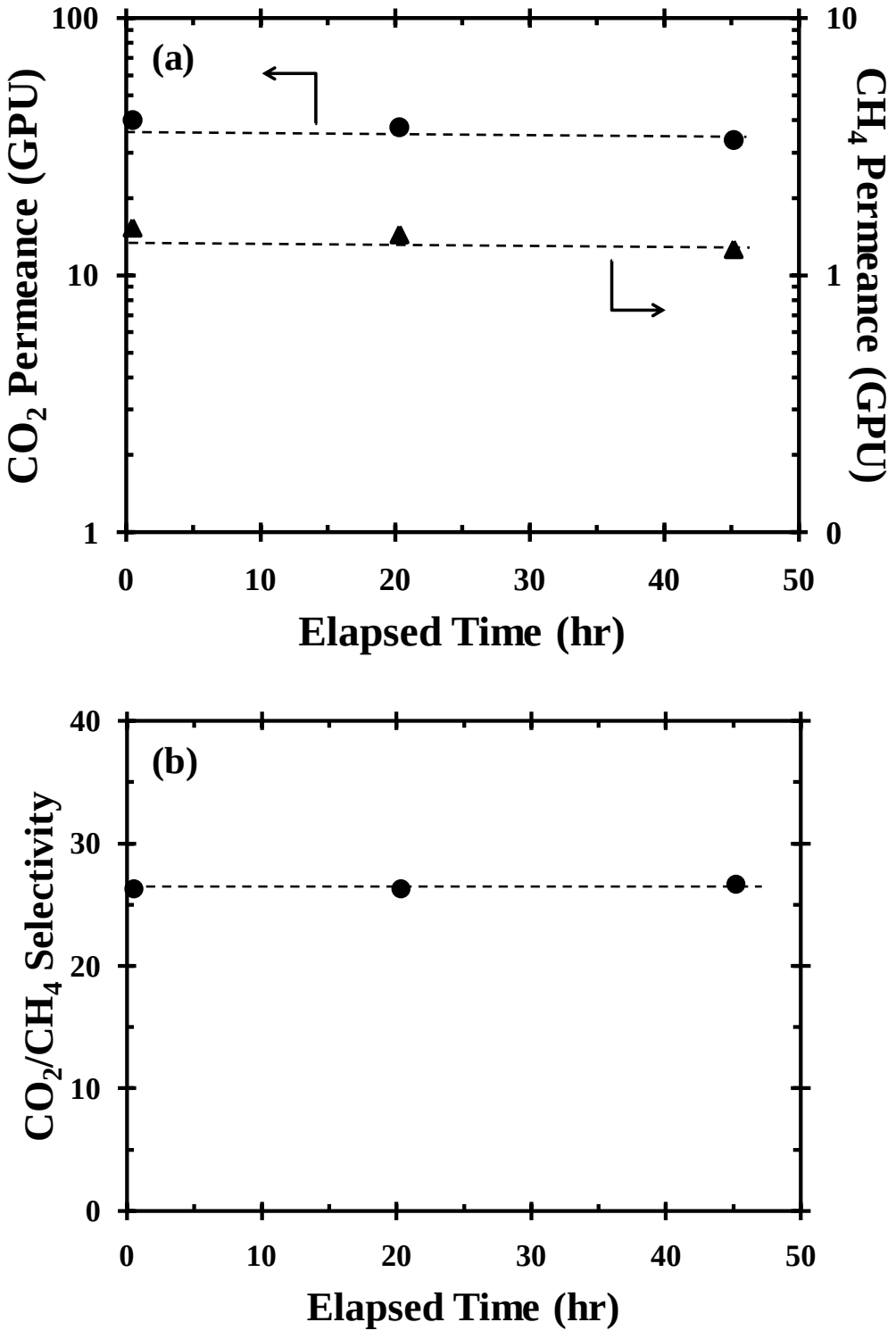

Figure 5.7: Stability over time of (a) CO_2 and CH_4 permeance (b) CO_2/CH_4 selectivity of 350 ℃ crosslinked fibers under 70% CO_2/30% CH_4 mixed gas feed at 1000 psia, 35 ℃. Permeances were calculated using fugacity.

5.4.3 Effects of operating temperature

The effects of temperature on separation performance of glassy polymer have been studied [7-9]. The increased polymer chain mobility at elevated temperature increases diffusion coefficients of all penetrants, but to different degrees. For CO_2/CH_4 separation, the larger molecule (CH_4) is affected to a larger extent, thereby decreasing the diffusion advantage of CO_2 over CH_4. Moreover, the sorption advantage of CO_2 over CH_4 is greatly reduced with increasing temperature. Given the combined decrease in diffusion and sorption advantages of CO_2 with increasing temperature, lower temperature is generally preferable for CO_2/CH_4 separation. However, the increasingly sorbed CO_2 at lower temperature also can lead to stronger plasticization effects [10, 11].

The effects of operating temperature on crosslinked fibers were investigated by mixed permeation with a 50% CO_2/50% CH_4 feed at 1000 psia. As described in section 2.2.3, the temperature dependence of permeability (P) or permeance (P/l) can be expressed by an Arrhenius type equation:

$$P = P_0 \exp\left[\frac{-E_p}{RT}\right] \tag{5.1}$$

Figure 5.8 shows the CO_2 and CH_4 permeances plotted as functions of temperature in an Arrhenius form for crosslinked fibers, and the activation energies for permeation (E_p) were computed and summarized in Table 5.1 along with other glassy polymers. As shown in Figure 5.8, there is higher temperature dependence for CH_4 permeance than CO_2 permeance of crosslinked fibers, also indicated by higher activation energy for CH_4 shown in Table 5.1. The activation energies for crosslinked fibers are smaller than other glassy polymers, indicating that crosslinked fibers are less sensitive to

changes in operating temperature, possibly due to controlled chain mobility by crosslinking.

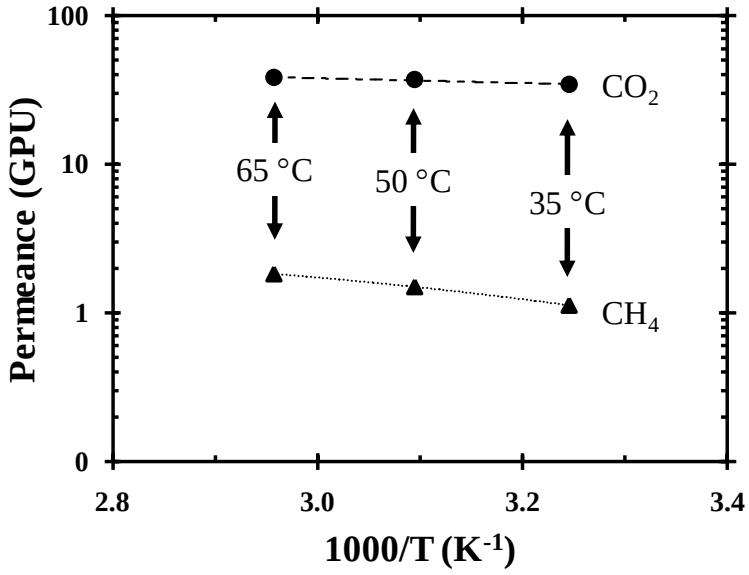

Figure 5.8: Temperature dependence of CO_2 and CH_4 permeances in an Arrhenius type plot. Test conditions: 50% CO_2/50% CH_4 mixed gas feed at 1000 psia, 35-65 ℃. Permeances were calculated using fugacity.

Table 5.1: Activation energies for permeation (E_p) for CO_2 and CH_4 in crosslinked fibers and other glassy polymers.

	E_p (kJ/mol)	
	CO_2	CH_4
Crosslinked polymer (this study)	3.1	14
Polycarbonate [12]	20.3	33
Kapton® [8]	12.6	26
6FDA-IPDA [8]	5.0	24
6FDA-6FmDA [7]	9.2	31
6FDA-6FpDA [7]	3.0	18

The elevated temperature tests (50 ℃ and 65 ℃) were conducted to simulate the crosslinked fiber performance under typical field operating conditions. Table 5.2 summarizes the permeance and selectivity changes from 35 ℃ to 50 ℃ and 65 ℃. As test temperature increases, CO_2/CH_4 selectivity decreases as expected, suggesting that lower operating temperature is preferable. It should be noted that, as mentioned earlier, lower temperature is preferable in terms of intrinsic selectivity, but can lead to membrane swelling due to higher sorption of plasticizing components. The capability of the crosslinked fiber to operate in aggressive environments (high CO_2 partial pressure discussed in this chapter and presence of condensable hydrocarbons discussed in the next chapter) allows its use under wider operating conditions to optimize membrane performance for specific applications.

Table 5.2: Permeance and selectivity changes from 35 ℃ to 50 ℃ and 65 ℃.

Temperature (℃)	CO_2 permeance % increase	CO_2/CH_4 selectivity % decrease
50	8	19
65	11	32

5.4.4 Effects of permeate pressure

An increase in permeate pressure reduces permeation flux as the driving force across the membrane decreases, thus increasing membrane area requirement. Therefore, operating at the lowest-possible permeate pressure is generally preferable from the stand

point of membrane cost. In practical operation, optimal permeate pressure also depends on how the permeate stream is further processed. For example, if the permeate is to be vented or flared, the permeate pressure is generally slightly above ambient pressure (about 20 psia). If the permeate is to be recompressed and delivered to a second membrane stage or re-injected into a well, increased permeate pressure (50-100 psia) reduces the required compressor power and size [13]. However, the increased permeate pressure also increases the average CO_2 concentration in the membrane, and may cause membrane swelling, thereby reducing selectivity. Figure 5.9 shows schematics of CO_2 concentration profiles in a polymeric membrane under various testing conditions. Most characterization of polymeric membranes in the literature are conducted under a low feed pressure with a vacuum permeate pressure. As shown in Figure 5.9 (a), under these idealistic conditions, the CO_2 concentration throughout the membrane is below the threshold concentration required to induce plasticization. Therefore, the membrane exhibits intrinsic high selectivity as it is in its glassy state. Some studies tested membranes at higher feed pressure to simulate real gas stream, but still with an idealistic vacuum permeate. As shown in Figure 5.9 (b), although majority of the membrane is in plasticized state (shaded area), the thin layer adjacent to downstream side is still in glassy state due to the vacuum permeate. The membrane may still show acceptable selectivity since separation is governed by the glassy region due to its higher transport resistance. In some practical operations as shown in Figure 5.9 (c), high feed pressure and non-zero permeate pressure can increase CO_2 concentration to above the threshold value, and thus swell the entire membrane. This example demonstrates the importance of testing membrane under practical permeate pressure for aggressive feeds.

In this work, all measurements were carried out with a permeate pressure of ambient pressure or above as discussed here. To evaluate fiber performance under various realistic operating conditions, the effects of permeate pressure were investigated. A 50% CO_2/50% CH_4 mixture was used as feed and the feed pressure was kept at 1000 psia while the permeate pressure was increased from 20 to 100 psia via a back pressure regulator attached to bore/permeate side of the fiber module. With accounting proper transmembrane driving force in permeance calculation, both permeance and selectivity are not affected with increasing permeate pressure as shown in Figure 5.10. These results suggest that crosslinked fibers can maintain good separation performance over a range of practical permeate pressures.

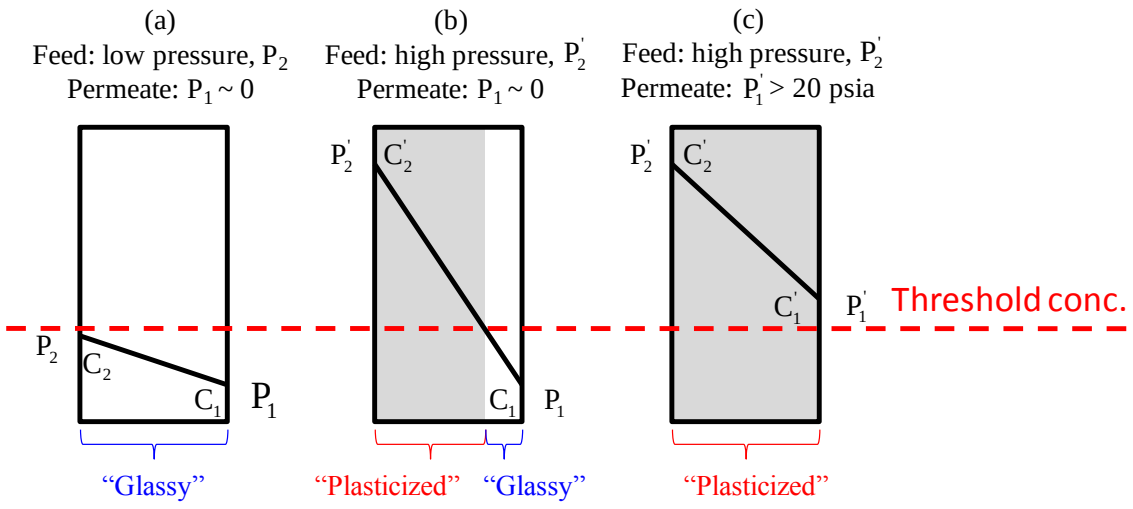

Figure 5.9: Schematic showing CO_2 concentration profiles in a polymeric membrane under various testing conditions: (a) low feed pressure with vacuum permeate, (b) high feed pressure with vacuum permeate, (c) high feed pressure with permeate above ambient pressure. Red dash line represents the threshold concentration of sorbed CO_2 required to induce plasticization. Shaded areas indicate plasticized regions where sorbed CO_2 is above the threshold concentration.

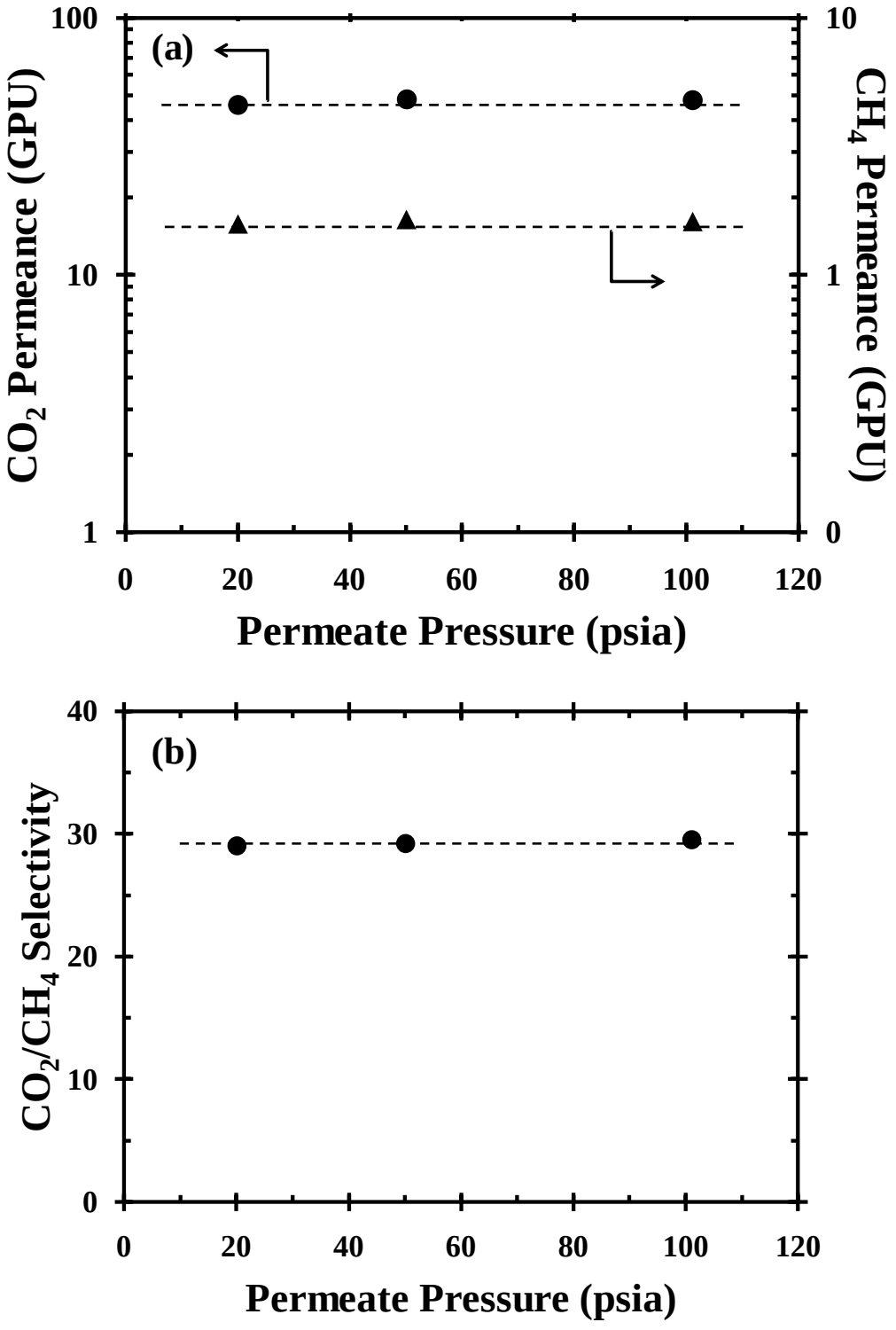

Figure 5.10: Effects of permeate pressure on (a) CO_2 and CH_4 permeance (b) CO_2/CH_4 selectivity of 350 ℃ crosslinked fibers under 50% CO_2/50% CH_4 mixed gas feed at 1000 psia with permeate pressure of 20-100 psia. Permeances were calculated using fugacity.

5.5 Effect of physical aging

The history of crosslinked fibers can be divided into two time periods: before crosslinking (precursor fiber age) and after crosslinking (crosslinked fiber age). The effect of aging on CO_2 permeance of fibers crosslinked at various precursor fiber ages is shown in Figure 5.11. All crosslinked fibers fall on the same line, indicating that aging behavior of crosslinked fibers is essentially independent of precursor fiber age. The thermal treatment used to crosslink fibers accelerates the aging process [14]; indeed, the extent of aging during thermal treatment outweighs the extent of aging at room temperature before thermal treatment. The CO_2 permeance of crosslinked fibers dropped ~35% in ~100 days but leveled off afterward. The aged crosslinked fibers show less permeance reduction as compared to aged uncrosslinked/precursor fibers (>70% permeance reduction).

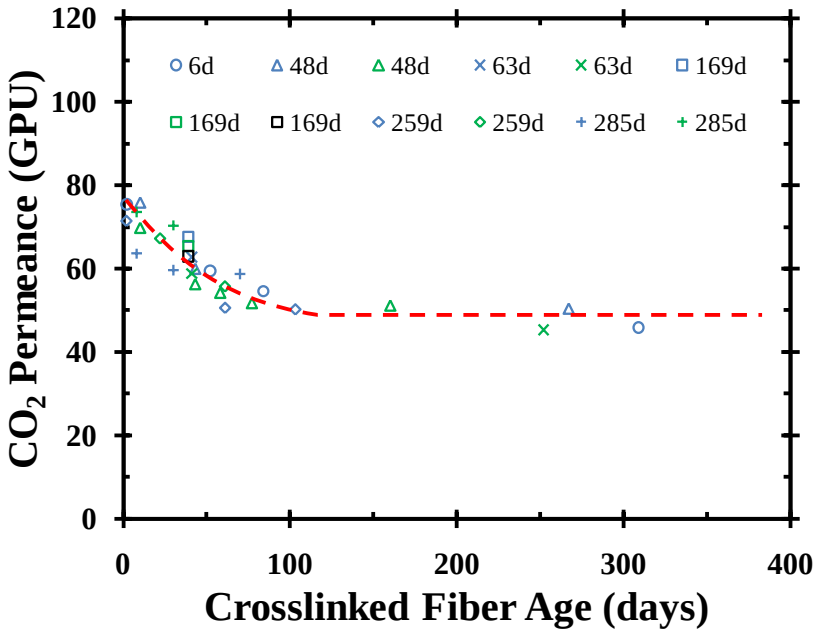

Figure 5.11: Effects of aging on CO_2 permeance of crosslinked fibers of various precursor fiber ages (numbers beside symbols). Test conditions: 50% CO_2/50% CH_4 mixed gas feed at 200 psia, 35 °C. Permeances were calculated using fugacity.

5.6 CO_2 conditioning on crosslinked fibers

As reviewed in section 2.3.4, the use of a highly sorbing penetrant, like CO_2, as a conditioning agent to tune the separation properties of glassy polymers has been reported [15-22]. Therefore, the effects of CO_2 conditioning on crosslinked fibers were investigated to explore its potential as a useful and practical tool to improve membrane productivity. Exposing a CO_2 conditioned membrane to vacuum [19] or atmosphere [21] has been shown to result in a rapid loss of the permeability enhancement, so a gas exchange protocol was employed to keep the module pressurized at all times. The fiber module was tested using a 50% CO_2/50% CH_4 mixed gas feed at 200 psia before conditioning to determine the initial performance. Then, the module was subjected to the conditioning treatment by exchanging the mixed gas feed with the CO_2 conditioning feed at the preset pressure without being exposed to the atmosphere. Note that although the CO_2 was applied from the shell side of the module during conditioning, the CO_2 pressure equilibrated quickly throughout the module since the bore side was isolated from the atmosphere after the residual CH_4 was purged out. When the conditioning treatment was completed, the CO_2 was exchanged with a 50% CO_2/50% CH_4 mixed gas feed to monitor the "after-effects" of conditioning on membrane performance. Four conditioning pressures were studied, including low-pressure (100 psig), medium-pressure (200 and 400 psig), and above-critical pressure (1500 psig). Permeance and selectivity are normalized to the values measured before conditioning to compare the relative changes in separation performance resulting from various conditioning treatments in different fibers.

The effects of CO_2 conditioning at 100 psig on crosslinked fibers were investigated. As shown in Figure 5.12 (a), there is a 15% increase in CO_2 permeance after

conditioning, and the permeance enhancement remained stable over 70 hr testing. The CO_2 permeance enhancement following conditioning can be attributed to the loosening of the polymer matrix and the reduction of the effective thickness of the dense skin [21]. The less permeance enhancement compared to another 6FDA-based polyimide fiber [21] is likely due to the restricted polymer chain mobility by crosslinking. Figure 5.12 (b) shows that CO_2 conditioning at 100 psig has a negligible effect on CO_2/CH_4 selectivity.

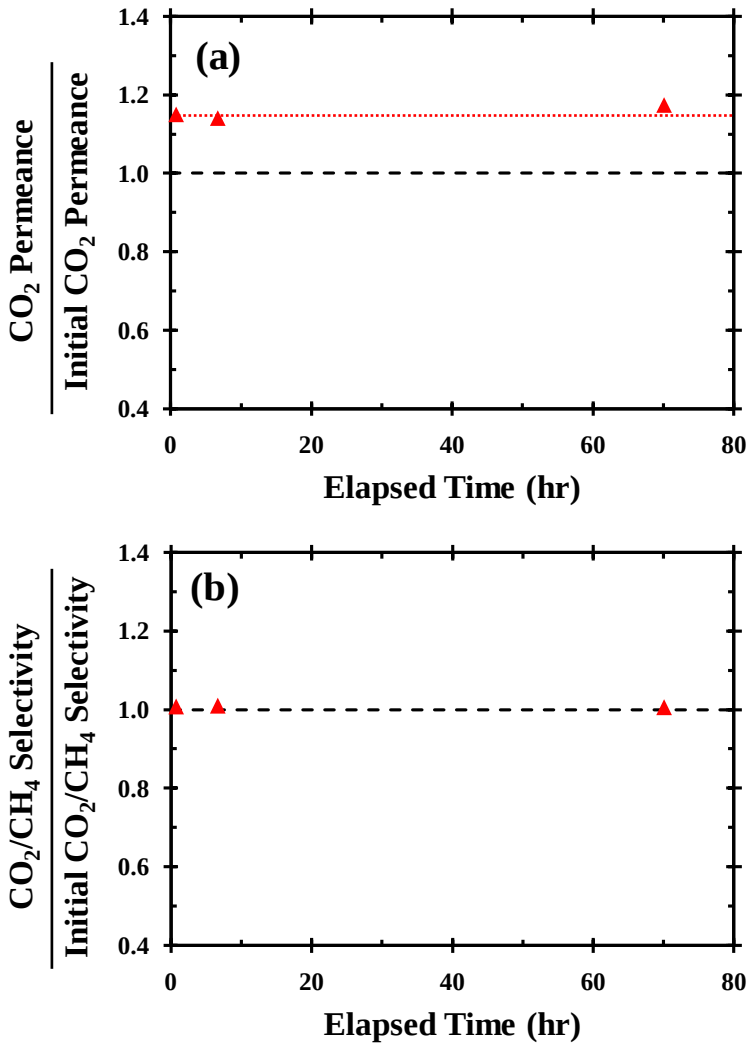

Figure 5.12: Effects of conditioning with 100 psig CO_2 for 21 hr on 350 ℃ crosslinked fibers. Test conditions: 50% CO_2/50% CH_4 mixed gas feed, 35 ℃. Permeances were calculated using fugacity. The lines are used to guide the eye.

Higher pressure CO_2 (200 psig) was applied to pursue higher permeance enhancement. Figure 5.13 (a) shows that CO_2 conditioning at 200 psig led to a maximum increase of ~35% in CO_2 permeance, which is significantly higher than that observed in the 100 psig CO_2 conditioned fiber. In addition, the conditioning treatment resulted in a small reduction in CO_2/CH_4 selectivity as shown in Figure 5.13 (c). The permeance enhancement decreased with time due to polymer chain relaxations. Note that the permeance seems to follow a logarithmic decline with time, as suggested in the plot of the permeance versus the log of the time shown in Figure 5.13 (b). The logarithmic relaxation behavior of conditioned membranes has also been observed in other glassy polymers [21, 23].

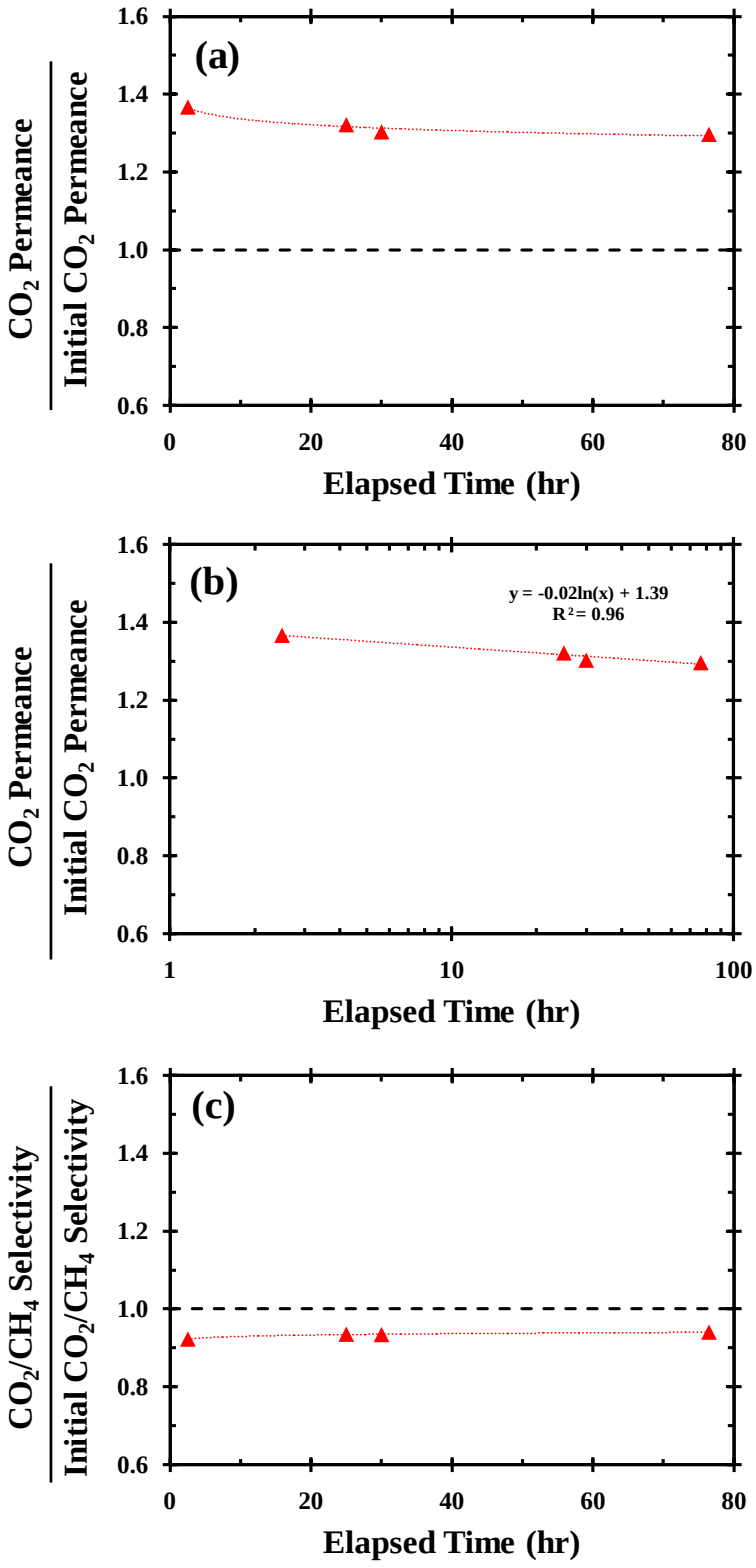

Figure 5.13: Effects of conditioning with 200 psig CO_2 for 21 hr on crosslinked fibers. Test conditions: 50% CO_2/50% CH_4 mixed gas feed, 35 ℃. Permeances were calculated using fugacity. The logarithmic trend lines are used to guide the eye.

As shown in Figure 5.13, the conditioned fiber seems to approach to a new state of enhanced permeance after three days of polymer relaxation. The conditioned fiber was tested for an extended period (50 days) to monitor the long term effects of conditioning on fiber performance and the results are shown in Figure 5.14. A steady decline of permeance enhancement over time was observed after the first three days. The magnitude (20%) and the time scale (47 days) of the permeance decline following the initial 3 days of faster decline is similar to the effects of physical aging shown in Figure 5.11. These results suggest that the conditioned fiber quickly reached a new "puffed-up" state, and then underwent physical aging similar to the unconditioned fibers.

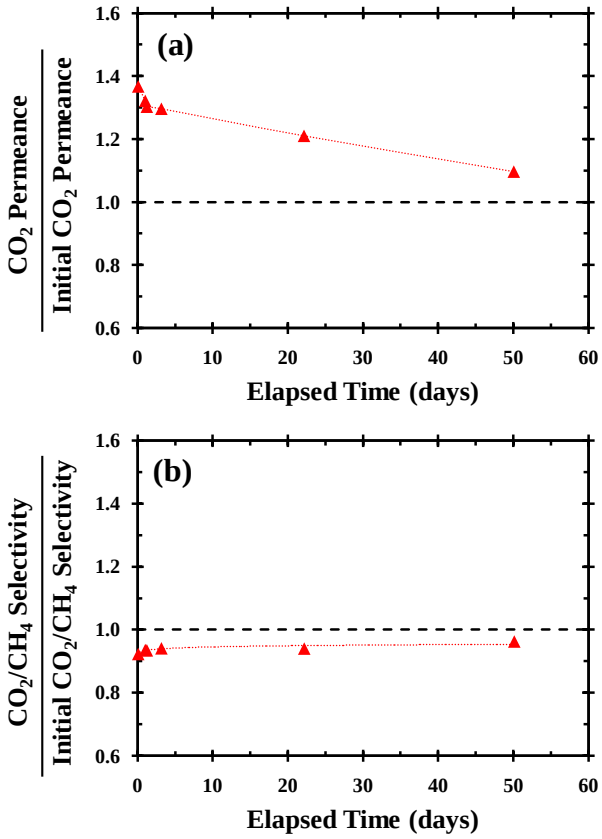

Figure 5.14: Long term effects of conditioning with 200 psig CO_2 for 21 hr on 350 ℃ crosslinked fibers. Test conditions: 50% CO_2/50% CH_4 mixed gas feed, 35 ℃. Permeances were calculated using fugacity. The lines are used to guide the eye.

Conditioning with 400 psig CO_2 was applied to the crosslinked fiber and separation performance was monitored for 45 days. As show in Figure 5.15 (b) and (c), CO_2 permeance increased ~47% with ~8% loss in selectivity immediately (within 1.5 hr) after conditioning and relaxed toward a new state of ~20% permeance enhancement with less than 5% loss in selectivity. Similar to the 200 psig conditioned fiber, a logarithmic relaxation behavior was observed in the initial 3 days as shown in Figure 5.15 (a). After the 3 day relaxation, no significant drifts were observed over protracted times (45 days), indicating that the permeance enhancement by high pressure CO_2 conditioning (400 psig) is semi-permanent as long as the CO_2/CH_4 mixture feed remains in contact with the module. Carbon dioxide conditioning has been shown to introduce semi-permanent alterations in the organization of the polymer matrix [18, 24] and the supermolecular morphology of the asymmetric membranes [21]. Similar to effects of plasticization and physical aging, the effects of conditioning are significantly pronounced in thin membrane structures, such as thin films [25] and asymmetric hollow fibers [21]. It should be noted that intensive conditioning treatments on asymmetric hollow fibers may destroy the selective skin [21] or lead to undesirable membrane compaction [26], possibly due to the dramatic drop in modulus caused by excessive swelling of the polymer matrix. The excellent plasticization resistance of crosslinked fibers offers the potential for tuning the separation performance by using high pressure CO_2 conditioning.

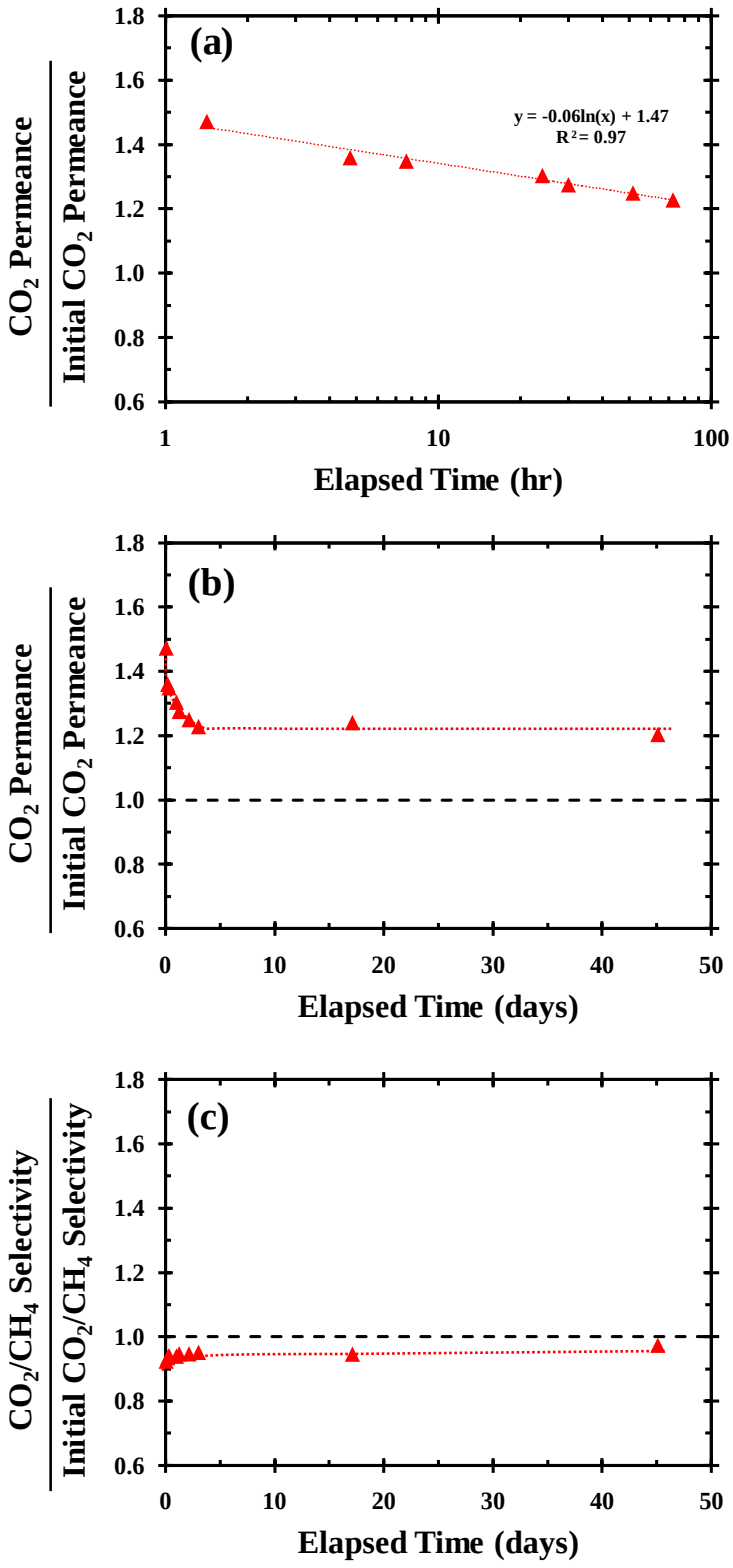

Figure 5.15: Long term effects of conditioning with 400 psig CO_2 for 22 hr on 350 ℃ crosslinked fibers. Test conditions: 50% CO_2/50% CH_4 mixed gas feed, 35 ℃. Permeances were calculated using fugacity. The lines are used to guide the eye.

To further explore the upper limit of conditioning pressure for crosslinked fibers, 1500 psig CO_2 was employed. This upper limit of 1500 psig is above the critical pressure of CO_2 (1070 psia). As shown in Figure 5.16 , the supercritical CO_2 conditioning led to a maximum increase of ~85% in CO_2 permeance with ~18% loss in selectivity. The expected logarithmic relaxation process was observed and the conditioned fiber relaxed toward a new state of ~38% increase in CO_2 permeance with ~10% reduction in selectivity after the 3 day relaxation. These results indicate that the crosslinked nature of the polymer not only maintains the size-discriminating ability under aggressive feeds but also provides mechanical strength to allow high pressure CO_2 conditioning for tuning membrane performance.

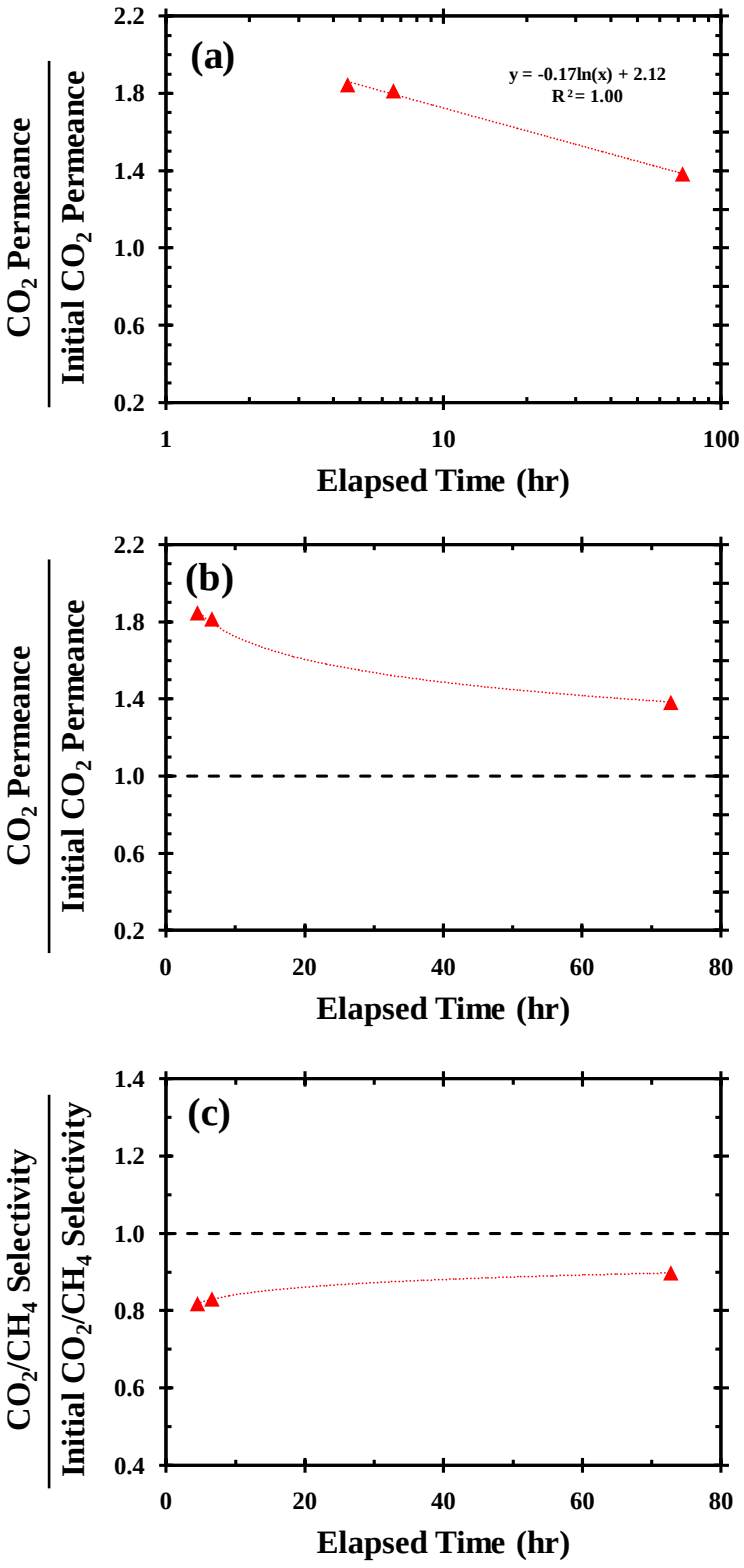

Figure 5.16: Effects of conditioning with 1500 psig CO_2 for 30 min on 350 ℃ crosslinked fibers. Test conditions: 50% CO_2/50% CH_4 mixed gas feed, 35 ℃. Permeances were calculated using fugacity. The lines are used to guide the eye.

5.7 Summary and conclusions

Thermally crosslinkable hollow fiber membranes were crosslinked at various conditions and characterized. Dissolution tests and mixed gas permeation measurements suggest that crosslinking occurs rapidly at sufficient temperature (350 ℃) while doping trace strong oxidizer (O_2 or N_2O) does not facilitate crosslinking at lower temperature (300 ℃). Crosslinking under open-air conditions caused severe skin and transition layer densification, and thus resulted in a reduction in both permeance and selectivity. Nevertheless, this undesirable effect can be avoided by crosslinking under a controlled environment, such as the most cost-efficient inert atmosphere using N_2 purge.

Crosslinking improves membrane efficiency and plasticization resistance as well as mechanical strength of fibers. The crosslinked fibers can maintain good separation performance under high CO_2 content feeds at a variety of feed pressures, temperatures, and permeate pressures. The initial stability tests showed that the crosslinked fibers have good potential for long-term operations in aggressive environments.

The aging behavior of crosslinked fibers was found to be essentially independent of precursor fiber age, but strongly affected by time after exposure to the crosslinking process. The CO_2 permeance of the crosslinked fiber showed less reduction with aging time as compared to the uncrosslinked fiber. Conditioning of membranes with a highly sorbing species, CO_2, was employed to “regain” fiber permeance by loosening the polymer matrix densified during thermal crosslinking and physical aging. The superior plasticization resistance and mechanical strength of crosslinked fibers allows CO_2 conditioning at high pressures (even above critical pressure). The permeance enhancement caused by high pressure CO_2 conditioning (400 psig) is long-lived as long

as the module remains in contact with the CO_2/CH_4 mixture feed.

5.8 References

1. A.M. Kratochvil and W.J. Koros, *Decarboxylation-induced cross-linking of a polyimide for enhanced CO_2 plasticization resistance.* Macromolecules, 2008. **41**(21): p. 7920-7927.

2. W.L. Qiu, C.C. Chen, L. Xu, L. Cui, D.R. Paul, and W.J. Koros, *Sub-T_g cross-linking of a polyimide membrane for enhanced CO_2 plasticization resistance for natural gas separation.* Macromolecules, 2011. **44**(15): p. 6046-6056.

3. W.L. Qiu, C.C. Chen, M.R. Kincer, and W.J. Koros, *Thermal analysis and its application in evaluation of fluorinated polyimide membranes for gas separation.* Polymer, 2011. **52**(18): p. 4073-4082.

4. A.F. Ismail and W. Lorna, *Penetrant-induced plasticization phenomenon in glassy polymers for gas separation membrane.* Separation and Purification Technology, 2002. **27**(3): p. 173-194.

5. J.D. Wind, D.R. Paul, and W.J. Koros, *Natural gas permeation in polyimide membranes.* Journal of Membrane Science, 2004. **228**(2): p. 227-236.

6. J.H. Kim, W.J. Koros, and D.R. Paul, *Effects of CO_2 exposure and physical aging on the gas permeability of thin 6FDA-based polyimide membranes - Part 1. Without crosslinking.* Journal of Membrane Science, 2006. **282**(1-2): p. 21-31.

7. L.M. Costello and W.J. Koros, *Thermally stable polyimide isomers for membrane-based gas separations at elevated-temperatures.* Journal of Polymer Science Part B-Polymer Physics, 1995. **33**(1): p. 135-146.

8. T.H. Kim, W.J. Koros, and G.R. Husk, *Temperature effects on gas permselection properties in hexafluoro aromatic polyimides.* Journal of Membrane Science, 1989. **46**(1): p. 43-56.

9. L.M. Costello and W.J. Koros, *Comparison of pure and mixed gas CO_2 and CH_4 permeabilities in polycarbonate: effect of temperature.* Industrial & Engineering Chemistry Research, 1993. **32**(10): p. 2277-2280.

10. X. Duthie, S. Kentish, C. Powell, K. Nagai, G. Qiao, and G. Stevens, *Operating temperature effects on the plasticization of polyimide gas separation membranes.* Journal of Membrane Science, 2007. **294**(1-2): p. 40-49.

11. A. Bos, I.G.M. Punt, M. Wessling, and H. Strathmann, *CO_2-induced plasticization phenomena in glassy polymers.* Journal of Membrane Science, 1999. **155**(1): p. 67-78.

12. L.M. Costello and W.J. Koros, *Temperature dependence of gas sorption and*

transport properties in polymers: measurement and applications. Industrial & Engineering Chemistry Research, 1992. **31**(12): p. 2708-2714.

13. B.D. Bhide and S.A. Stern, *Membrane processes for the removal of acid gases from natural gas. 1. Process configurations and optimization of operating conditions.* Journal of Membrane Science, 1993. **81**(3): p. 209-237.

14. Y. Huang and D.R. Paul, *Effect of temperature on physical aging of thin glassy polymer films.* Macromolecules, 2005. **38**(24): p. 10148-10154.

15. A.M. Kratochvil and W.J. Koros, *Effects of supercritical CO_2 conditioning on cross-linked polyimide membranes.* Macromolecules, 2010. **43**(10): p. 4679-4687.

16. A.M. Kratochvil, S. Damle-Mogri, and W.J. Koros, *Effects of supercritical CO_2 conditioning on un-cross-linked polyimide membranes for natural gas purification.* Macromolecules, 2009. **42**(15): p. 5670-5675.

17. W.J. Koros, S.M. Jordan, and G.K. Fleming *Processes to condition gas permeable membranes.* U.S. Patent 4755192, 1988.

18. S.M. Jordan, W.J. Koros, and G.K. Fleming, *The effects of CO_2 exposure on pure and mixed gas permeation behavior - comparison of glassy polycarbonate and silicone-rubber.* Journal of Membrane Science, 1987. **30**(2): p. 191-212.

19. S.M. Jordan, W.J. Koros, and J.K. Beasley, *Characterization of CO_2-induced conditioning of polycarbonate films using penetrants with different solubilities.* Journal of Membrane Science, 1989. **43**(1): p. 103-120.

20. S.M. Jordan and W.J. Koros, *Characterization of CO_2-induced conditioning of substituted polycarbonates using various exchange penetrants.* Journal of Membrane Science, 1990. **51**(3): p. 233-247.

21. S.M. Jordan, M.A. Henson, and W.J. Koros, *The effects of carbon-dioxide conditioning on the permeation behavior of hollow fiber asymmetric membranes.* Journal of Membrane Science, 1990. **54**(1-2): p. 103-118.

22. M.R. Coleman and W.J. Koros, *Conditioning of fluorine-containing polyimides. 2. Effect of conditioning protocol at 8% volume dilation on gas-transport properties.* Macromolecules, 1999. **32**(9): p. 3106-3113.

23. S.M. Jordan. *History-dependent permeation behavior of glassy polymers.* Ph.D. Dissertation, The University of Texas at Austin, Austin, TX, 1989.

24. G.K. Fleming and W.J. Koros, *Carbon dioxide conditioning effects on sorption and volume dilation behavior for bisphenol A-polycarbonate.* Macromolecules, 1990. **23**(5): p. 1353-1360.

25. N.R. Horn and D.R. Paul, *Carbon dioxide plasticization and conditioning effects in thick vs. thin glassy polymer films.* Polymer, 2011. **52**(7): p. 1619-1627.

26. M. Al-Juaied and W.J. Koros, *Performance of natural gas membranes in the presence of heavy hydrocarbons.* Journal of Membrane Science, 2006. **274**(1-2): p. 227-243.

CHAPTER 6

EFFECTS OF MINOR IMPURITIES ON PERFORMANCE OF THERMALLY CROSSLINKED HOLLOW FIBER MEMBRANES

6.1 Overview

In Chapter 5, the impact of crosslinking on fiber membrane performance was discussed. The excellent performance stability under high CO_2 content feeds at a variety of feed pressures, temperatures, and permeate pressures demonstrated that crosslinked fibers are indeed promising for aggressive natural gas applications. However, the mixed gas permeation data in the previous two chapters are limited to ideal, clean CO_2/CH_4 binary mixtures. In this chapter, crosslinked fibers were further characterized using more realistic feeds containing different concentrations of various impurities, including toluene, heptane, and ethylene glycol. The crosslinking and performance stability of crosslinked fibers under aggressive wet acid gas condition was also investigated.

6.2 Pretreatment for CO_2 removal membranes

Proper pretreatment is critical to all membrane systems, because inadequate pretreatment could undermine membrane performance and lifetime. The amount of pretreatment is dependent on the durability of membranes used and the quality of the gas to be processed. Robust membrane may require less pretreatment and further reduce the system footprint, which is especially important for offshore applications. A typical pretreatment train consists of a coalescing filter to remove liquid, a adsorbent bed to

remove heavy hydrocarbons, a particle filter to removes any dust from the adsorbent bed, and a heater to prevent liquid condensation [1, 2]. Large portions of heavy hydrocarbons are removed from raw natural gas for both practical and economical considerations [3]. Removal of the heavy hydrocarbons is needed to prevent condensation in the pipeline and recovery of these high value natural gas liquids (NGLs) from the process can be more profitable than the processed natural gas in some cases. However, it has been shown that event trace amount of these condensable impurities can cause severe and irreversible damage to polymeric membranes [4-6]. Although nowadays most membrane units are installed with pretreatment systems, it is impractical to completely remove all impurities. Moreover, any upsets in the pretreatment train, or a sudden surge in impurity content in the feed can cause accidental exposure to high levels of heavy hydrocarbon impurities and may result in destruction of the membranes. Therefore, it is necessary to determine membrane performance in the presence of various levels of condensable impurities. In this work, toluene and heptane are selected as the model aromatic and aliphatic impurities, respectively. The range of impurity content in the feed streams was selected to simulate the harsh environment may encounter in aggressive applications. Figure 6.1 shows the heavy hydrocarbon content before and after pretreatment in an enhanced oil recovery facility [2]. The highest content of hydrocarbon (C7) impurities tested in this work is 750 ppm, which is well above the un-pretreated feed in order to simulate the event of pretreatment failure. On the other hand, the lower limit of 30 ppm represents the typical impurity level of a pretreated feed.

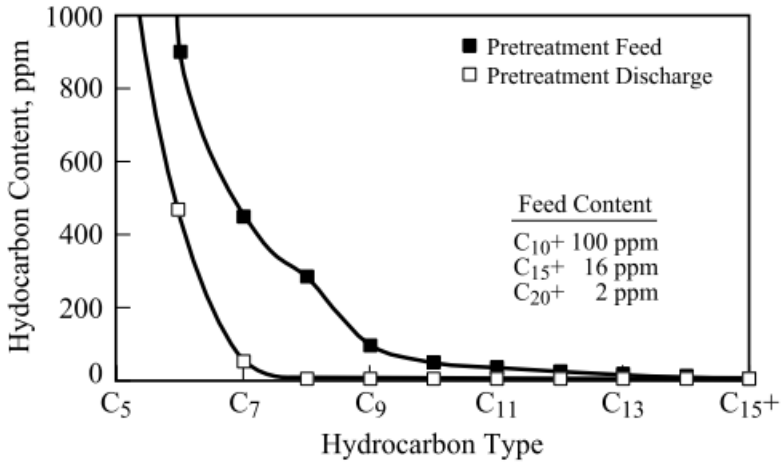

Figure 6.1: Performance of pretreatment for membranes used in an enhanced oil recovery application [2].

6.3 Effects of toluene impurity on CO_2/CH_4 separation

6.3.1 Crosslinked fiber performance in 50% CO_2 feeds with toluene

To investigate the impact of toluene impurity on separation performance, the crosslinked fibers were tested with a clean feed (50% CO_2/50% CH_4) and then exposed to toluene contaminated feeds with increasing concentration: 30 ppm, 100 ppm, 200 ppm, 500 ppm, and 750 ppm. The measurements were carried out at 35 ℃ and the results are shown in Figure 6.2. As mentioned in Chapter 5, the reduction in permeances and selectivity with increasing pressure (in the absence of toluene), is due to dual mode sorption effects. As shown in Figure 6.2 (a), there is no increase in CO_2 permeance with increasing pressure for all toluene contaminated feeds, indicating that toluene does not cause plasticization in all tested conditions. The greater reduction in permeance with increasing toluene concentration can be attributed to a combination of competitive sorption [7-11] and antiplasticization effects [9, 10, 12].

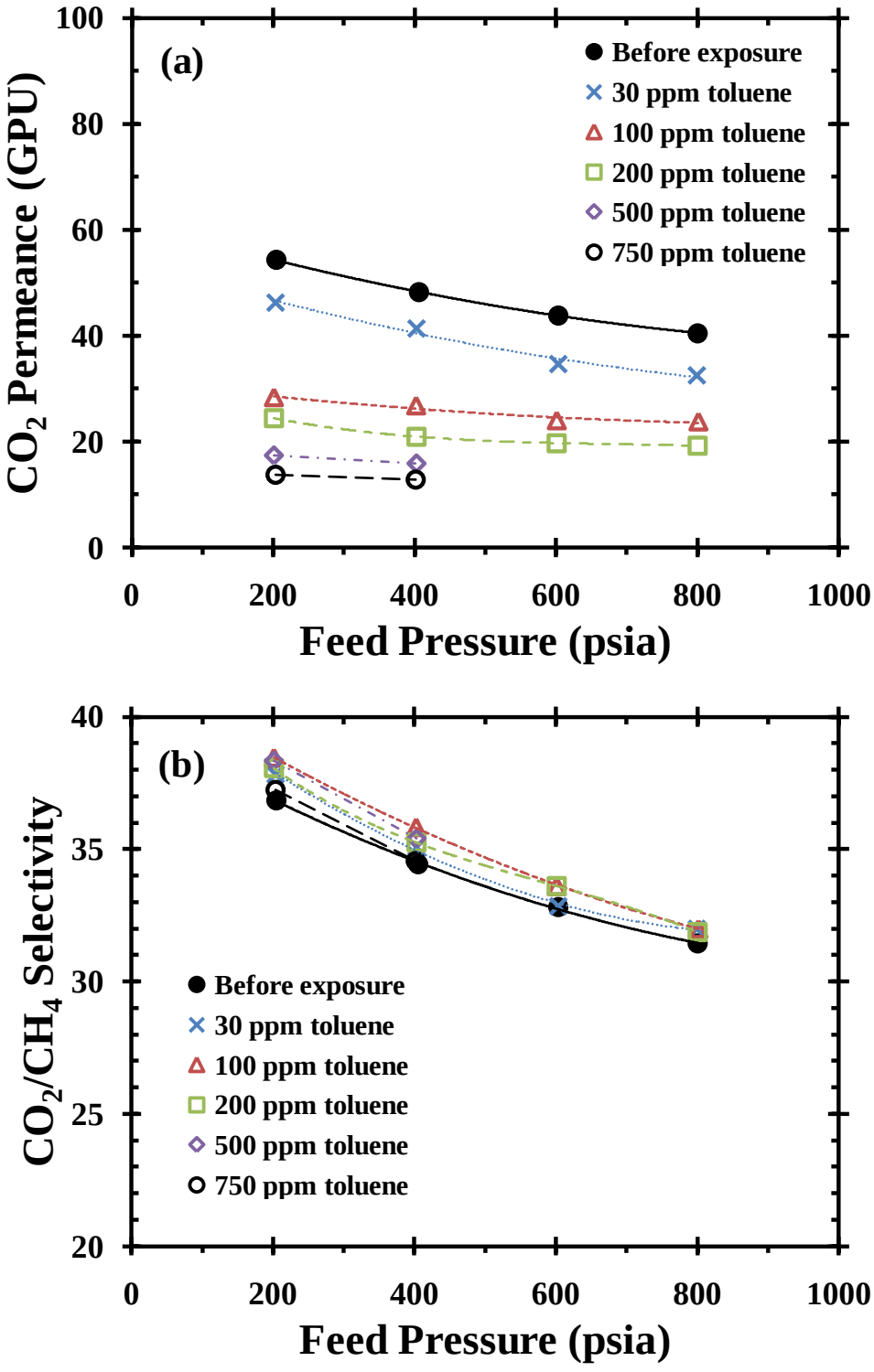

Figure 6.2: Effects of toluene on (a) CO_2 permeance and (b) CO_2/CH_4 selectivity of crosslinked fibers. Test conditions: ~50% CO_2, 0-750 ppm toluene balanced with CH_4; 35 °C. Permeances were calculated using fugacity at corresponding feed pressures. The lines are used to guide the eye.

Figure 6.3 illustrates the competitive sorption effects in the presence of a highly condensable component, such as toluene in this case. Since toluene is much more condensable than CO_2 and CH_4, toluene molecules can occupy unrelaxed free volume in the polymer matrix and block transport pathways [8]. The reduction in permeance and slight increase in selectivity shown in Figure 6.2 (b) cannot be explained by competitive sorption alone [9, 10]. Antiplasticization effects caused by toluene have been observed in Matrimid [12, 13] and an ester crosslinked polyimide [9, 10]. The sorbed toluene molecules act as antiplasticizers, retarding polymer chain segmental mobility, thereby decreasing the permeabilities of all penetrants. The slight selectivity enhancement can be attributed to the restricted chain mobility due to antiplasticization, in agreement with antiplasticized membranes reported elsewhere [9, 14, 15]. A detailed study of free volume in the membranes via sorption would help determine the extent of antiplasticization vs. competitive sorption. Such a study, however, was beyond the scope of this research.

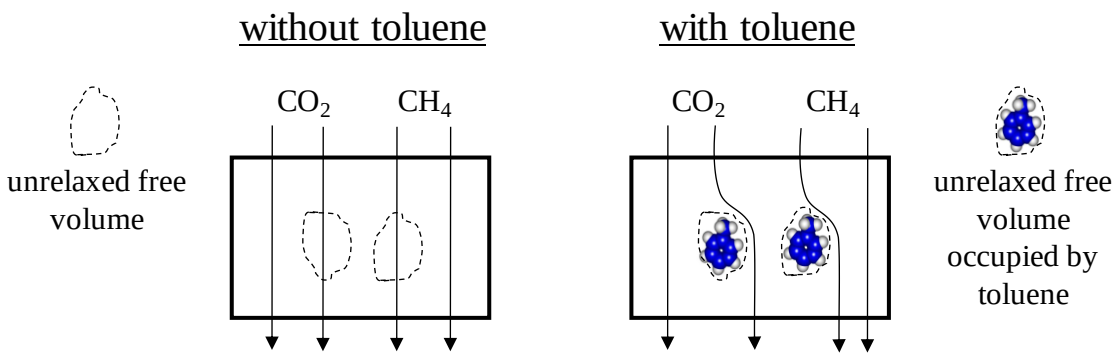

Figure 6.3: Schematics showing the competitive sorption effects of toluene on permeation. Adapted from Ref. [8].

Due to its highly condensable nature, instead of antiplasticization, toluene often causes membrane plasticization and results in a drastic loss in selectivity by as much as 50% [7, 13, 16, 17]. The transition from antiplasticization behavior at low impurity concentration to plasticization behavior at higher concentration has been observed in Matrimid® hollow fibers [13] as shown in Figure 6.5. Such transition was not observed in crosslinked fibers, even in the presence of high concentration of toluene. Moreover, strong swelling and plasticization of the polymer matrix may damage the selective skin layer and cause the compaction of the transition layer (shown in Figure 6.4) in the asymmetric hollow fiber structure [4, 8, 17]. These morphology alterations may be responsible for permanent and non-recoverable performance loss caused by heavy hydrocarbon contamination [4, 6, 17].

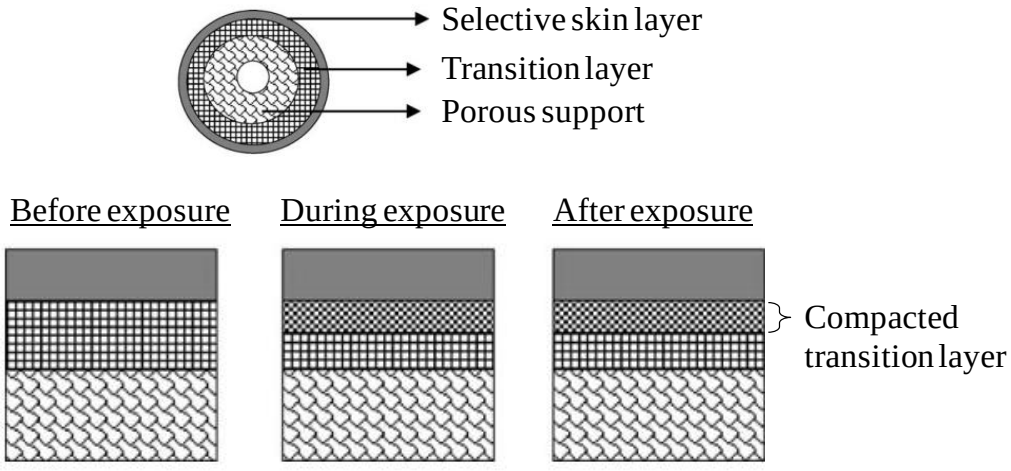

Figure 6.4: Schematic showing the compaction effect. The compacted transition layer adds a less selective resistance (e.g., Knudsen selective), thereby reducing overall selectivity. Adapted from Ref. [8].

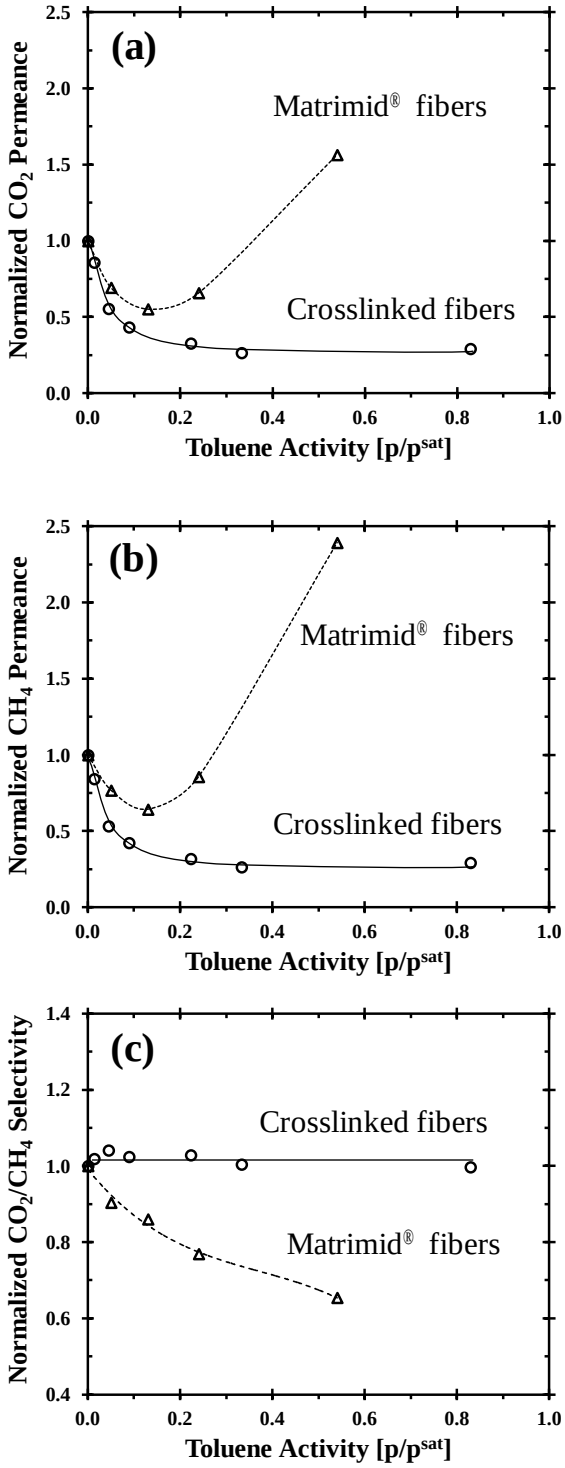

Figure 6.5: Effects of toluene on Matrimid® fibers [13] and crosslinked fibers at 35 °C. Matrimid® fibers were tested using 10% CO_2 feeds at 400 psia. Crosslinked fibers were tested using 50% CO_2 feeds at 400 psia except the data at the highest toluene activity (0.83) was measured at 1000 psia. Permeances and selectivity were normalized by those before toluene exposure. The lines are used to guide the eye.

6.3.2 Recovery of membrane performance after toluene exposure

The results from toluene exposure experiments show no evidence of skin plasticization or transition layer compaction by toluene over the range of aggressive conditions. The depressed permeance is the result of sorption competition and antiplasticization rather than permanent alteration of the membrane structure, suggesting that recovery of performance should be possible once sorbed toluene molecules are removed from the membrane. This section describes the reversibility of toluene exposure effects on membrane performance.

The fiber exposed to toluene contaminated feeds discussed in the previous section was purged/tested using a clean feed (50% CO_2/50% CH_4) and the results are shown in Figure 6.6. The large reduction in CO_2 permeance during exposure to 750 ppm toluene was readily recovered via purging with a clean feed, and reached ~95% of permeance before exposure. These results indicate that the permeance loss can be recovered by simply removing toluene in the feed. The recoverable permeance loss and maintained high selectivity again suggests that toluene impurity neither damaged the skin nor caused membrane compaction.

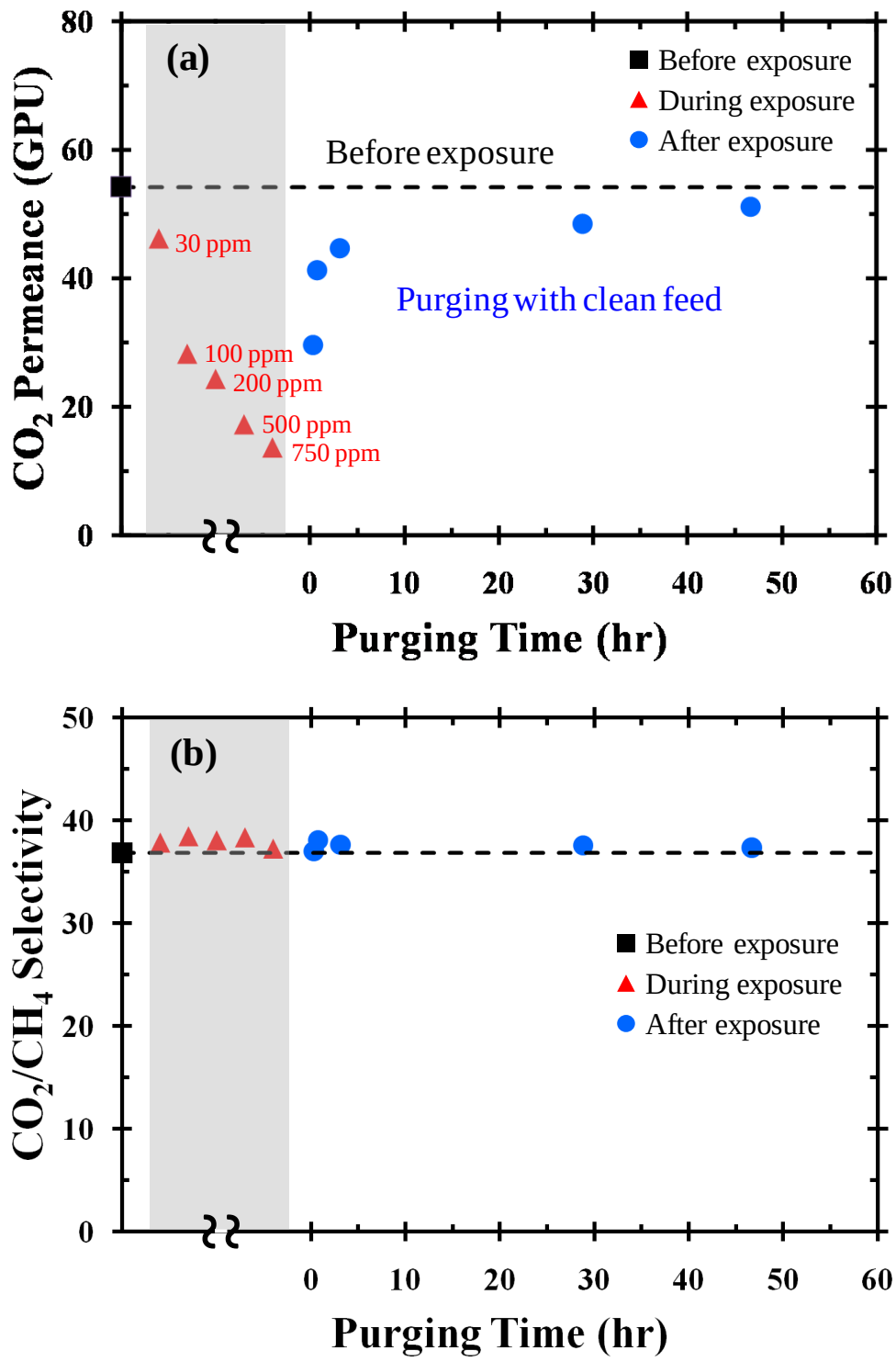

Figure 6.6: Crosslinked fiber performance under a clean feed (50% CO_2/50% CH_4) after toluene exposure with comparisons to crosslinked fiber performance before and during exposure to 30-750 ppm toluene. Dash line represents performance before exposure. Shaded areas represents during exposure. Test conditions: 200 psia, 35 ℃.

6.3.3 Temperature effects on toluene exposure

The effects of operating temperature on fiber performance in the presence of toluene were investigated. Results shown in Figure 6.7 indicate that 30 ppm toluene did not affect selectivity but reduced 15-20% of permeance. It is expected that the effect of toluene should be reduced at elevated temperature due to decreased sorption of toluene. Operating at 65 ℃ compensates for permeance loss caused by 30 ppm toluene, but at the cost of significant selectivity loss. The decrease in selectivity at 65 ℃ is due to the reduced sorption advantage of CO_2 over CH_4 with increasing temperature as discussed in section 5.4.3. These results suggest that operating at 35 ℃ is preferable for CO_2/CH_4 feeds containing 30 ppm toluene (typical concentration after pretreatment). As mentioned in section 5.4.3, lower temperature is generally preferable in terms of intrinsic CO_2/CH_4 selectivity for glassy polymers, but the catastrophic failure upon heavy hydrocarbon exposure may require membranes to operate at higher temperature to mitigate the damage. The ability of crosslinked fiber to process toluene contaminated feeds over a range of temperature provides more flexibility for performance optimization.

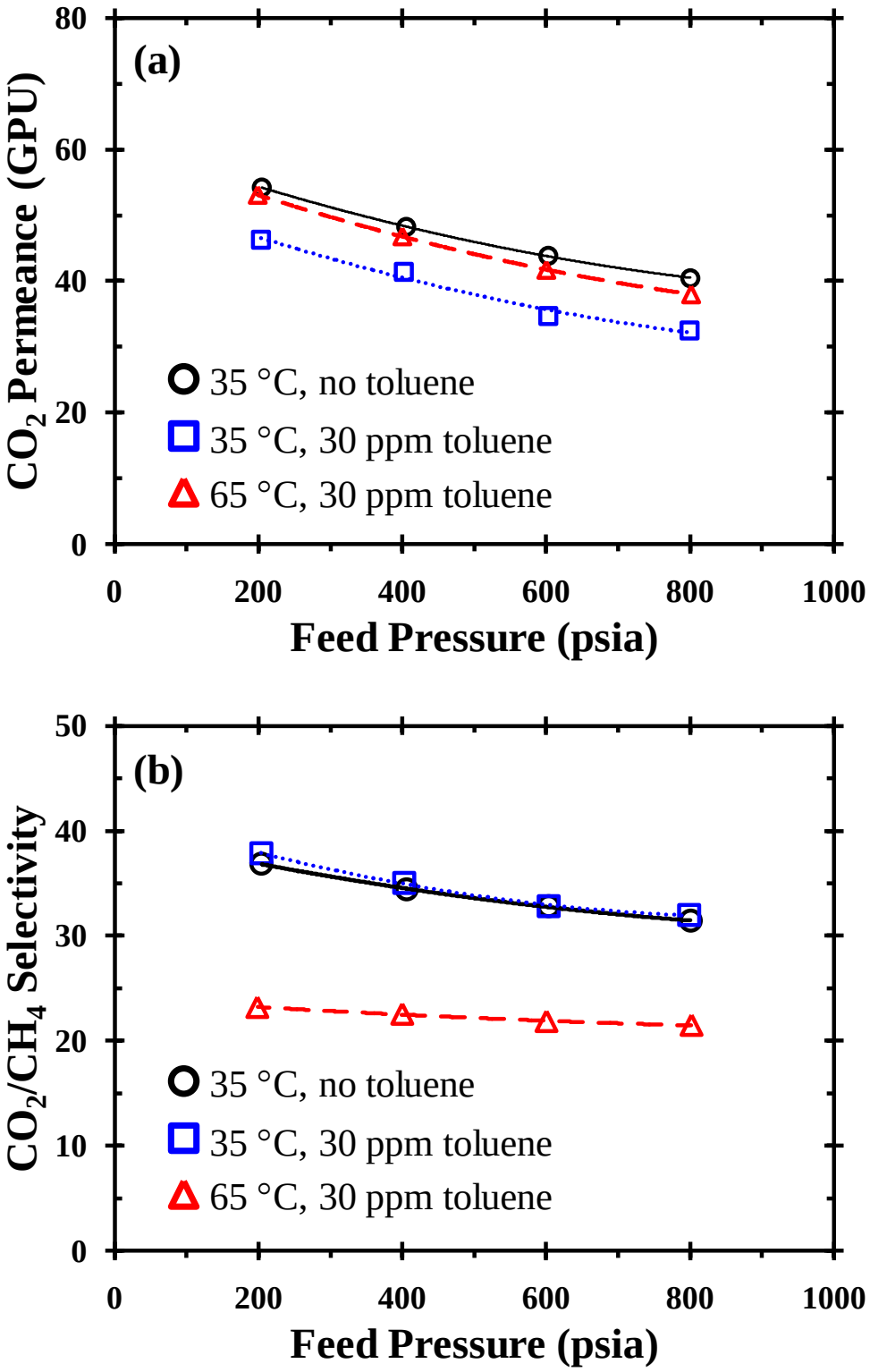

Figure 6.7: Effect of operating temperature on toluene exposure. Test conditions: ~50% CO_2, with or without 30 ppm toluene balanced with CH_4; 200 psia, 35 ℃ or 65 ℃. Permeances were calculated using fugacity. The lines are used to guide the eye.

6.3.4 Performance stability under high pressure feeds with toluene

To simulate the event of pretreatment failure, the performance stability over time was tested using a toluene-containing feed (750 ppm toluene, 50% CO_2 balanced with CH_4) at 1000 psia and the results are shown in Figure 6.8. The results of the time stability test showed negligible drifting of permeances and selectivity over 68 hr testing under a high toluene activity (~0.83) feed. These results indicate that the crosslinked fibers have good hydrocarbon resistance.

The greatly depressed permeance (65-70% reduction compared to toluene-free feed) suggests that toluene content should be reduced for higher productivity; however, recall that the permeance loss upon toluene exposure can be recovered after toluene is removed from the feed. Therefore, despite temporary productivity loss, the crosslinked fibers can withstand accidental exposure to high levels of toluene. The impurity-tolerant ability should allow the crosslinked fibers to survive the events of catastrophic pretreatment failures or a sudden surge of impurity content in the feed.

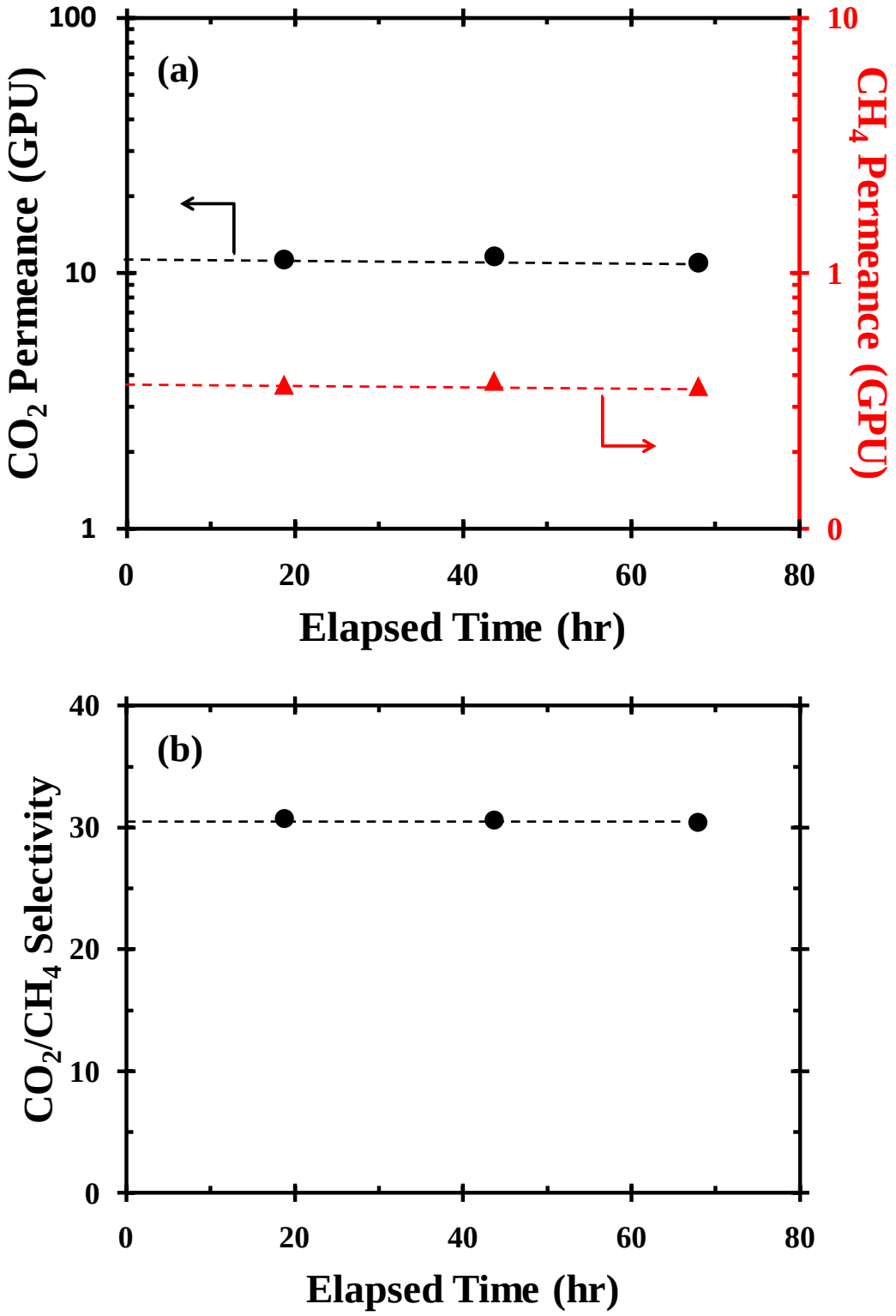

Figure 6.8: Stability over time under a toluene contaminated feed: (a) CO_2 and CH_4 permeance (b) CO_2/CH_4 selectivity. Test conditions: 750 ppm toluene, 50% CO_2 balanced with CH_4; 1000 psia, 35 °C. Permeances were calculated using fugacity.

6.4 Effects of heptane impurity on CO_2/CH_4 separation

6.4.1 Crosslinked fiber performance in 50% CO_2 feeds with heptane

Effects of heptane, as a model aliphatic contaminant, on separation performance were also investigated. In this study, two levels of heptane concentration, 33.4 and 750 ppm, in mixed gas feeds (~50% CO_2 balanced with CH_4) were evaluated to compare with the effects of toluene impurity at the same levels. The results are shown in Figure 6.9 along with data from toluene exposure experiments for comparison. Given the results from toluene impurity studies, it is expected that the presence of heptane in the feeds should not damage the crosslinked fibers, evidenced by the maintained high selectivities shown in Figure 6.9 (b). Similar to the reduction in CO_2 permeance seen in the toluene impurity studies, heptane contamination also caused permeance loss, but to much less extent as compared to toluene contamination at the same concentration level. This may be attributed to stronger interactions from π-electrons in the aromatic ring between toluene molecules and aromatic groups in polymer chains. Strong sorption of aromatic compounds has been observed in polyimides. For example, toluene (aromatic) has more than twice higher equilibrium sorption in Matrimid® than heptane (linear aliphatic) at 35 ℃ [18]. A detailed sorption study would facilitate a better understanding of the fundamental mechanism responsible for the stronger effects of toluene compared to heptane. Such a study, however, was beyond the scope of the present work.

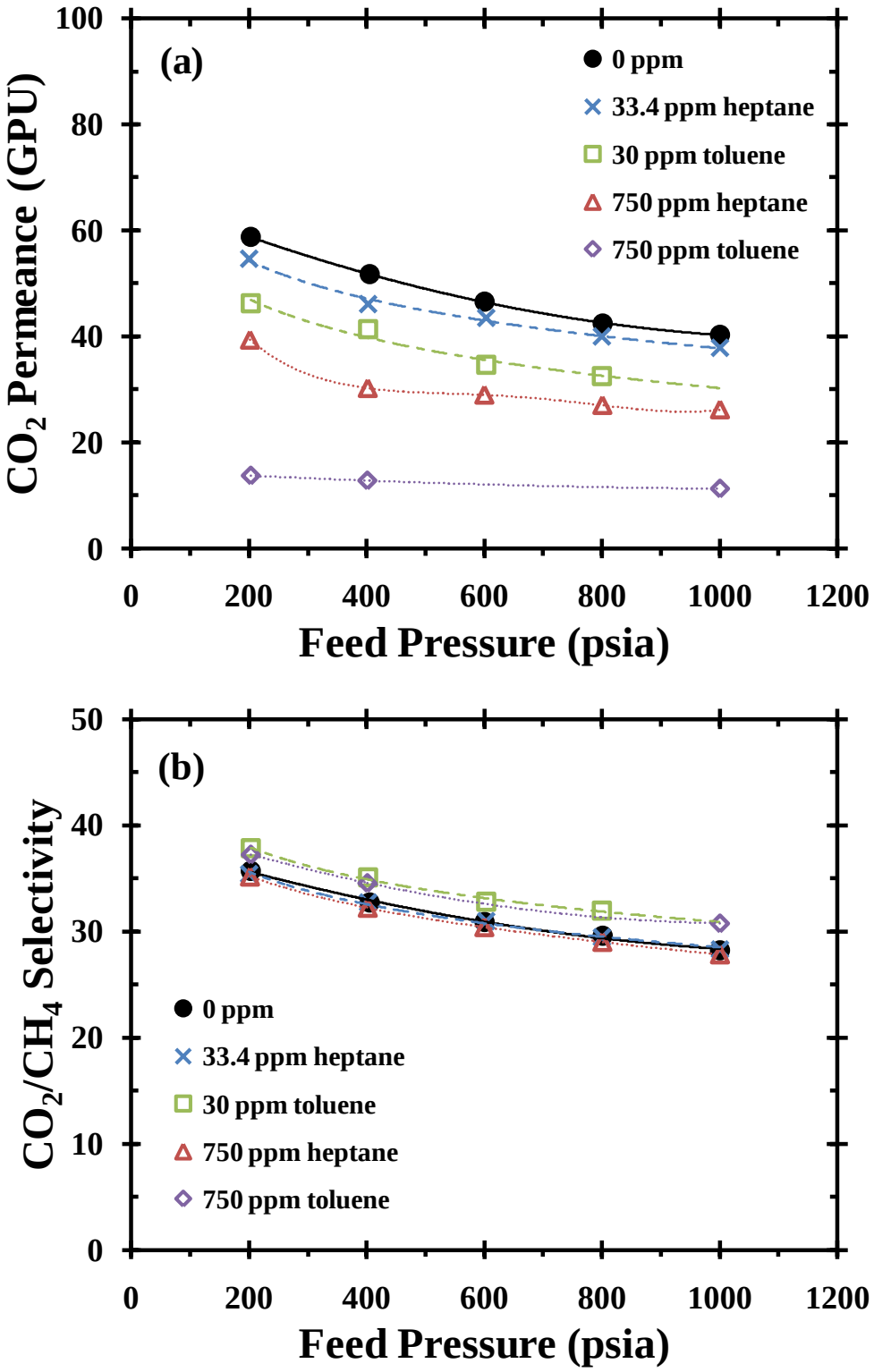

Figure 6.9: Effects of heptane on (a) CO_2 permeance, and (b) CO_2/CH_4 selectivity of crosslinked fibers. Test conditions: ~50% CO_2, 33.4 or 750 ppm heptane balanced with CH_4; 35 ℃. Permeances were calculated using fugacity at corresponding feed pressures. Data from toluene exposure experiments are shown for comparison.

6.4.2 Performance stability under high pressure feeds with heptane

The performance stability over time under low and high heptane activity feeds was tested using heptane-containing feeds (33.4 ppm or 750 ppm heptane, 50% CO_2 balanced with CH_4) at 1000 psia. The results of the time stability test are shown in Figure 6.10. These results indicate that the crosslinked fibers remained stable over 52 hr testing with 33.4 ppm heptane contaminated feed and 69 hr testing with 750 ppm heptane contaminated feed. The good performance stability once again demonstrated the hydrocarbon resistance of crosslinked fibers.

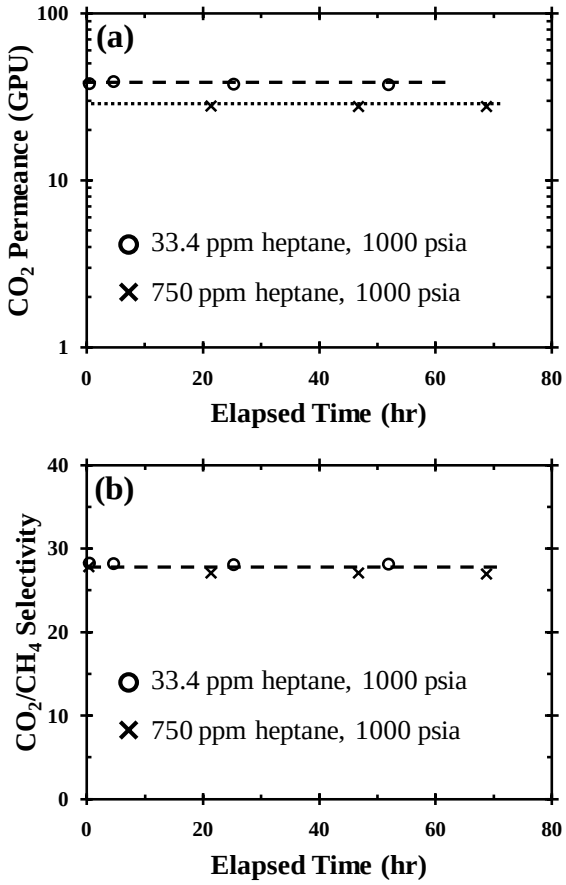

Figure 6.10: Stability over time under heptane contaminated feeds: (a) CO_2 and CH_4 permeance (b) CO_2/CH_4 selectivity. Test conditions: 33.4 ppm or 750 ppm heptane, 50% CO_2 balanced with CH_4; 1000 psia, 35 °C. Permeances were calculated using fugacity.

6.4.3 Recovery of membrane performance after heptane exposure

To observe the reversibility of heptane exposure effects, after the fiber had been subjected to heptane contaminated feeds, it was purged and tested using a clean feed (50% CO_2/50% CH_4) to monitor the performance recovery. As shown in Figure 6.11, the permeance loss during heptane exposure was recovered, as expected, after few hours of clean feed purging. The slightly higher permeance after exposure may be due to conditioning effects during ~3 day exposure to high heptane activity (> 0.5) feed.

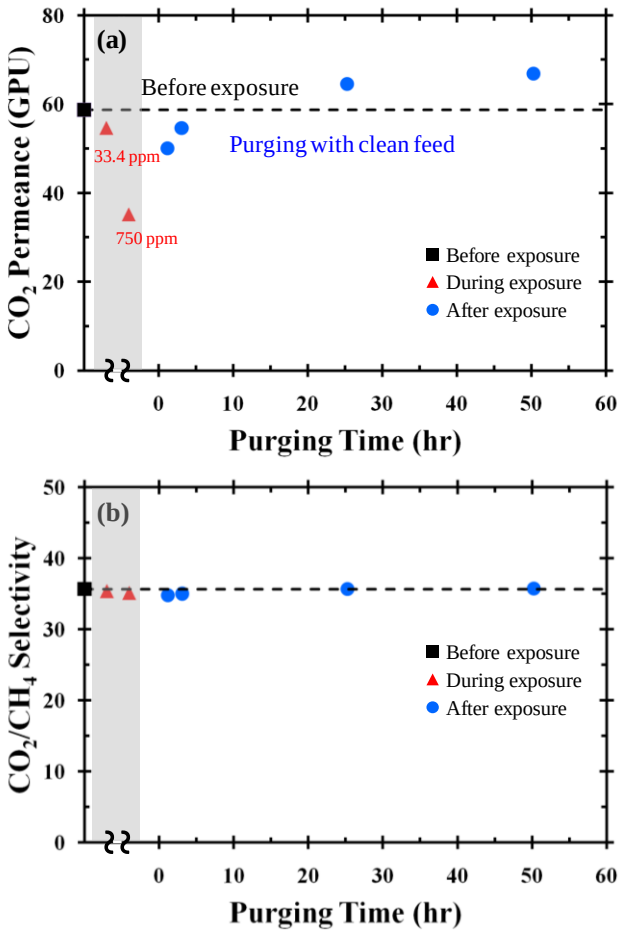

Figure 6.11: Crosslinked fiber performance with a clean feed (50% CO_2/50% CH_4) after heptane exposure with comparisons to crosslinked fiber performance before and during exposure to 33.4 and 750 ppm heptane. Dash line represents performance before exposure. Shaded areas represents during exposure. Test conditions: 200 psia, 35 ℃.

6.5 Stability against water-saturated acid gas

Natural gas also contains water and is usually removed at or near the wellhead to avoid hydrate formation and corrosion in the pipeline. The most widely used technology for natural gas dehydration is glycol absorption, which usually reduce water concentration to ~100 ppm. However, this trace amount of water can still be problematic for some membranes. For example, cellulose acetate membranes have been shown to be particularly sensitive to water. Moisture levels higher than 20% RH can cause an irreversible loss in flux due to membrane compaction [19]. Strong water-induced plasticization effects were observed in polyethersulfone and polysulfone films, resulting in a drastic loss in selectivity (~45% and ~37% loss for polyethersulfone and polysulfone films, respectively) [20]. Moreover, some types of crosslinkage (such as ester linkages [21] or amide linkages) as well as polymer backbones can potentially be hydrolyzed in aggressive acid gas conditions present in high CO_2 feed streams. Therefore, the hydrolytic stability of crosslinked fibers was evaluated.

Similar to previous hydrocarbon impurity studies, this experiment attempts to simulate the worst case scenario of pretreatment failures by exposing the crosslinked fiber to a high pressure water-saturated acid gas feed. The crosslinked fiber was tested before and after exposure to a water-saturated 50% CO_2/50% CH_4 mixture at 1000 psia for ~5 hr at room temperature (~22 ℃). Due to the limitation of experimental equipment, separation performance was not measured during wet acid gas exposure. The separation performances of the crosslinked fiber before exposure, after exposure, and after simple drying are shown in Figure 6.12. The decrease in CO_2 permeance after exposure is likely due to the sorbed water molecules occupying unrelaxed free volume (Langmuir sorption

sites), as indicated by the permeance seems to fall to a level where permeation occurs through Henry's mode alone. Sorption analysis would help confirm this, though it was beyond the scope of the present work. After permeation tests, simple drying was then pursued by storing the module in a box with desiccants at room temperature followed by vacuum drying in a oven at 110 ℃. The maintained high selectivities, good plasticization resistance and the recovered permeance upon simple drying suggest that wet acid gas neither plasticized the membrane nor jeopardized the efficacy of crosslinking.

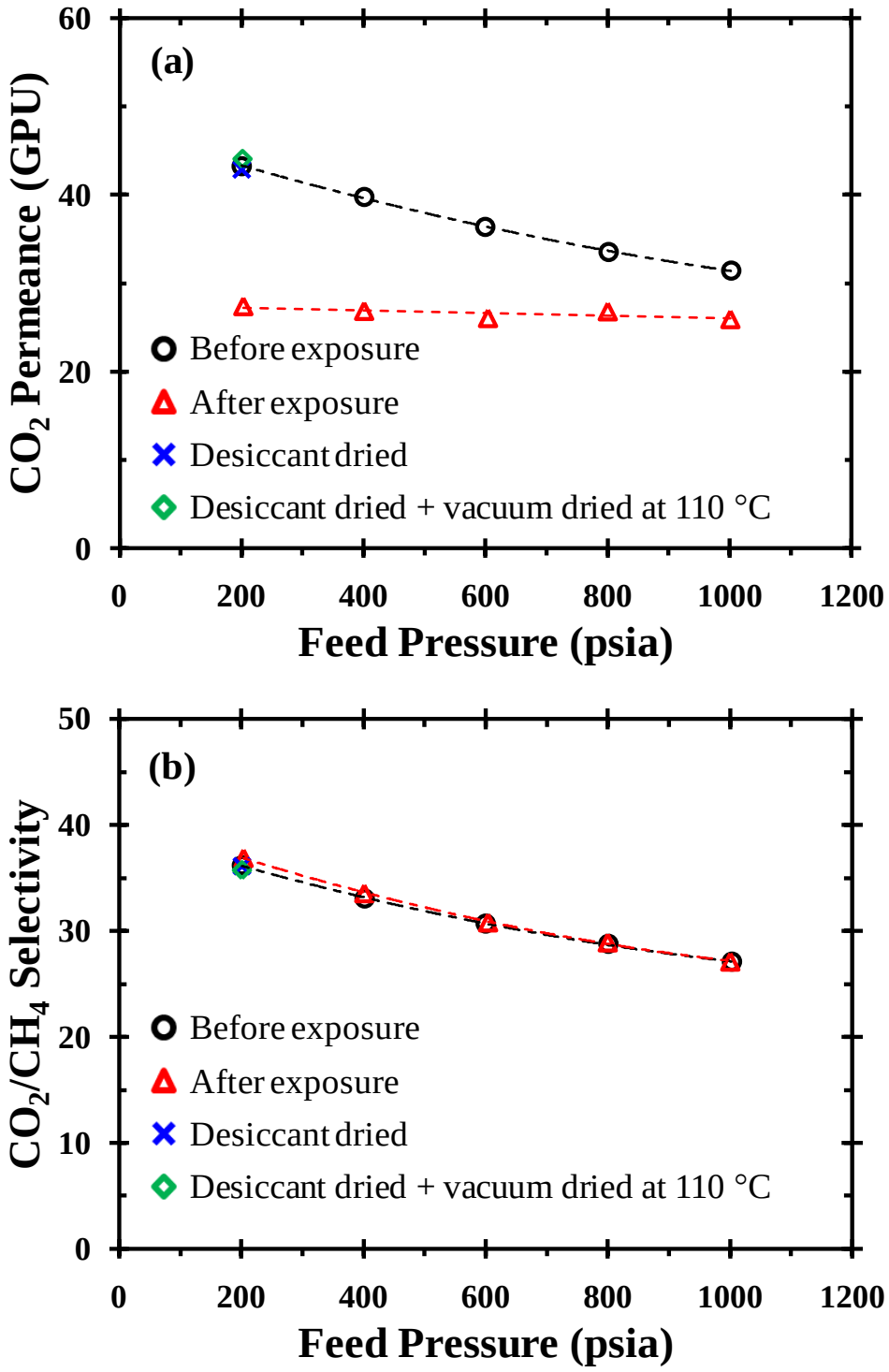

Figure 6.12: Effects of wet acid gas exposure on (a) CO_2 permeance, and (b) CO_2/CH_4 selectivity. The fiber was tested before and after exposed to water-saturated 50% CO_2/50% CH_4 mixtures at 1000 psia for ~5 hr at room temperature. Drying: desiccant dried for ~4 days, vacuum dried at 110 ℃ for ~ 2 days. Test conditions: 50% CO_2/50% CH_4 mixed gas feed, 35 ℃. Permeances were calculated using fugacity at corresponding feed pressures.

6.6 Effects of glycol impurity on CO_2/CH_4 separation

As mentioned in the previous section, glycol is widely used for natural gas dehydration and is commonly carried over from dehydration units as vapor and in entrained liquid form. Similar to hydrocarbon impurities, glycol is generally removed from the gas stream during pretreatment, as it may damage polymeric membranes [6]. The objective here is, again, to test membrane durability during pretreatment failure or upset. To investigate the effects of glycol carryover on the membrane performance, the crosslinked fiber was tested using a 32 ppm ethylene glycol contaminated feed. The separation performances of the crosslinked fiber before exposure, during exposure and after exposure to the ethylene glycol contaminated feed are shown in Figure 6.13. The results indicate that presence of ethylene glycol does not affect membrane performance. Note that vapor pressure of ethylene glycol at 35 ℃ is very low (~0.004 psia), 32 ppm indeed represents high level of contamination. Ethylene glycol partial pressures in all test conditions are higher than its saturation pressure, i.e. ethylene glycol may contact the membrane in both vapor and liquid form, similar to the event of severe carryover due to inadequate pretreatment.

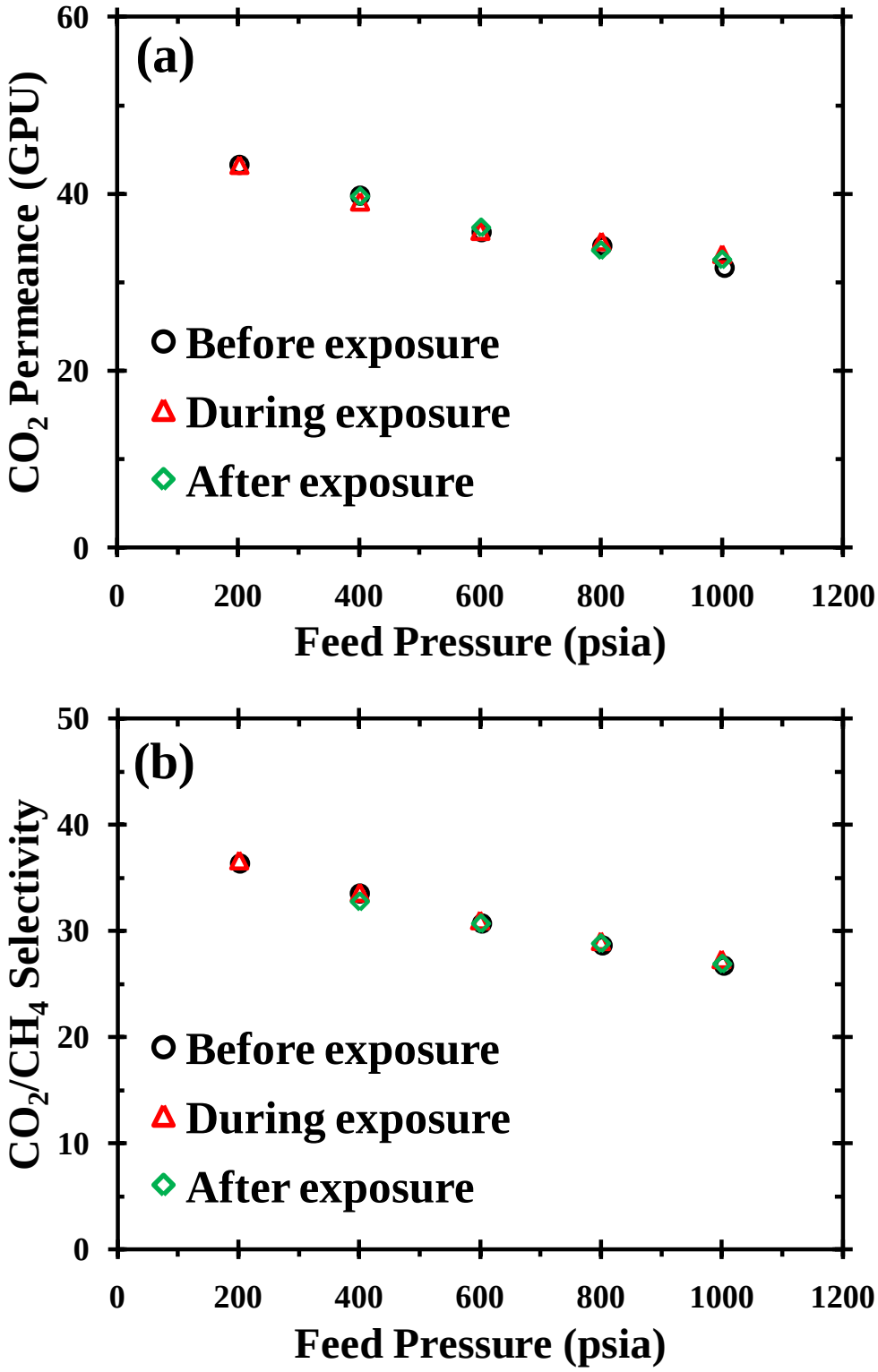

Figure 6.13: Effects of ethylene glycol on membrane performance. Test conditions: 49.8% CO_2, with or without 32 ppm ethylene glycol balanced with CH_4; 35 ℃. Permeances were calculated using fugacity at corresponding feed pressures.

6.7 Summary and conclusions

Effects of condensable heavy hydrocarbons on separation performance of crosslinked fibers were investigated. No indication of membrane plasticization was observed over ~3 days of stability tests using a high pressure feed that is highly contaminated with either toluene or heptane. Both heptane and toluene contamination caused a reduction in permeance, possibly due to competitive sorption and antiplasticization. Stronger reduction in permeance was observed in toluene contaminated feeds than in heptane contaminated feeds. These results suggest that proper pretreatment is essential to membrane productivity. Nevertheless, the maintained high selectivity and recovered permeance after removal of impurities demonstrate the durability of the crosslinked fibers against accidental exposure to high levels of heavy hydrocarbon impurities. Moreover, the unimpaired selectivities and plasticization resistance after exposure to a high pressure wet acid gas indicate the good hydrolytic stability of the crosslinks, in agreement with previous dense film studies [21, 22]. Finally, the presence of ethylene glycol was found to have negligible effects on separation performance of the crosslinked fibers.

6.8 References

1. D.R. Koch, W.R. Buchan, and T. Cnop, *Proper pretreatment systems reduce membrane replacement element cost and improve reliability*, 2005, UOP LLC: Des Plaines.

2. D. Dortmundt and K. Doshi, *Recent developments in CO_2 removal membrane technology*, 1999, UOP LLC: Des Plaines.

3. D.Q. Vu, W.J. Koros, and S.J. Miller, *Effect of condensable impurities in CO_2/CH_4 gas feeds on carbon molecular sieve hollow-fiber membranes.* Industrial & Engineering Chemistry Research, 2003. **42**(5): p. 1064-1075.

4. N. Tanihara, H. Shimazaki, Y. Hirayama, S. Nakanishi, T. Yoshinaga, and Y. Kusuki, *Gas permeation properties of asymmetric carbon hollow fiber membranes prepared from asymmetric polyimide hollow fiber.* Journal of Membrane Science, 1999. **160**(2): p. 179-186.

5. J.W. Simmons, S. Kulkarni, and O.M. Ekiner. *Method for separating hydrocarbon-containing gas mixtures using hydrocarbon-resistant membranes.* U.S. Patent 7025804 B2, 2006.

6. C.T. Ratcliffe, A. Diaz, C. Nopasit, and G. Munoz. *Application of membranes in co2 separation from natural gas: pilot plant tests on offshore platforms*: *Laurence Reid Gas Conditioning Conference*. 1999. Norman, OK.

7. R. Hasan, C.A. Scholes, G.W. Stevens, and S.E. Kentish, *Effect of hydrocarbons on the separation of carbon dioxide from methane through a polyimide gas separation membrane.* Industrial & Engineering Chemistry Research, 2009. **48**(11): p. 5415-5419.

8. M. Al-Juaied and W.J. Koros, *Performance of natural gas membranes in the presence of heavy hydrocarbons.* Journal of Membrane Science, 2006. **274**(1-2): p. 227-243.

9. J.K. Ward and W.J. Koros, *Crosslinkable mixed matrix membranes with surface modified molecular sieves for natural gas purification: II. Performance characterization under contaminated feed conditions.* Journal of Membrane Science, 2011. **377**(1-2): p. 82-88.

10. I.C. Omole, D.A. Bhandari, S.J. Miller, and W.J. Koros, *Toluene impurity effects on CO_2 separation using a hollow fiber membrane for natural gas.* Journal of Membrane Science, 2011. **369**(1-2): p. 490-498.

11. W.J. Koros, R.T. Chern, V. Stannett, and H.B. Hopfenberg, *A model for permeation of mixed gases and vapors in glassy polymers.* Journal of Polymer

Science: Polymer Physics Edition, 1981. **19**(10): p. 1513-1530.

12. J.S. Lee, W. Madden, and W.J. Koros, *Antiplasticization and plasticization of Matrimid® asymmetric hollow fiber membranes-Part A. Experimental.* Journal of Membrane Science, 2010. **350**(1-2): p. 232-241.

13. J.S. Lee, W. Madden, and W.J. Koros, *Antiplasticization and plasticization of Matrimid® asymmetric hollow fiber membranes. Part B. Modeling.* Journal of Membrane Science, 2010. **350**(1-2): p. 242-251.

14. F.A. Ruiz-Trevino and D.R. Paul, *Gas permselectivity properties of high free volume polymers modified by a low molecular weight additive.* Journal of Applied Polymer Science, 1998. **68**(3): p. 403-415.

15. Y. Maeda and D.R. Paul, *Effect of antiplasticization on gas sorption and transport .1. Polysulfone.* Journal of Polymer Science Part B-Polymer Physics, 1987. **25**(5): p. 957-980.

16. L.S. White, T.A. Blinka, H.A. Kloczewski, and I.F. Wang, *Properties of a polyimide gas separation membrane in natural-gas streams.* Journal of Membrane Science, 1995. **103**(1-2): p. 73-82.

17. G. Djoekita. *Characterization and analysis of asymmetric hollow fiber membranes for natural gas purification in the presence of hydrocarbons.* M.S. Thesis, The University of Texas at Austin, Austin, TX, 2000.

18. J.S. Lee, R.T. Adams, W. Madden, and W.J. Koros, *Toluene and n-heptane sorption in Matrimid® asymmetric hollow fiber membranes.* Polymer, 2009. **50**(25): p. 6049-6056.

19. E.W. Funk, S.S. Kulkarni, and A.X. Swamikannu, *Effect of impurities on cellulose acetate membrane performance.* AIChE Symp. Series, 1986. **250**.

20. C. Scholes, S. Kentish, and G. Stevens, *Effects of minor components in carbon dioxide capture using polymeric gas separation membranes.* Separation and Purification Reviews, 2009. **38**(1): p. 1-44.

21. W.L. Qiu, C.C. Chen, M.R. Kincer, and W.J. Koros, *Thermal analysis and its application in evaluation of fluorinated polyimide membranes for gas separation.* Polymer, 2011. **52**(18): p. 4073-4082.

22. A.M. Kratochvil and W.J. Koros, *Decarboxylation-induced cross-linking of a polyimide for enhanced CO_2 plasticization resistance.* Macromolecules, 2008. **41**(21): p. 7920-7927.

CHAPTER 7

SUMMARY AND FUTURE DIRECTIONS

7.1 Summary

The overarching goal of this research was to develop robust asymmetric hollow fiber membranes for CO_2 removal from aggressive natural gas feed streams and to understand their properties. The objectives described in Chapter 1 are summarized and progress toward these goals is reviewed.

1. **Develop crosslinkable defect-free asymmetric hollow fiber membranes from a novel polyimide, 6FDA-DAM:DABA (3:2).**

Successful spinning of asymmetric hollow fiber membranes is a prerequisite for practical membranes. An initial attempt of spinning resulted in hollow fibers with slightly defective skin, which was found to suffer from severe and irreparable loss in selectivity during thermal crosslinking. After subsequent optimization of dope composition and spinning conditions, crosslinkable asymmetric hollow fibers with defect-free selective skin layers on an optimized porous support substructure were successfully spun at a commercially relevant production rate of 50 m/min.

2. **Investigate the effect of thermal treatment on degree of crosslinking, fiber morphology, and separation performance.**

Post-spin thermal crosslinking was implemented for the successful asymmetric hollow fiber membranes related to objective 1. Thermal treatment conditions, which

promote sufficient crosslinking without introducing defects or undesired substructure resistance, were identified. It was found that crosslinking improves membrane efficiency and plasticization resistance as well as mechanical strength of fibers. The superior stability under high pressure feeds (with CO_2 partial pressure up to 700 psia) suggests that the crosslinked fibers have good potential for long-term operations in aggressive environments.

3. Demonstrate the efficacy of thermally crosslinked hollow fiber membranes under aggressive feed streams and realistic operating conditions.

The third objective is of a practical nature and is intended to evaluate membrane performance under realistic operating conditions as well as durability and resistance against impurities in the event of a pretreatment upset. The crosslinked fibers were found to maintain good separation performance under high CO_2 content feeds (50-70% CO_2) at a variety of feed pressures (up to 1000 psia), temperatures (35-65 °C), and permeate pressures (up to 100 psia). This capability allows the crosslinked fibers to be used under a wide range of operating conditions to optimize separation performance for specific applications. In the studies of condensable hydrocarbon impurities, it was found that crosslinked fibers were resistant to plasticization by toluene and heptane, even at high activity levels. Although significant reduction in membrane productivity was observed in highly contaminated feeds, standard pretreatment of the feeds is sufficient to remove impurity to an acceptable level. Moreover, the contaminated membranes can be regenerated by simply purging with a contaminant-free feed. Besides hydrocarbon impurities, crosslinked fibers were also found to be resistant to glycol and water—two other common impurities may damage polymeric membranes.

7.2 Future directions

The results presented in this dissertation demonstrate that successful crosslinked hollow fiber membranes are achievable and can exhibit good separation performance as well as durability required for practical applications. This final section contains recommendations for future directions of this project.

1. Performance evaluation under H_2S contaminated feeds

Hydrogen sulfide is another common acid gas component presented in many gas reserves. The effects of H_2S on membrane performance and stability were not studied in this work. It is expected that H_2S can induce stronger plasticization effects than CO_2 due to its higher condensability. Moreover, in the presence of moisture, H_2S forms sulfuric acid, which is more acidic than carbonic acid formed by CO_2. Given the superior solvent resistance and hydrolytic stability shown in this work, crosslinked fibers may be used in H_2S contaminated gas fields.

2. Investigation of low temperature route for crosslinking

As mentioned in Chapter 5, high temperature thermal treatment required to promote crosslinking can cause skin layer densification, and thus result in a decrease in permeance. Although the addition of oxidizers (O_2 and N_2O) was not successful to facilitate crosslinking at lower temperature, some other approaches may be worth pursuing. For example, since the crosslinking mechanism involves the formation of phenyl free radicals, thermal free radical initiators are potential catalysts for crosslinking. Moderate crosslinking temperature (150-300 ℃) is preferable, since it could provide sufficient polymer chain mobility to bring reactive sites together. Therefore, relatively

stable organic hydroperoxides, such as cumene hydroperoxide and t-butyl hydroperoxide, with high half-life temperatures [1] are selected as catalyst candidates. The stability at room temperature allows these catalysts to remain inactive after being imbibed into fibers during solvent exchange steps while decomposing and forming free radicals at elevated temperatures during subsequent drying/crosslinking steps.

3. Exploration of potential applications

Excellent plasticization resistance to heavy hydrocarbon suggests that crosslinked hollow fiber membranes have great potential for use in diverse aggressive applications, even beyond the CO_2/CH_4 example explored in this work. Examples of such potential applications include olefin/paraffin separation and aromatic/aliphatic separation. Some preliminary tests were performed in this work to explore these possibilities. Propylene permeation was conducted and the results are shown in Figure 7.1. Early onset of plasticization was observed in uncrosslinked fibers while crosslinked fibers were not plasticized by propylene, a strong plasticizer in propane/propylene separation. Nevertheless, detailed characterization is needed to determine the feasibility of the crosslinked fibers for these separations.

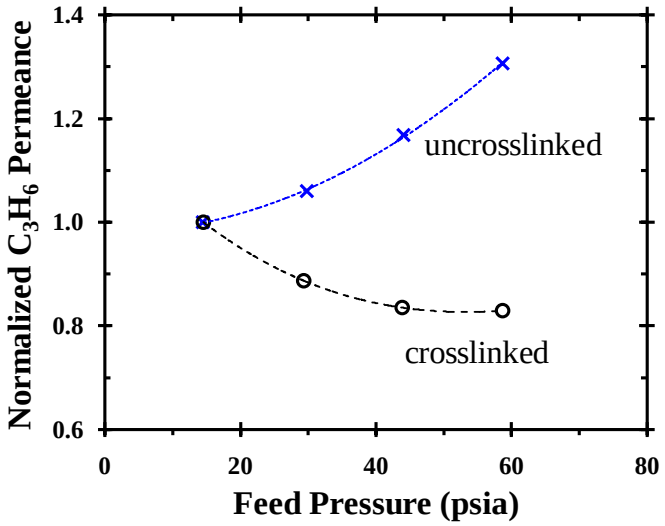

Figure 7.1: Propylene permeation isotherm of crosslinked and uncrosslinked fibers. Test temperature: 35 ℃.

If the current structure (3:2 DAM:DABA ratio) does not offer good separation performance for a specific application, transport properties can be tailored via (1) change of monomer ratio: polymers with higher DABA contents are expected to have more pronounced effect on plasticization resistance due to the higher crosslinking density. In addition, polymer with higher DABA content show higher selectivity compared to its lower DABA content counterpart [2, 3]. However, the increased DABA content will also increase the hydrophilicity of the polymers, thereby spinning of these materials will be more challenging; (2) substitution of DAM moiety: the class of crosslinkable polyimide used in this work has proven to be extremely flexible, having an essentially unlimited number of possible structure by varying or modifying dianhydride and diamine monomers. For example, DAM moiety has been shown to provide higher permeability but lower selectivity as compared to mPDA moiety, due to the bulky methyl groups on DAM which inhibit chain packaging [4, 5]. Therefore, replacing DAM moiety in the

current structure by mPDA is expected to create a less open structure, and thus increase selectivity at some expense of permeability. The structures of 6FDA-DAM: DABA and 6FDA-mPDA:DABA are shown in Figure 7.2.

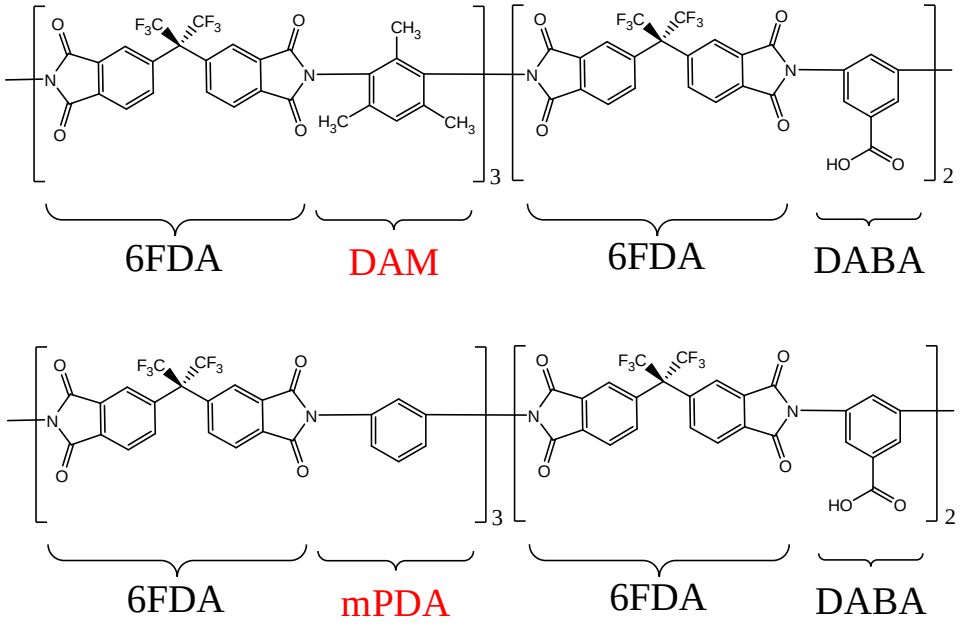

Figure 7.2: Chemical structures of 6FDA-DAM:DABA (3:2) (top) and 6FDA-mPDA:DABA (3:2) (bottom).

4. Analysis of antiplasticization vs. competitive sorption effects

As discussed in Chapter 6, permeance reduction observed in the presence of condensable hydrocarbons (toluene or heptane) can be attributed to combined effects of antiplasticization and competitive sorption. Detailed sorption analysis can provide essential information needed to decouple the two effects, i.e., to determine how much of the depression in permeance is due to antiplasticization vs. competitive sorption.

7.3 References

1. *Organic Peroxides - Arkema Inc.* http://arkemaus.com/literature/pdf/320.pdf. (accessed 09/2011).

2. C. Hibshman, C.J. Cornelius, and E. Marand, *The gas separation effects of annealing polyimide-organosilicate hybrid membranes.* Journal of Membrane Science, 2003. **211**(1): p. 25-40.

3. J.D. Wind. *Improving Polyimide Membrane Resistance to Carbon Dioxide Plasticization in Natural Gas Separations* Ph.D. Dissertation, The University of Texas at Austin, Austin, TX, 2002.

4. K. Tanaka, M. Okano, H. Toshino, H. Kita, and K.I. Okamoto, *Effect of Methyl Substituents on Permeability and Permselectivity of Gases in Polyimides Prepared from Methyl-Substituted Phenylenediamines.* Journal of Polymer Science Part B-Polymer Physics, 1992. **30**(8): p. 907-914.

5. I.C. Omole. *Crosslinked Polyimide Hollow Fiber Membranes for Aggressive Natural Gas Feed Streams.* Ph.D. Dissertation, Georgia Institute of Technology, Atlanta, GA, 2008.

APPENDIX A

POLYMER SYNTHESIS PROCEDURE

As described in Chapter 3, the thermally crosslinkable polyimide, 6FDA-DAM:DABA (3:2), was synthesized by a two-step polycondensation reaction. The procedure is outlined as follows.

1. Monomer purification

a. Dry both dianhydride and diamine in vacuum ovens ~20 ℃ below their actual sublimation temperature overnight.

b. Assemble the sublimation apparatus with monomer inside.

c. Sublimate monomers at a given temperature.

d. After sublimation, note down the yield and store the monomers in an airtight place (use the sublimated monomer as soon as possible).

e. Dry slight excess amount of monomers in vacuum ovens again ~2 days before synthesis.

2. Solvent drying

Start ~3 days before synthesis

a. Dry molecular sieves in different flasks under vacuum in an oven for at least one day at 150 ℃.

b. Seal the flasks with rubber septum, needle transfer ~1.5 times of calculated amount of NMP and acetic anhydride (AcAn) solvents to the flasks 2~3 days before synthesis.

c. Seal flasks with parafilm.

3. Polyamic acid formation

a. Assemble synthesis reactor. Thoroughly clean and dry all glassware, stirrer, and thermometer.

b. After the whole assembly is done, purge it with inert gas for couple of hours to get rid of any unwanted moisture.

c. Flame the whole reactor with propane torch under purging.

d. Needle transfer ~60% of required NMP to the reactor with a syringe (rest of it will be required after monomer addition step).

e. Carefully weigh the amount of diamines required.

f. Under stirring and purging, add diamines into the reactor, rinse the neck of the reactor with NMP using a syringe, and seal the neck with rubber septum.

g. Cool the reactor with an ice-water bath.

h. Wait until diamines are dissolved, and temperature reaches below 5 ℃.

i. Carefully weigh ~1/4 amount of required dianhydride, add it to reactor, rinse the neck with NMP, and seal with rubber septum.

j. Keep temperature below 5 ℃, and wait till all the dianhydride dissolves.

k. Repeat this step, added all the pre-calculated dianhydride partially in 3~4 times.

l. Keep the reaction below 5 ℃ for several hours till viscosity rise significantly, let reaction go at room temperature.

m. After total reaction continues for 24 hr under purging, starting imidization process.

4. Chemical imidization

a. Add calculated amount of beta-picoline via syringe into the reactor.

b. Let it dissolve in the solution completely.

c. Add calculated amount of acetic anhydride (AcAn) slowly via syringe.

d. Let the reaction go for 24 hr at room temperature under purging.

5. Precipitation

a. Pour methanol in a large container.

b. Pour the polyimide solution into methanol slowly, polymer will phase separate easily.

c. Blend polymer, and collect the polymer with pressure filtration.

d. Soak polyimide in methanol overnight.

e. Filtrate polymer, wash the polymer with methanol 2~3 times.

f. Dry the polymer in a hood at room temperature until most solvent was evaporated (at least overnight).

g. Dry the polymer in a vacuum oven at 200 ℃ for 24 hr.

APPENDIX B

HOLLOW FIBER POST-TREATMENT (PDMS COATING) [1]

Hollow fibers can be treated to "plug" minor defects in the fiber skin. This treatment usually involves coating the fibers with a second layer of a highly permeable, flexible polymer that can prevent Knudsen flow through the fibers as outlined by Henis and Tripodi [2].

In this research, a crosslinkable polydimethylsiloxane, Sylgard 184® available from Dow Corning was used to post-treat the fibers. The procedure is outlined as follows.

1. A 3 wt % solution of Sylgard® in heptane was heated at 75 ℃ for 1 hr to obtain branching and chain extension.
2. The fiber module was filled with the heptane solution and the module shaken to swirl the contents. The fibers were then allowed to soak in the solution for 5 minutes. The solution was drained out of the module.
3. Step 2 was repeated.
4. The module was placed in a vacuum oven at 75 ℃ for 2 hr.

References

1. D.W. Wallace. *Crosslinked hollow fiber membranes for natural gas purification and their manufacture from novel polymers.* Ph.D. Dissertation, The University of Texas at Austin, Austin, TX, 2004.

2. J.M.S. Henis and M.K. Tripodi, *Composite hollow fiber membranes for gas separation - the resistance model approach.* Journal of Membrane Science, 1981. **8**(3): p. 233-246.